Problems in Analysis, Control, and Design

of

Switching Inverters and Rectifiers

Thesis by

Ramaswamy Mahadevan

In Partial fulfillment of the Requirements

for the Degree of

Doctor of Philosophy

California Institute of Technology

Pasadena, California

1987

(Submitted July 1, 1986)

to my parents

Acknowledgements

I thank my advisor Professor R. D. Middlebrook and co-advisor Professor Slobodan Ćuk for kindling my interest in Power Electronics. They have provided me with constant encouragement, counsel, and support during my stay at Caltech. I also thank Professor A. Sabanović of Energoinvest, Yugoslavia, for introducing me to the fascinating field of sliding mode control during his stay as Visiting Professor of Electrical Engineering at Caltech from 1983–85.

I also wish to acknowledge the financial support provided by Caltech in the form of Graduate Teaching Assistantships, and Garrett AiResearch, General Dynamics Corporation Fort Worth, and Caltech's Program in Advanced Technologies, sponsored by Aerojet General, General Motors, GTE, and TRW for the Graduate Research Assistantships.

I am grateful to the many members of the Power Electronics Group, especially Khai Ngo and Ram Venkataramanan, for the numerous stimulating discussions and brainstorming sessions. My thanks to my friends in the Electrical Engineering Department and the Institute, who have made my stay at Caltech an enjoyable and memorable experience.

Abstract

Control and *analysis techniques* in switched-mode *inversion (dc-ac)* and *rectification (ac-dc)* are examined in this thesis. *Current programming* and *sliding mode control* are used to provide *regulation* and obtain desired *dynamic responses.* The basic *buck, boost, flyback, and buck-boost* topologies are used to illustrate the different methods of control and analysis. For illustration, embodiments employ *fast switching* converters, but the techniques described can be applied to any general converter.

Different possibilities for the current programming of dc-ac inverters and ac-dc rectifiers are explored and the more practical and advantageous methods noted. Current reference programming improves the dynamic response of the converter and simplifies the design of the main regulatory loop. It also protects the switches from excessive current stresses and enables the parallel operation of many converters to support a common load. Constant frequency current reference programmed converters are, however, subject to oscillations under certain operating conditions.

Describing equations are used to obtain the *low frequency* characterization of current programmed converters. The system representation is first obtained in the *stationary abc* reference frame and then transformed to the *rotating dq* coordinate frame. In the *dq* coordinate system, the low frequency characterizations of all *balanced, polyphase* ac converter systems are represented by a set of *continuous, time-invariant* differential equations. The steady-state and linearized, small signal dynamic responses are then obtained in this rotating reference frame.

Sliding mode control is applied to inverters and rectifiers to provide regulation and ensure the stability of the system in the presence of small and large signal disturbances. This is a natural method of control for variable structure systems and enables the design of a robust controller that can provide stability and performance in the face of plant uncertainities. However, it requires that all or many of the states of the system be accessible and results in a variable switching frequency in the converter.

The *equivalent control* method is used to obtain the low frequency properties of the sliding mode system, and can also be used to obtain the low frequency models of duty ratio programmed converters. Different switching strategies can be used to provide sliding mode control, as well as to optimize responses, maximize efficiency, or minimize switching losses. Practical aspects such as hardware implementation, switch realization, and measurement techniques are also discussed.

Contents

Introduction

The field of switched-mode power conversion extends over myriad applications in the areas of energy processing systems. The four major areas of switched-mode power conversion pertain to *dc-dc conversion, inversion, rectification, and cycloconversion.* Switched-mode converters in each of these areas have been used in various applications ranging from computers and motor drives to uninterruptable power supplies and switched-mode amplifiers. Various topologies and modulation strategies have been used depending on the application and power level involved.

The analysis and design of dc-dc converter systems has progressed over a considerable period of time towards it present state. Many good analysis and design methods, and control techniques have been developed for dc-dc systems. Polyphase inversion, rectification, and cycloconversion systems, however, pose a much more difficult problem from the point of view of analysis and control. This difficulty stems from the multiple-input, multiple-output nature of polyphase converters in which the nonlinearity cannot be approximated easily using linear approximations, as is done in the case of dc-dc systems. Different analysis and control methods have been used depending on the application and are predominantly related to the areas of motor drives. Many of these evolved from slow switching converters that were utilized for high power applications; the switching frequency and size, weight and dynamic limitations of the converters being effectively determined by the power-speed limitations of the semiconductor devices used.

The advent of new semiconductor devices with higher power-speed limitations,

such as MOSFETs and GTOs, has enabled the development of polyphase conversion systems that use high switching frequencies. Consequently, converters with low ac harmonics, smaller size and weight, and improved dynamic responses, have emerged. Adequate analysis and control methods are required to exploit the full potential available in these converters. Different methods of analysis and control of polyphase converters are discussed in this thesis.

The first three chapters pertain to fast-switching, sinusoidally pulse width modulated, inverters and rectifiers. The basic converter topologies and pulse width modulation schemes are reviewed in Chapter 1. The low frequency representation of the system is obtained using describing functions, but can also be obtained (through a more lengthy procedure) using state space averaging techniques. This low frequency representation of the converter adequately describes the properties of interest for most real-life applications. However, the presence of large signal time-varying states in the system, cross-coupling of outputs, and the presence of nonlinearities, make it difficult to apply simple single loop design techniques to design a regulator for the MIMO system.

Current programming of polyphase inverters and rectifiers is considered in Chapter 2. Techniques for current programming of polyphase converters are explored and seen to be more advantageous for some topologies than for others. Current programming helps reduce the distortion in ac waveforms, as well as improve the dynamic responses of the converter. In some cases, it helps reduce the cross-coupling between input-output pairs and simplifies the design of the MIMO controller by reducing it to a series of single loop controllers. Current programming also provides inherent protection for the semiconductor devices of the converter. The analysis of the current programmed buck-boost converter is discussed in detail in Chapter 3.

The latter three chapters are devoted to the sliding mode control of polyphase

converter systems. Sliding mode is a method of control that has been utilized in, and is especially suitable for, variable structure systems. The concepts and notations used in sliding systems, and the sliding mode control of dc-dc converters, are reviewed in Chapter 4. A generalized method of sliding mode control for polyphase converters, based on the topological classification of the converters, is discussed in Chapters 5 and 6. Different techniques are used to obtain conditions required for sliding motion, and to obtain nonconservative estimates for the sliding domain. Appendix A reviews the mathematical fundamentals used to obtain the conditions necessary for sliding motion to exist in the system.

Chapter 1

Review of Fast-Switching Sinusoidal PWM Inverters and Rectifiers

Three phase and single phase alternating current systems are the backbone of electrical power generation and distribution systems. However, many modern electric and electronic systems utilize direct current power supplies, and so many present day applications require the conversion of electrical power from ac to dc form. Similarly, there are numerous applications such as motor drives and uninterruptable power supplies, where electric power has to be converted from dc to ac form. This transformation of power from ac to dc form is done using a *rectifier* and the process is known as *rectification.* The corresponding transformation of electrical power from dc to ac form is labelled as *inversion* and is performed by an *inverter.* Alternating current systems may consist of single phase or balanced polyphase outputs. However, only the latter kind of systems with *constant instantaneous power flow* are discussed in this thesis.

Inverters can be classified under three main categories based on the value of the switching frequency compared to the inversion frequency. The first class of inverters consists of those converters switched at the inversion frequency. In these "slow-switching" inverters, the switching harmonics are close to the inversion frequency and cannot be effectively filtered from the desired output. The six-stepped voltage-source and current-source inverters [1,2,3] fall in this category. The second group comprises invert-

ers whose switching frequency is approximately an order of magnitude higher than the inversion frequency. Some stepped-synthesis inverters and PWM inverters implemented using thyristor switches belong to this group [4,5,6]. Although the switching frequency is higher, the switching harmonics are still not separated well enough from the inversion frequency to be attenuated effectively using filters which are small in size.

The third category consists of inverters whose switching frequency is two or more orders of magnitude higher than the inversion frequency. Consequently, small filters are used to suppress the switching harmonics. Switched-mode power amplifiers, resonant inverters, and sinusoidal PWM inverters belong to this category [7,8,9].

Rectifiers can also be classified in a manner similar to that described above.

This chapter reviews fast switching sinusoidal PWM inverters and rectifiers. Section 1.1 describes the topology and PWM modulation schemes used for some of the basic converters belonging to this family. Though the topologies and modulation can be utilized for general polyphase systems, they are illustrated using three phase systems. The method of describing the system using state equations is discussed in Section 1.2 as are the necessary transformations to convert the time-varying system of equations into a time-invariant form. From these equations, the steady-state and dynamic models are obtained in Section 1.3.

1.1 Description of Topology and PWM Modulation

The following subsections describe the topology and operation of the buck, boost, and flyback *fast-switching, pulse width modulated* inverters and rectifiers. In all cases, the switching frequency is presumed to be two or more decades above the inversion frequency or source frequency of operation. The term "high frequency, sinusoidal pulse width modulation" is used to refer to the operation of switches that are pulse width

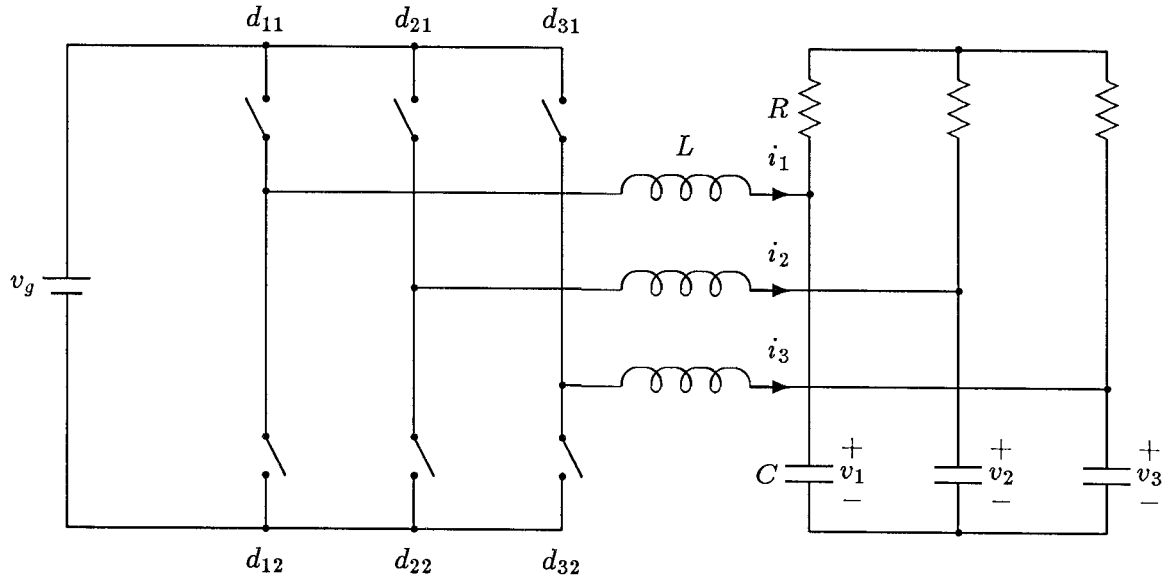

Figure 1.1: Three phase buck inverter with three, sinusoidally pulse width modulated, double-throw switches.

modulated at a high switching frequency with the duty ratios varied according to sinusoidal functions or segments of sinusoidal functions. The converters are described using duty ratios for the various switches, and not with switch timing waveforms, as most of the properties of the converter depend only on the duty ratios and not on the specific switching sequence. Any constraints imposed on the operation of the switches by the topology itself, or by practical considerations, are noted as and when they arise.

1.1.1 Buck Topology

The three phase *buck inverter* and *buck rectifier* are derived from the buck dc-dc converter. The buck inverter, Fig. 1.1, consists of a *single-pole, double-throw* switch for each phase of the balanced polyphase output. Each of the double-throw switches can operate *independently* and the only constraint imposed by the topology is that the top

and bottom throws of each switch should be *non-overlapping* to prevent *shoot through* faults. The duty ratio of each switch consists of a dc offset and a *continuous, or piecewise continuous, sinusoidal* modulation. One way of implementing this is by using:

$$d_{w1} = \frac{1}{2} + \frac{d_m}{2}\cos[\theta_m - (w-1)\frac{2\pi}{3}] \tag{1.1}$$

$$d_{w2} = 1 - d_{w1} \tag{1.2}$$

where

$$\theta_m = \int_0^t \omega(\tau)\, d\tau \quad , \quad d_m \leq 1 \quad \text{and} \quad 1 \leq w \leq 3 \tag{1.3}$$

The *effective duty ratio* is given by

$$d_w = d_{w1} - \frac{1}{3}\sum_{z=1}^{3} d_{z1} = \frac{d_m}{2}\cos[\theta_m - (w-1)\frac{2\pi}{3}] \tag{1.4}$$

A *different* modulation strategy would only change the *amplitude* of the *effective duty ratio* and not the basic properties of the circuit. This is analogous to having a pulse width modulator with a different gain in the modulator. The *instantaneous modulation frequency* ω can assume any real value that is sufficiently lower in magnitude than the switching frequency. A negative frequency ω signifies a reversal in the phase sequence. The above mentioned duty ratios can be realized by different switching functions and the actual drive depends on the ease of implementation and on second order effects. All switches in the buck inverter are *voltage unidirectional, current bidirectional* switches and can be implemented using a transistor and anti-parallel diode for each throw of the switch.

The three phase buck rectifier of Fig. 1.2 consists of two *single-pole, triple-throw* switches. The input voltages are assumed to be balanced, three phase, ac voltages and represented by

$$v_{gk} = v_g \cos[\theta_g - (k-1)\frac{2\pi}{3}], \quad (1 \leq k \leq 3) \tag{1.5}$$

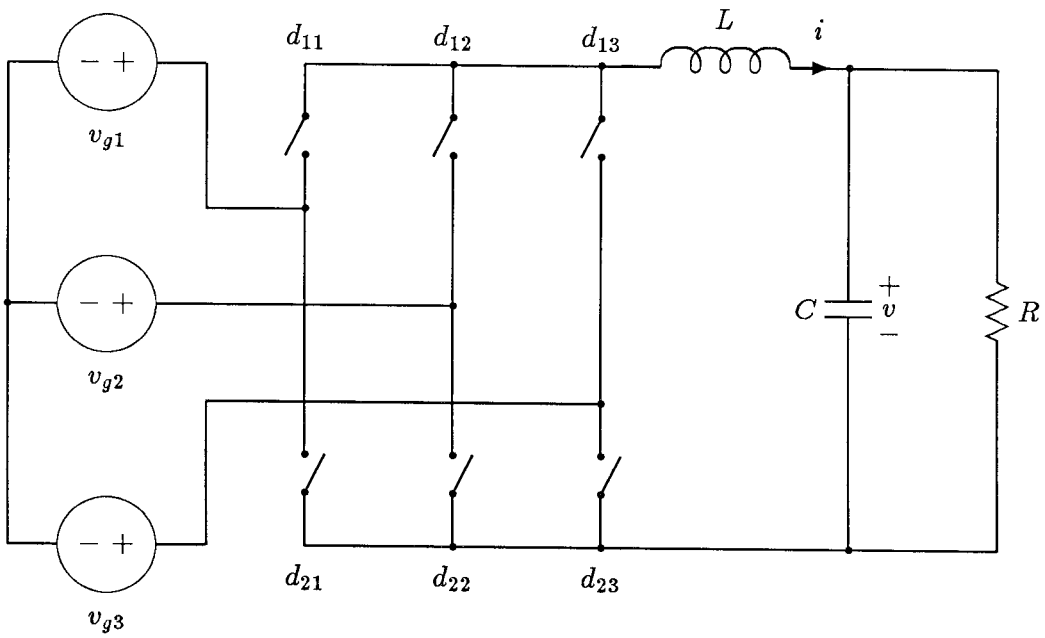

Figure 1.2: Three phase buck rectifier with two triple-throw switches pulse width modulated by sinusoidal functions.

where

$$\theta_g = \int_0^t \omega_g(\tau)\, d\tau + \phi_g \tag{1.6}$$

The lower case v_g and ω_g denote the *instantaneous source amplitude* and *frequency,* respectively. The *sinusoidally pulse width modulated* duty ratios are given by

$$d_{1k} = \frac{1}{3} + \frac{d_m}{3}\cos[\theta_m - (k-1)\frac{2\pi}{3}], \quad (1 \le k \le 3) \tag{1.7}$$

$$d_{2k} = \frac{1}{3} - \frac{d_m}{3}\cos[\theta_m - (k-1)\frac{2\pi}{3}], \quad (1 \le k \le 3) \tag{1.8}$$

where

$$d_m \le 1 \text{ and } \theta_m = \int_0^t \omega_g(\tau)\, d\tau + \phi_m \tag{1.9}$$

The *effective duty ratios* that affect the circuit properties of the inverter are given by

$$d_k = d_{1k} - d_{2k} = \frac{2d_m}{3}\cos[\theta_m - (k-1)\frac{2\pi}{3}] \tag{1.10}$$

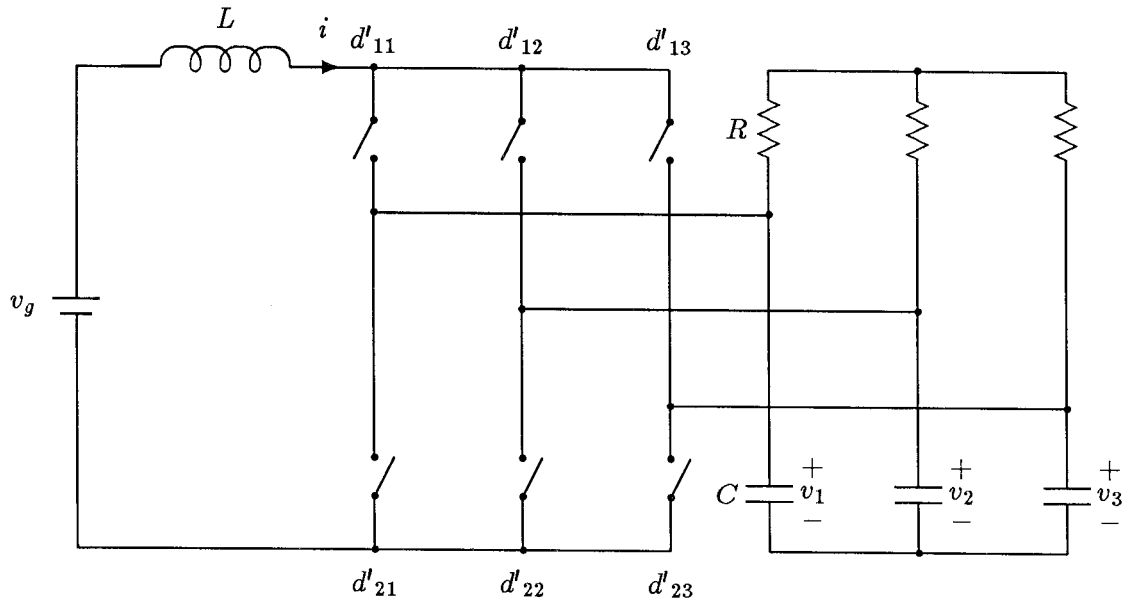

Figure 1.3: Three phase boost inverter with two, sinusoidally pulse width modulated, triple-throw switches

The LC low pass filter attenuates the switching harmonics only and does not have to filter low frequency harmonics of the source frequency. Elimination of the source frequency and its harmonics from the dc output is primarily a result of the sinusoidal pulse width modulation, and not the LC filter. This enables the use of a small filter, unlike the slow-switching rectifier whose filter has to attenuate harmonics of the source frequency.

1.1.2 Boost Topology

This subsection describes the boost inverter and boost rectifier, both of which are derived from the boost dc-dc converter. The boost inverter, Fig. 1.3, can also be obtained by interchanging the inputs and outputs of a buck rectifier in the same way as in the case of the boost and buck dc-dc converters. The boost inverter consists of two *single-pole, triple-throw* switches which are *current unidirectional, voltage bidirectional*

in nature. This is a current-fed topology and the inductor acts like a dc current source which is steered to the three phase outputs by the two triple-throw switches. The duty ratios of the switches are similar to those of the buck rectifier and are given by

$$d'_{1w} = \frac{1}{3} + \frac{d'_m}{3}\cos[\theta_m - (w-1)\frac{2\pi}{3}] \tag{1.11}$$

$$d'_{2w} = \frac{1}{3} - \frac{d'_m}{3}\cos[\theta_m - (w-1)\frac{2\pi}{3}] \tag{1.12}$$

where

$$d'_m \leq 1 \quad , \quad \theta_m = \int_0^t \omega(\tau)\, d\tau + \phi_m \quad \text{and} \quad 1 \leq w \leq 3 \tag{1.13}$$

The prime on the duty ratios is used to indicate that the switch lies on the output side of the circuit. The resulting *effective duty ratios* are

$$d'_w = d'_{1w} - d'_{2w} = \frac{2d'_m}{3}\cos[\theta_m - (w-1)\frac{2\pi}{3}] \quad , \quad 1 \leq w \leq 3 \tag{1.14}$$

The boost rectifier, Fig. 1.4, is obtained from the boost dc-dc converter or by reverse operation of the buck inverter. It is a current fed topology like the boost inverter or boost dc-dc converter. The three phase boost rectifier comprises three *small* inductors that transform the three phase source voltages into a set of balanced three phase currents. The three *single-pole, double-throw* switches on the output side transform these ac currents into a dc current for the load. This topology results in smooth input currents with low source frequency harmonics even with small input inductors because the switches operate at a high frequency and the duty ratios are sinusoidally pulse width modulated. The three phase source voltages are as specified in Eqs. (1.5) and (1.6). The duty ratios of the switches are

$$d'_{k1} = \frac{1}{2} + \frac{d'_m}{2}\cos[\theta_m - (k-1)\frac{2\pi}{3}] \quad , \quad (1 \leq k \leq 3) \tag{1.15}$$

$$d'_{k2} = 1 - d'_{k1} \quad , \quad (1 \leq k \leq 3) \tag{1.16}$$

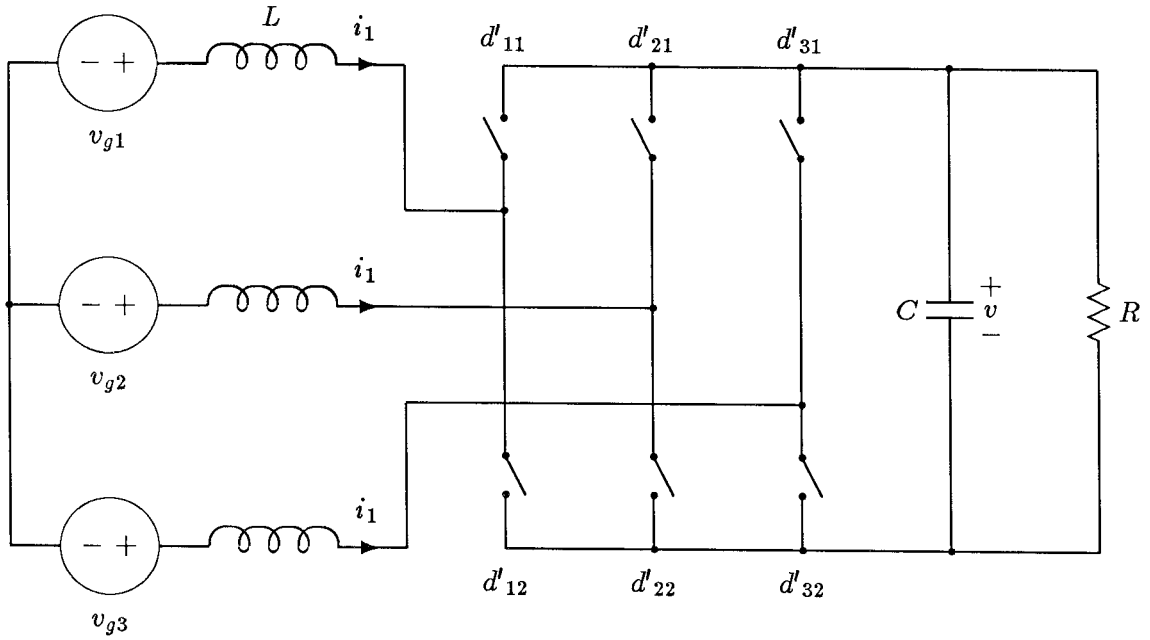

Figure 1.4: Three phase boost rectifier with three, sinusoidally pulse width modulated, double-throw switches.

where

$$d'_m \leq 1 \quad \text{and} \quad \theta_m = \int_0^t \omega_g(\tau)\, d\tau + \phi_m \tag{1.17}$$

The *effective duty ratio* of each phase is given by

$$d'_k = \frac{d'_m}{2} \cos[\theta_m - (k-1)\frac{2\pi}{3}] \quad , \quad (1 \leq k \leq 3) \tag{1.18}$$

The boost rectifier uses high frequency, pulse width modulation to generate a clean dc output in which harmonics of the source frequency are eliminated without the use of a bulky filter at the source frequency.

1.1.3 Flyback Topology

The flyback inverter originates from the flyback dc-dc converter. Again, this is a current-fed topology as seen in the three phase flyback inverter of Fig. 1.5. The

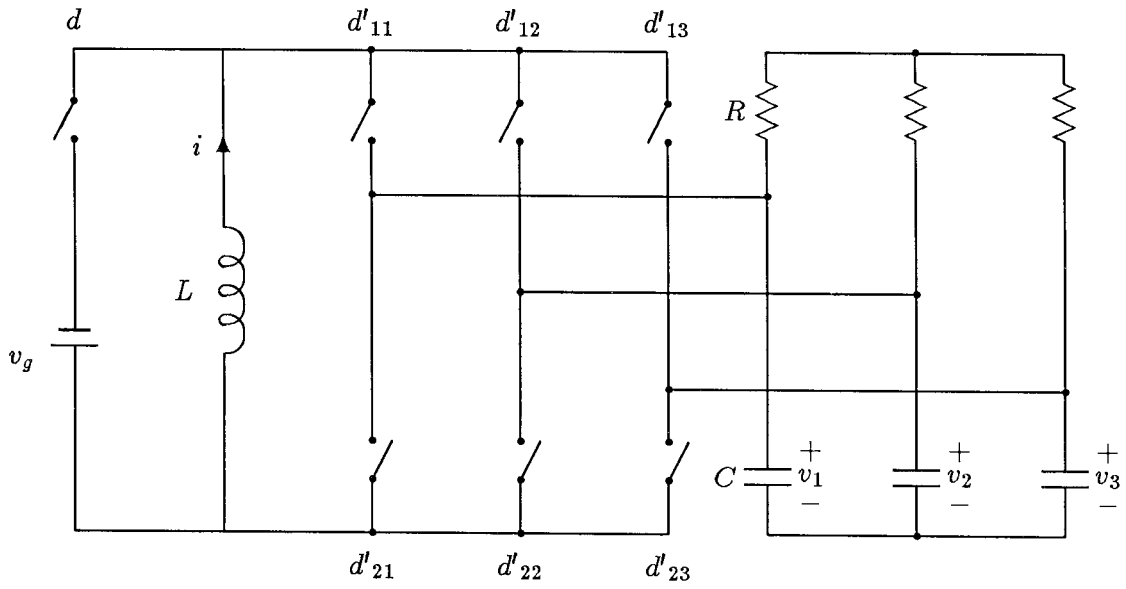

Figure 1.5: Three phase flyback inverter with one triple-throw and one quadruple-throw switch.

inductor, L, is connected across the dc source for a portion of each switching period to store energy in it. This stored energy is then steered to the three phase outputs using the switches on the load side in a manner analogous to that of the boost inverter. The duty ratios of the switches on the load side are given by

$$d'_{1w} = \frac{d'}{3} + \frac{d'_m}{3}\cos[\theta_m - (w-1)\frac{2\pi}{3}] \tag{1.19}$$

$$d'_{2w} = \frac{d'}{3} - \frac{d'_m}{3}\cos[\theta_m - (w-1)\frac{2\pi}{3}] \tag{1.20}$$

where

$$d' = 1 - d \ , \ d'_m \leq d' \ \text{ and } \ 1 \leq w \leq 3 \tag{1.21}$$

and θ_m is the instantaneous phase of the modulation, as defined before. The effective duty ratios d'_w are as given by Eq. (1.14) along with the constraint that $d'_m \leq d'$. The high frequency, sinusoidal pulse width modulation enables the flyback inverter to produce

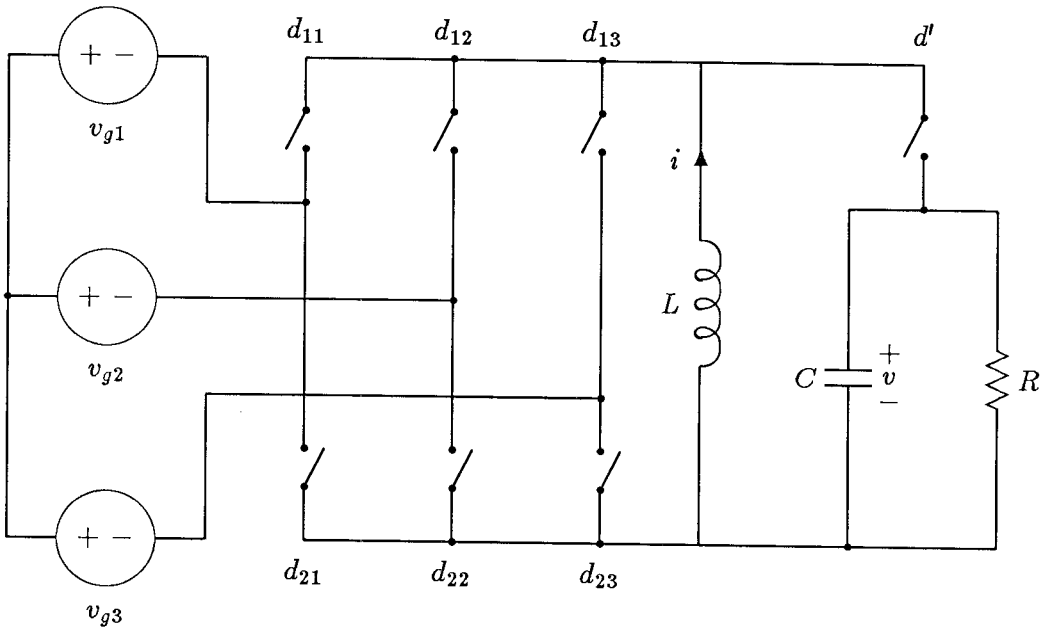

Figure 1.6: Three phase flyback rectifier with one triple-throw and one quadruple-throw switch.

output voltages with low inversion frequency harmonics.

The flyback rectifier is akin to reverse operation of the flyback inverter. The three phase flyback rectifier, Fig. 1.6, has one triple-throw switch and one quadruple-throw switch like the flyback inverter. Every switching cycle is partitioned into an energy storage period dT_s and an energy release period $d'T_s$. During dT_s, the input throws are activated according to the duty ratios

$$d_{1k} = \frac{d}{3} + \frac{d_m}{3}\cos[\theta_m - (k-1)\frac{2\pi}{3}] \tag{1.22}$$

$$d_{2k} = \frac{d}{3} - \frac{d_m}{3}\cos[\theta_m - (k-1)\frac{2\pi}{3}] \tag{1.23}$$

where

$$d_m \leq d \ , \ 1 \leq k \leq 3 \ \text{ and } \ \theta_m = \int_0^t \omega_g(\tau)\, d\tau + \phi_m \tag{1.24}$$

with the source voltages as defined by Eqs. (1.5) and (1.6). The output throw then diverts

the inductor current to the load during the period $d'T_s$, where

$$d' = 1 - d \tag{1.25}$$

The effective duty ratio that results is

$$d_k = d_{1k} - d_{2k} = \frac{2d_m}{3}\cos[\theta_m - (k-1)\frac{2\pi}{3}] \tag{1.26}$$

where $d_m \leq d$. The three phase ac source voltages are rectified by the throws on the input side to produce a dc current in the inductor during the period dT_s. The inductor then supplies energy to the load side during the period $d'T_s$ to produce a dc output which is free of source frequency harmonics.

1.2 System Description

This section first obtains the state space representation of the system in terms of the switching functions d_i^* of the switches[10]. The exact describing equations are then averaged over the switching period to obtain the low frequency state space representation of the system. This average state space description consists of a system of differential equations with time varying coefficients. This averaged system is then transformed into a time invariant system of equations using suitable transformations. Thus, the ac sinusoidally time varying quantities are transformed into dc quantities in the new co-ordinate reference frame. Standard methods can then be used to obtain steady-state and dynamic models. The procedure is illustrated using the three phase buck-boost inverter of Fig. 1.7.

1.2.1 Describing Equations

In this subsection, the switching equations of the converter are obtained so that the averaged state space model can be found without enumerating each and every switched network and writing state space equations for each one.

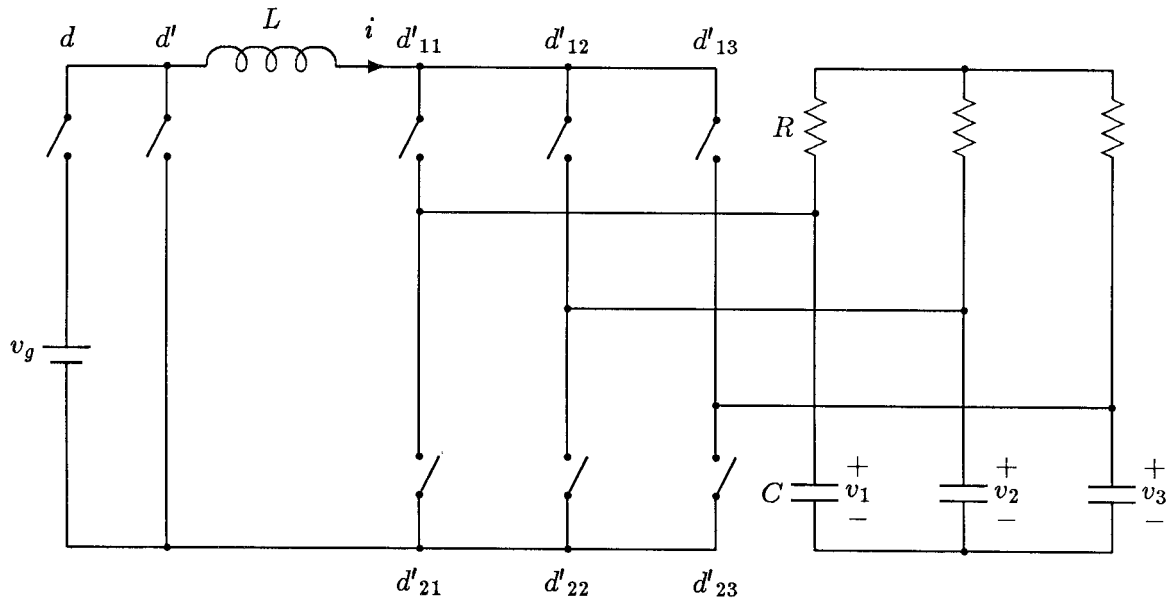

Figure 1.7: Three phase buck-boost inverter with two, sinusoidally pulse width modulated, triple-throw switches and one pulse width modulated, double-throw switch.

Consider the three phase buck-boost inverter of Fig. 1.7. The symbols i^* and v_w^*, with the asterisk (*), are used for the exact values of the states and the d_{kw}^* represent the switching functions of the switches. Following Kirchhoff's voltage law around the loop containing the source, switches, inductor, and capacitors, the following switching equation is obtained for the inductor:

$$L\frac{di^*}{dt} = d^*\, v_g - \sum_{w=1}^{3}(d'^*_{1w} - d'^*_{2w})\, v_w^* \tag{1.27}$$

Similarly, application of Kirchhoff's current law at the positive node of each capacitor results in

$$C\frac{dv_w^*}{dt} = i^*(d'^*_{1w} - d'^*_{2w}) - \frac{1}{R}(v_w^* - \frac{1}{3}\sum_{z=1}^{3} v_z^*) \quad , \quad (1 \le w \le 3) \tag{1.28}$$

Any general switched-mode converter includes S switches, each with t_s throws

for $1 \leq s \leq S$. The total number of controllable throws T_c that result is given by

$$T_c = \sum_{s=1}^{S} (t_s - 1) \tag{1.29}$$

If switching functions d_n^* , $1 \leq n \leq T_c$ are assigned to each of these controllable throws, then the *exact* state space *switching equation* of the ideal converter can be expressed as

$$\mathbf{P}\,\dot{\mathbf{x}}^* = \sum_{n=0}^{T_c} d_n^* (\mathbf{A}_n \mathbf{x}^* + \mathbf{B}_n \mathbf{u}) \tag{1.30}$$

where

$d_0^* = 1$,

$\mathbf{x}^*$ is the $N \times 1$ state vector,

$\mathbf{P}$ is the $N \times N$ LC matrix,

$\mathbf{A}_n$ is the $N \times N$ constant matrix,

$\mathbf{u}$ is the $M \times 1$ source vector,

$\mathbf{B}_n$ is the $N \times M$ constant matrix.

The terms with subscript 0 represent the contributions owing to the dependent throws of the switches in the switched-mode converter.

The sources and duty ratios of a fast-switching PWM converter vary at a slow rate compared to the switching frequency. The LC time constants of the converter are also generally chosen to be much longer than the switching period in order to minimize the switching ripple. Under these conditions, Eq. (1.30) can be averaged over the switching time period to obtain the low frequency representation of the system. The switching function d_n^* is approximated by its duty ratio d_n and the exact state vector $\mathbf{x}^*$ by its principal component $\mathbf{x}$. Thus, for frequencies sufficiently below the switching frequency, the system of Eq. (1.30) can be modelled by

$$\mathbf{P}\,\dot{\mathbf{x}} = (\mathbf{A}\,\mathbf{x} + \mathbf{B}\,\mathbf{u}) \tag{1.31}$$

where

$$\mathbf{A} = \sum_{n=0}^{T_c} d_n \mathbf{A}_n \quad \text{and} \quad \mathbf{B} = \sum_{n=0}^{T_c} d_n \mathbf{B}_n \tag{1.32}$$

In the case of the buck-boost inverter, the switching equations of Eqs. (1.27) and (1.28) result in the following vectors and matrices:

$$\mathbf{P} = \begin{bmatrix} L & 0 & 0 & 0 \\ 0 & C & 0 & 0 \\ 0 & 0 & C & 0 \\ 0 & 0 & 0 & C \end{bmatrix}, \quad \mathbf{x} = \begin{bmatrix} i \\ v_1 \\ v_2 \\ v_3 \end{bmatrix}$$

$$\mathbf{A} = \begin{bmatrix} 0 & -d'_1 & -d'_2 & -d'_3 \\ d'_1 & -2/3R & 1/3R & 1/3R \\ d'_2 & 1/3R & -2/3R & 1/3R \\ d'_3 & 1/3R & 1/3R & -2/3R \end{bmatrix}, \quad \mathbf{B} = \begin{bmatrix} d \\ 0 \\ 0 \\ 0 \end{bmatrix}, \quad \mathbf{u} = v_g \tag{1.33}$$

where d'_w are the effective duty ratios as defined by Eq. (1.14) and d is the duty ratio of the input switch. In this example, $\mathbf{P}$ and $\mathbf{B}$ are constant matrices, but $\mathbf{A}$ contains time varying terms as the effective duty ratios are chosen to be sinusoidally varying functions.

1.2.2 Transformation

The low frequency representation of any switched-mode converter in the stationary frame of reference, Eq. (1.31), may contain constant or time varying duty ratios depending on whether the converter is dc or ac. Time invariant systems are generally easier to analyze using standard techniques than time varying ones. Hence, an ac system is transformed into an equivalent dc one whenever possible.

Many transformations can be used to convert a set of balanced three phase sinusoids into an equivalent dc form [11]. The one chosen is the "dq" transformation,

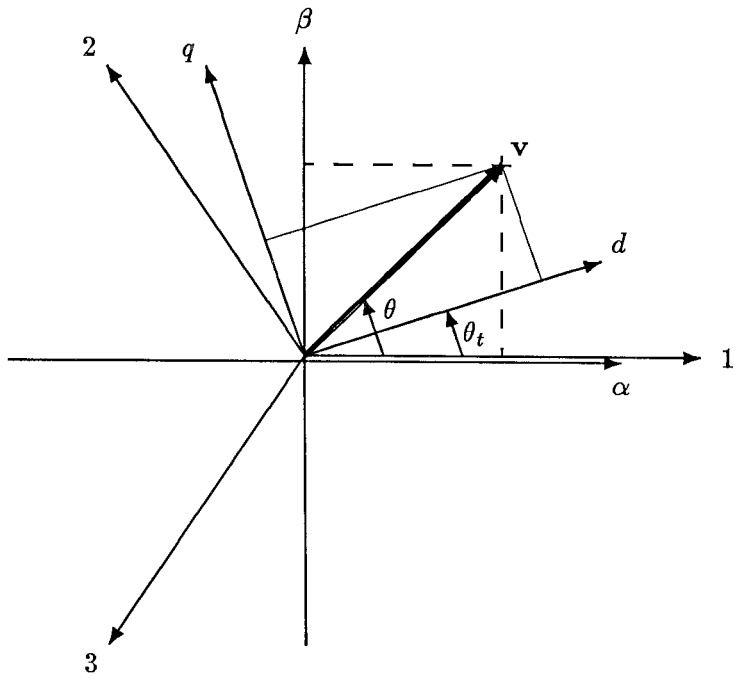

Figure 1.8: Transformation from the three phase ac, stationary frame to the rotating dq reference frame.

which is often used in the analysis of ac machines. The transformation is split in two parts as shown in Fig. 1.8. The first part of the transformation, $\mathbf{T}_1$, converts a set of balanced three phase sinusoids into an equivalent two phase set. The second transformation, $\mathbf{T}_2$, transforms the two phase system to a moving "dq" reference frame which is rotating at the same instantaneous angular frequency as the vector $\mathbf{v}$.

A vector $\mathbf{v}$ in the stationary reference is transformed into a vector $\breve{\mathbf{v}}$ in the two phase $\alpha\beta$ reference frame by

$$\mathbf{v} = \mathbf{T}_1\breve{\mathbf{v}} \quad \text{or} \quad \breve{\mathbf{v}} = \mathbf{T}_1^{-1}\mathbf{v} \tag{1.34}$$

where

$$\breve{\mathbf{v}} = \begin{bmatrix} v_\alpha \\ v_\beta \\ v_o \end{bmatrix} \text{ and } \mathbf{v} = \begin{bmatrix} v_1 \\ v_2 \\ v_3 \end{bmatrix} \tag{1.35}$$

and

$$\mathbf{T}_1^{-1} = [\mathbf{T}_1]^T = \sqrt{\frac{2}{3}} \begin{bmatrix} \cos(0) & \cos(\frac{2\pi}{3}) & \cos(\frac{4\pi}{3}) \\ \sin(0) & \sin(\frac{2\pi}{3}) & \sin(\frac{4\pi}{3}) \\ 1/\sqrt{2} & 1/\sqrt{2} & 1/\sqrt{2} \end{bmatrix} \tag{1.36}$$

A vector $\breve{\mathbf{v}}$ in the $\alpha\beta$ reference is then transformed to the vector $\tilde{\mathbf{v}}$ in the rotating dq reference frame according to

$$\breve{\mathbf{v}} = \mathbf{T}_2\tilde{\mathbf{v}} \text{ or } \tilde{\mathbf{v}} = \mathbf{T}_2^{-1}\breve{\mathbf{v}} \tag{1.37}$$

where

$$\tilde{\mathbf{v}} = \begin{bmatrix} v_d \\ v_q \\ v_o \end{bmatrix} \tag{1.38}$$

and

$$\mathbf{T}_2^{-1} = [\mathbf{T}_2]^T = \begin{bmatrix} \cos\theta_t & \sin\theta_t & 0 \\ -\sin\theta_t & \cos\theta_t & 0 \\ 0 & 0 & 1 \end{bmatrix} \tag{1.39}$$

where θ_t is the transformation angle given by

$$\theta_t = \theta - \phi_t = \int_0^t \omega(\tau)\, d\tau - \phi_t \tag{1.40}$$

in terms of the instantaneous angular frequency ω of the vector $\mathbf{v}$.

The low frequency representation of the converter, Eq. (1.31), is transformed to the dq reference frame using the transformations $\mathbf{T}_1$ and $\mathbf{T}_2$ to transform the ac quantities. The state vector $\mathbf{x}$ is transformed to the dq co-ordinate frame using

$$\mathbf{x} = \mathbf{T}\tilde{\mathbf{x}} \text{ or } \tilde{\mathbf{x}} = \mathbf{T}^{-1}\mathbf{x} \tag{1.41}$$

and the system becomes

$$\tilde{\mathbf{P}}\,\dot{\tilde{\mathbf{x}}} = \tilde{\mathbf{A}}\,\tilde{\mathbf{x}} + \tilde{\mathbf{B}}\,\tilde{\mathbf{u}} \tag{1.42}$$

where

$$\begin{aligned} &\tilde{\mathbf{A}} = \mathbf{T}^{-1}\mathbf{A}\mathbf{T} - \mathbf{T}^{-1}\mathbf{P}\dot{\mathbf{T}} \quad , \qquad \tilde{\mathbf{P}} = \mathbf{T}^{-1}\mathbf{P}\mathbf{T} \\ &\tilde{\mathbf{B}}\tilde{\mathbf{u}} = \mathbf{T}^{-1}\mathbf{B}\mathbf{u} \end{aligned} \tag{1.43}$$

The buck-boost inverter of Eq. (1.33) is transformed to the dq reference frame using

$$\tilde{\mathbf{x}} = \mathbf{T}^{-1}\mathbf{x} = \begin{bmatrix} 1 & \mathbf{o}_3^T \\ \mathbf{o}_3 & \mathbf{T}_2^{-1}\mathbf{T}_1^{-1} \end{bmatrix} \mathbf{x} \tag{1.44}$$

where $\mathbf{o}_3$ is the 3×1 zero vector. The resulting system matrices are

$$\begin{aligned} \tilde{\mathbf{P}} &= \begin{bmatrix} L & 0 & 0 & 0 \\ 0 & C & 0 & 0 \\ 0 & 0 & C & 0 \\ 0 & 0 & 0 & C \end{bmatrix} \quad , \quad \tilde{\mathbf{A}} = \begin{bmatrix} 0 & -d'_e\cos\phi_t & -d'_e\sin\phi_t & 0 \\ d'_e\cos\phi_t & -1/R & \omega C & 0 \\ d'_e\sin\phi_t & -\omega C & -1/R & 0 \\ 0 & 0 & 0 & 0 \end{bmatrix} \\ \tilde{\mathbf{B}} &= \begin{bmatrix} d \\ 0 \\ 0 \\ 0 \end{bmatrix} \qquad\qquad , \quad \tilde{\mathbf{u}} = v_g \end{aligned} \tag{1.45}$$

in which d'_e is the effective amplitude of modulation and ϕ_t is due to the phase of the transformation. In Eq. (1.45), it is noted that the "o" component of the capacitor voltages is given by $C\dot{v}_o = 0$. Subsequently, the value of v_o is determined by initial conditions only and in practice will be zero. Thus, the "o" component(s) are trivial state(s) and are eliminated from the system representation. The reduced order system is expressed in the form

$$\mathbf{P}_r\,\dot{\tilde{\mathbf{x}}}_r = (\mathbf{A}_r + \mathbf{A}_d\,d'_e + \mathbf{A}_\omega\,\omega)\tilde{\mathbf{x}}_r + \mathbf{B}_r\,\tilde{\mathbf{u}} + \mathbf{B}_d\,d\,\tilde{\mathbf{u}} \tag{1.46}$$

with the control parameters outside the matrices in order to show their effects on the operation of the converter. For the buck-boost inverter example, the system matrices and state vector are

$$\mathbf{P}_r = \begin{bmatrix} L & 0 & 0 \\ 0 & C & 0 \\ 0 & 0 & C \end{bmatrix}, \quad \mathbf{A}_r = \begin{bmatrix} 0 & 0 & 0 \\ 0 & -1/R & 0 \\ 0 & 0 & -1/R \end{bmatrix}, \quad \mathbf{A}_\omega = \begin{bmatrix} 0 & 0 & 0 \\ 0 & 0 & C \\ 0 & -C & 0 \end{bmatrix}$$

$$\mathbf{A}_d = \begin{bmatrix} 0 & -\cos\phi_t & -\sin\phi_t \\ \cos\phi_t & 0 & 0 \\ \sin\phi_t & 0 & 0 \end{bmatrix}, \quad \mathbf{B}_d = \begin{bmatrix} 1 \\ 0 \\ 0 \end{bmatrix}, \quad \mathbf{B}_r = \begin{bmatrix} 0 \\ 0 \\ 0 \end{bmatrix}, \quad \tilde{\mathbf{x}}_r = \begin{bmatrix} i \\ v_d \\ v_q \end{bmatrix} \tag{1.47}$$

1.3 Steady-State and Dynamic Analysis

In this section, steady-state and dynamic low frequency models are obtained from the reduced order, low frequency representation of the system. The system is linearized around the steady-state operating point to arrive at the small signal dynamic responses. The method used is similar to that used in the case of dc-dc converters[12].

1.3.1 Steady-State Analysis

The inputs in Eq. (1.46) take on *dc* values D'_e, Ω, $\tilde{\mathbf{U}}$, D under steady-state conditions. The resulting state vector $\tilde{\mathbf{X}}_r$, is also dc and is found by setting its derivative to zero in Eq. (1.46). Capital letters are used to represent steady-state quantities — dc, as well as sinusoidally time varying ones, which appear as dc in the *dq* reference frame. The steady-state solution is:

$$\tilde{\mathbf{X}}_r = -\mathbf{A}_o{}^{-1}\mathbf{B}_o\tilde{\mathbf{U}} \tag{1.48}$$

where

$$\begin{aligned} \mathbf{A}_o &= \mathbf{A}_r + D'_e\mathbf{A}_d + \Omega\mathbf{A}_\omega \\ \mathbf{B}_o &= \mathbf{B}_r + D\mathbf{B}_d \end{aligned} \tag{1.49}$$

The steady-state results of the buck-boost inverter are found from Eq. (1.47) setting d'_e, ω, $\tilde{\mathbf{u}}$, d and $\dot{\tilde{\mathbf{x}}}_r$ to D'_e, Ω, V_g, D and 0, respectively. The resulting inductor current and capacitor voltages are:

$$\begin{aligned} V_d &= \frac{V_g D}{D'_e}\left[1+\left(\frac{\Omega}{\omega_p}\right)^2\right]^{\frac{1}{2}}\cos(\phi_t-\phi_1) \\ V_q &= \frac{V_g D}{D'_e}\left[1+\left(\frac{\Omega}{\omega_p}\right)^2\right]^{\frac{1}{2}}\sin(\phi_t-\phi_1) \\ I &= \frac{V_g D}{RD'^2_e}\left[1+\left(\frac{\Omega}{\omega_p}\right)^2\right] \end{aligned} \tag{1.50}$$

where

$$\begin{aligned} \phi_1 &= \arctan\left(\frac{\Omega}{\omega_p}\right) \\ \omega_p &= \frac{1}{RC} \end{aligned} \tag{1.51}$$

and

$$D'_e = \sqrt{\frac{2}{3}}D'_m \tag{1.52}$$

for the modulation scheme chosen. The phase voltages and currents can be obtained by transforming $\tilde{\mathbf{X}}_r$ back to the stationary reference frame. In the stationary reference frame, the steady-state capacitor voltages are:

$$V_w = \frac{V_g D}{D'_m}\left[1+\left(\frac{\Omega}{\omega_p}\right)^2\right]^{\frac{1}{2}}\cos[\theta_m-\phi_1-(w-1)\frac{2\pi}{3}] \tag{1.53}$$

1.3.2 Dynamic Analysis

The dynamic analysis considered in this section is restricted to dynamics in the *small signal* sense only as the converter is in general nonlinear. Thus, it predicts

the response of the system to small perturbations around a quiescent operating point. The response to perturbations is studied in the dq reference frame as the equations representing the system have constant coefficients in this frame.

In the presence of perturbations, the system inputs and outputs are represented by:

$$\begin{aligned} \tilde{\mathbf{x}}_r &= \tilde{\mathbf{X}}_r + \hat{\tilde{\mathbf{x}}} \\ \tilde{\mathbf{u}} &= \tilde{\mathbf{U}} + \hat{\tilde{\mathbf{u}}} \\ d'_e &= D'_e + \hat{d'_e} \\ \omega &= \Omega + \hat{\omega} \\ d &= D + \hat{d} \end{aligned} \tag{1.54}$$

where the terms with carets represent the perturbation terms. The perturbation terms are substituted into Eq. (1.46) and the equations linearized to give the small signal model:

$$\mathbf{P}_r \dot{\hat{\tilde{\mathbf{x}}}}_r = \mathbf{A}_o \hat{\tilde{\mathbf{x}}}_r + \mathbf{B}_o \hat{\tilde{\mathbf{u}}} + \mathbf{A}_d \tilde{\mathbf{X}}_r \hat{d'_e} + \mathbf{A}_\omega \tilde{\mathbf{X}}_r \hat{\omega} + \mathbf{B}_d \tilde{\mathbf{U}} \hat{d} \tag{1.55}$$

The small signal transfer functions of interest, at the desired operating point, are found from Eq. (1.55). It is noted that the dynamics are dependent on the steady-state values of the variables.

For the buck-boost inverter of Eq. (1.47), the matrices in the small signal model are:

$$\mathbf{A}_o = \begin{bmatrix} 0 & -D'_e & 0 \\ D'_e & -1/R & \Omega C \\ 0 & -\Omega C & -1/R \end{bmatrix}, \quad \mathbf{B}_o = \begin{bmatrix} D \\ 0 \\ 0 \end{bmatrix}$$

$$\mathbf{A}_d \tilde{\mathbf{X}}_r = \begin{bmatrix} -V_d \\ I \\ 0 \end{bmatrix}, \quad \mathbf{A}_\omega \tilde{\mathbf{X}}_r = \begin{bmatrix} 0 \\ CV_q \\ -CV_d \end{bmatrix}, \quad \mathbf{B}_d \tilde{\mathbf{U}} = \begin{bmatrix} V_g \\ 0 \\ 0 \end{bmatrix} \tag{1.56}$$

where ϕ_t has been assumed to be zero for convenience, and the steady-state values V_d, V_q, and I are:

$$\begin{aligned} V_d &= \frac{D}{D'_e} V_g \\ V_q &= -\frac{\Omega}{\omega_p} \frac{D}{D'_e} V_g \\ I &= \left[1 + \left(\frac{\Omega}{\omega_p}\right)^2\right] \frac{D}{D'^2_e} \frac{V_g}{R} \end{aligned} \tag{1.57}$$

All the small signal transfer functions have the same denominator, $K(s)$, given by

$$K(s) = s^3 \left(\frac{RLC^2}{D'^2_e}\right) + s^2 \left(\frac{2LC}{D'^2_e}\right) + s \left(RC + \frac{L}{RD'^2_e} + \Omega^2 \frac{RLC^2}{D'^2_e}\right) + 1 \tag{1.58}$$

The denominator is of the third order and can be approximated by

$$K(s) \approx \left(1 + \frac{s}{\omega_p}\right) \left(1 + \frac{s}{\omega_o Q_o} + \frac{s^2}{\omega_o^2}\right) \tag{1.59}$$

where

$$\omega_p = \frac{1}{RC} \quad , \quad \omega_o = \frac{D'_e}{\sqrt{LC}} \quad , \quad Q_o = D'_e R \sqrt{\frac{C}{L}} \tag{1.60}$$

if the inequality

$$\frac{\Omega^2}{\omega_o^2} \ll 1 \tag{1.61}$$

is satisfied. The dc gains and zeros of some of the transfer functions are given in Table 1.1.

Function	DC Gain	Zeros
$\frac{\hat{v}_d}{\hat{d}'_e}$	$-\frac{D}{D'^2_e}V_g$	$\left(1+\frac{s}{\omega_p}\right)\left(1-\frac{s}{\omega_{z1}}\right)$
$\frac{\hat{v}_q}{\hat{d}'_e}$	$\frac{\Omega D}{\omega_p D'^2_e}V_g$	$\left(1-\frac{s}{\omega_{z1}}\right)$
$\frac{\hat{v}_d}{\hat{\omega}}$	$-\frac{2D\Omega V_g}{D'_e\omega_p\omega_o^2}$	$s\left(1+\frac{s}{\omega_{z2}}\right)$
$\frac{\hat{v}_q}{\hat{\omega}}$	$\frac{DV_g}{D'_e\omega_p}$	$\left(1+\frac{s}{\omega_o Q_q}+\frac{s^2}{\omega_o^2}\right)$
$\frac{\hat{v}_d}{\hat{d}}$	$\frac{D}{D'_e}$	$\left(1+\frac{s}{\omega_p}\right)$
$\frac{\hat{v}_q}{\hat{d}}$	$\frac{D\Omega}{D'_e\omega_p}$	1

where $\omega_p = \frac{1}{RC}$; $\omega_o = \frac{D'_e}{\sqrt{LC}}$; $\omega_{z1} = \frac{RD'^2_e}{L[1+(\Omega/\omega_p)^2]}$

$$\omega_{z2} = 2\omega_p \ ; \ Q_q = \frac{RD'^2_e}{\omega_o L[1-(\Omega/\omega_p)^2]}$$

Table 1.1: DC gains and zeros of some of the small signal transfer functions of the buck-boost inverter.

Chapter 2

Current Programmed Inverters and Rectifiers

A vast array of control methods can be used for the design of switching regulators. Current mode control has become widely accepted as a useful technique for improving the performance of dc-dc regulators. The popularity of current mode control stems from its inherent ability to provide protection in a switching converter. Current mode control can be implemented in many different ways. In all the methods, the switch duty ratio is determined by the instants at which the switch current reaches one or two threshold values. If two threshold values are used, it results in a variable switching frequency [13]. A single threshold value can be used, along with a reference clock, to obtain a fixed switching frequency [14]. The latter method is referred to as *current reference programming* and abbreviated as CRP.

Current reference programming of dc-dc converters is reviewed in Section 2.1.1. The basic principles, advantages, and disadvantages are discussed. Stability of dc-dc converters in current reference programmed mode is discussed in Section 2.1.2.

The above technique can also be used in inverters or rectifiers. There are different ways of programming the inductor current depending on the presence or absence of a switch on the dc side of the converter. In all cases, the aim is to control the switch or inductor current on a cycle-to-cycle basis, at the switching frequency. Application of current reference programming to inverters and rectifiers is discussed in Sections 2.2 and 2.3.

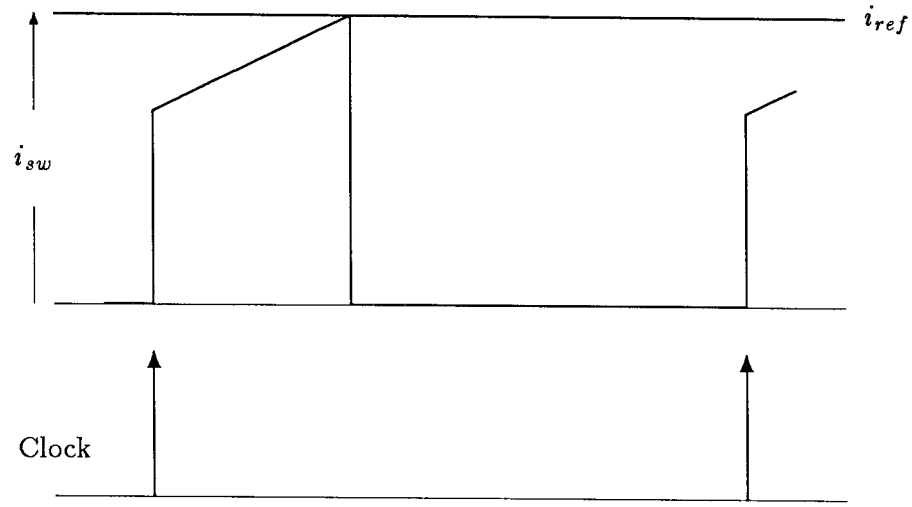

Figure 2.1: The current waveform of a constant-frequency current programmed switch shows how it is turned ON periodically and switches OFF when the current through it reaches a threshold level.

2.1 Current Reference Programmed DC-DC Converters

2.1.1 Principle of Operation

The technique of current reference programming is illustrated in Fig. 2.1. The switch is turned ON by a clock pulse at the beginning of each switching cycle. The switch is subsequently turned OFF when the current through it reaches a reference level. If the switch conducts the inductor current when it is ON, then it can be used to restrict the inductor current to a neighborhood of the reference current I_{ref}. The reference current, I_{ref}, can then be used as a control input instead of the duty ratio. Hence, the current programmed switch forms an inner loop around which the final outer loop of the regulator is designed.

The current reference programmed mode of operation has many advantages over the conventional duty ratio control scheme. If the maximum value of I_{ref} is limited, current programming automatically protects the switch from excessive current stresses. This also protects the dc-dc converter against deleterious effects owing to overloads and enables the parallel operation of several converters to support a common load, without load-sharing problems. Current programming constrains the inductor current and moves the pole caused by the inductor above the bandwidth of interest [15,16]. As a result, the effective order of the system is reduced by one and simplifies the design of the main regulation loop.

Constant-frequency current programmed dc-dc converters are subject to oscillations under certain operating conditions, even in the absence of regulator feedback. This potential instability, and techniques for its elimination, are discussed in the following section. These oscillations have been labelled as instability in the Lyapunov sense and refers to the stability of the desired steady-state limit cycle. When the current programmed converter is subject to sub-harmonic oscillations, it operates in an undesirable limit cycle, or in a chaotic mode.

2.1.2 Stability in Current Reference Programmed Mode

Current reference programming constitutes an inner feedback loop and the system can be unstable even without any regulatory external loop. Figure 2.2 depicts the steady-state current waveform, as well as the propagation of a disturbance from one switching cycle to the next. A disturbance Δ_1 at the beginning of the first switching cycle results in a disturbance Δ_2 at the beginning of the second, and so on. For stable operation, the disturbance should decay towards zero. Thus, the system will be stable if the Δ_i constitute an absolutely convergent sequence.

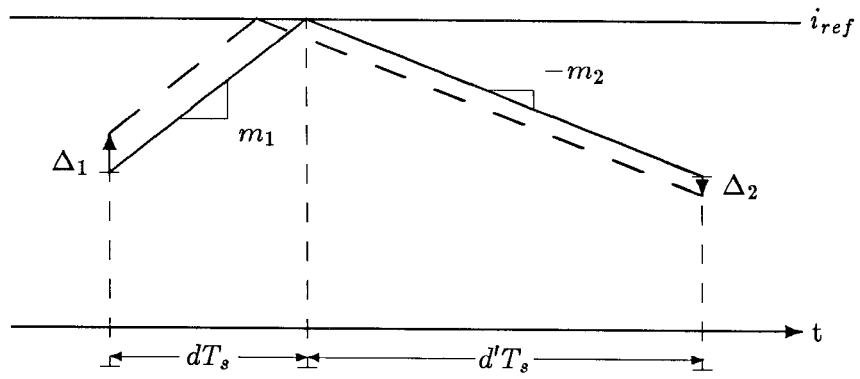

Figure 2.2: Propagation of a disturbance in the programmed current of a current reference programmed dc-dc converter. Instability exists for $D > 0.5$.

The stability of the current programmed mode can be obtained in many ways. Approaches that have been used include sampled data modelling, geometric approximations, and modelling of the current loop [15,16,17,18]. The simplest method is the geometric approach, which utilizes a linear approximation for the inductor current for each position of the switch. This linear approximation is adequate for most pulse width modulated switching converters as the time constants of the converter are large compared to the switching period. The resulting gain, k, for the disturbance is:

$$k = \frac{\Delta_2}{\Delta_1} = -\frac{m_2}{m_1} = -\frac{d}{d'} \tag{2.1}$$

If the magnitude of k is less than unity, the disturbance decays to zero and subharmonic oscillations are not sustained. Under steady-state conditions, the slopes m_1 and m_2 are constant (first order approximation) and the duty ratio of the current reference programmed switch does not vary. The current loop results in oscillations if the duty ratio exceeds 0.5.

The stable region of operation can be extended to duty ratios above 0.5 by

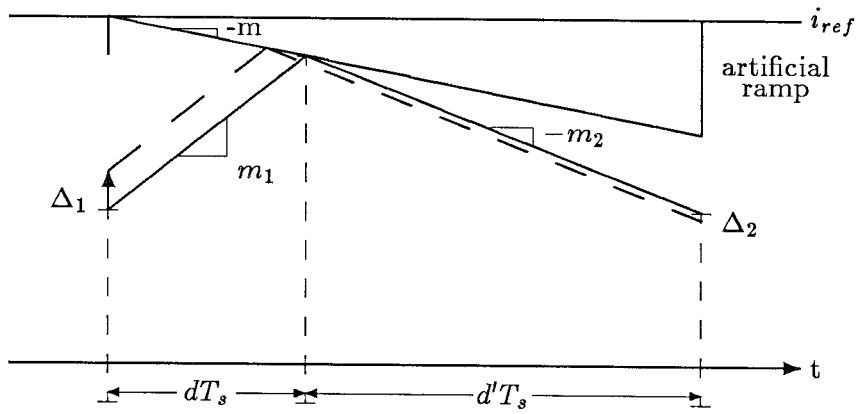

Figure 2.3: Propagation of a perturbation in the programmed current in the presence of an auxiliary ramp. A suitable ramp can be used to maintain stable operation for all D.

adding an auxiliary ramp to the current reference, as shown in Fig. 2.3. In the presence of a ramp of slope $-m$, the gain is:

$$k = -\frac{m_2 - m}{m_1 + m} = -\left(\frac{m_2}{m_1}\right)\left(\frac{1 - \frac{m}{m_2}}{1 + \frac{m}{m_1}}\right) \tag{2.2}$$

Hence, for a given value of m, $0 < m \leq m_2$, the region of stable operation will extend for duty ratios greater than 0.5. In particular, if the value of m is chosen equal to m_2, any perturbation in the programmed current is eliminated in one cycle. This optimum condition, however, is dependent on the operating point.

The problem of stability in current reference programmed mode does not exist in certain dc-dc converters, such as the ideal, three-switched network flyback converter [19]. In these converters, stability is ensured by the presence of an idling interval during which the programmed current has zero slope (ideal case). This is illustrated in the waveform of Fig. 2.4. Non-idealities, such as the magnetization current of the current

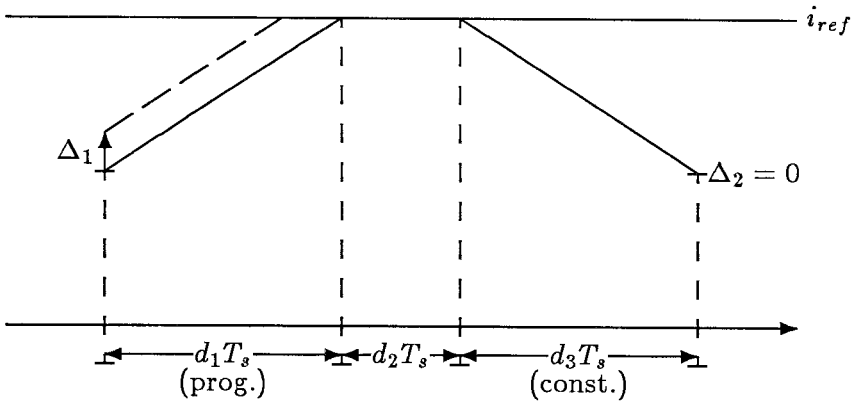

Figure 2.4: Inductor current of the ideal, three switched-network flyback dc-dc converter in current programmed mode. Perturbations in the programmed current are eliminated within one cycle.

transformer and voltage drops of the switches, can cause instability in practical implementations of these converters.

2.2 Application of Current Programming to Inverters

Current reference programming in dc-dc converters can be interpreted as a method of programming the energy processed by the converter. When the current programmed switch is ON, energy is stored in the reactive elements of the converter. The current programmed switch turns OFF when the programmed current, and hence stored energy, reaches a threshold level; consequently, the stored energy is released into the load. The quantity of power being processed is regulated in this manner.

The energy processing viewpoint is useful for the extension of current programming to inverters and rectifiers. In any balanced polyphase inverter, many switches are used to process power from the dc source to the load. Any single switch in the inverter may not be adequate for altering the operation of the inverter from energy storage to

energy release mode. If there is a switch on the dc side of the inverter and its duty ratio is not modulated during normal steady-state operation, then it may be used for current programming. The flyback and buck-boost inverters are examples of inverters in which such a switch exists. In other inverter topologies, current programming using a single switch current is not possible.

In many of the inverter topologies, there is no independent switch on the dc side of the converter. The boost inverter is an example of a topology in which there is no switch on the dc side of the converter: the average current in the inductor is dc under steady-state conditions. In other topologies, such as the buck inverter, there are six switches on the dc side and no single switch can be programmed separately without destroying the waveforms of the outputs. It is therefore necessary to program the inductor current itself using all the switches. In the buck inverter, the result is further complicated by the presence of three inductors carrying sinusoidally varying currents. The method used for current programming of inverters is largely dependent on the inverter and there is no universally applicable scheme.

Application of current programming results in lower harmonic distortion in the ac waveforms of an inverter. In a duty ratio programmed inverter, the regulatory loop does not affect the quality of the waveforms generated. In a practical inverter, the harmonics arise from nonidealities present such as voltage drops across switches, imbalances in the ac loads, and finite switching frequency. If the output voltages are distorted, the inductor current contains harmonics of the inversion frequency. The harmonics present in the inductor current again induce distortion in the outputs and this leads to a kind of positive feedback. Current programming constrains the inductor current and limits the harmonics of the inversion frequency in the inductor current, thereby breaking the positive feedback loop that tends to increase the distortion. It should be noted, however,

that the distortion in the output waveforms is low even in the duty ratio programmed, fast switching, sinusoidally pulse width modulated inverter.

Current programming helps to isolate source voltage variations from the output. It also essentially reduces the order of the system by one, as the inductor current is constrained, and so the dynamic behavior of the inverter is improved. Other advantages of current reference programming include protection of the inverter from fault conditions and possibility of parallel operation of many regulators.

2.2.1 Flyback and Buck-Boost Inverters

First consider those inverters which have an independent control on the input side, such as the flyback and buck-boost inverters. In both these inverters, there is a switch on the dc side of the converter, which conducts the inductor current when it is ON. The steady-state inductor current is dc in nature with a switching ripple and can be programmed using the input switch. This is possible because the duty ratio of the input switch is not sinusoidally modulated in the duty ratio programmed mode of operation. The switches on the ac side are operated independently of the input switch in the buck-boost inverter. In the flyback inverter, the duty ratio of the current programmed switch limits the maximum value that the amplitude of modulation d'_m can assume. Except for this constraint, the duty ratios of the output switches can be assigned independently of the input switch. In both cases, current reference programming of the input switch constrains the inductor current to remain in the neighborhood of the reference current and converts the dc input voltage into a dc current source, which feeds the ac outputs. The modulation of the switches on the ac side can be used to provide the regulation of the outputs.

The current reference programmed flyback inverter is stable for all operating conditions if the suggested mode of operation is used. In this case, the reference current

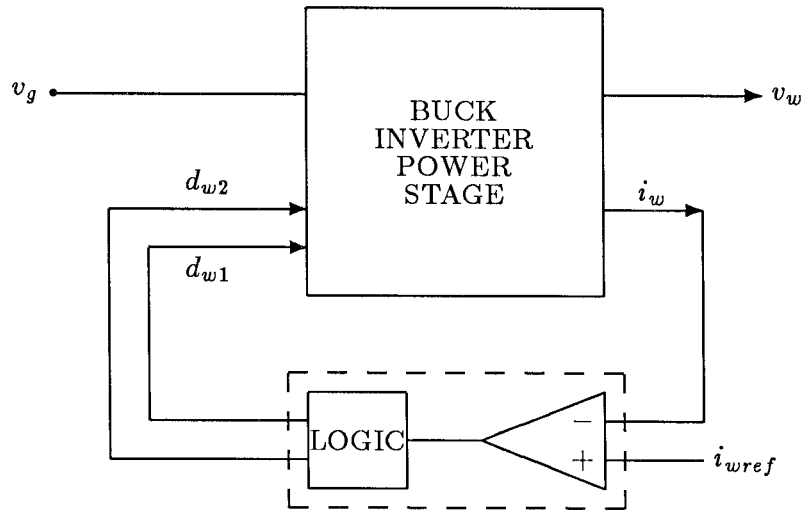

Figure 2.5: The fixed-frequency current programmed buck inverter.

can be kept fixed and the regulation achieved using the duty ratio modulation of the switches on the output side. Sub-harmonic oscillations occur in the current reference programmed buck-boost inverter for certain operating conditions. The buck-boost case can be considered to be similar to a current reference programmed buck dc-dc converter followed by a boost inverter, and is discussed in greater detail in the next chapter.

2.2.2 Buck Inverter

In the buck inverter, the magnitude and phase of the inductor currents are programmed using the six switches on the input side. Fixed-frequency current programming can be implemented by using the inductor current in each phase to control the double-throw switch of that phase, as shown in Fig. 2.5. The three reference currents are not independent, however, and must sum to zero. In steady state, the references cor-

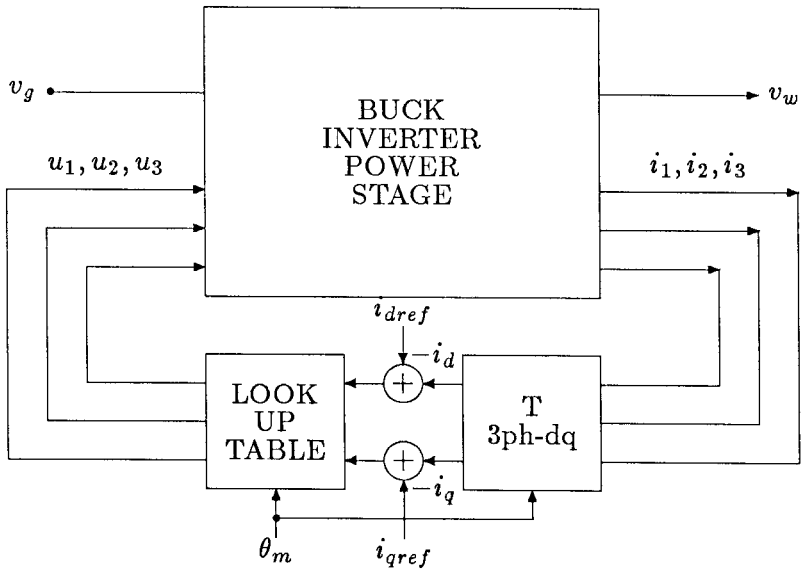

Figure 2.6: Current programmed buck inverter using the sliding mode method of control. This results in a variable switching frequency.

respond to a three phase sine wave set with the desired magnitude and phase. Though this method is simple to implement, it is not a very desirable strategy for two primary reasons. First, the three current loops are not independent and interact with other, and compensating ramps have to be used to prevent subharmonic oscillations. Second, the current references are large signal, time-varying quantities even in steady-state operation. This method is not general and cannot be adapted to the boost inverter.

The preferable alternative is to apply current programming using a variable switching frequency. This method programmes the components i_d and i_q of the inductor current and the control is in the dq reference frame. The controller constrains i_d and i_q to lie within an error band on either side of their respective reference values. Sliding mode control is used and the controller is implemented using a simple look-up table to

determine the control inputs from the current errors and the modulation angle. Figure 2.6 shows the block diagram of the current programmed buck inverter which uses the sliding mode method of control. The control u_w represents the position of the double-throw switch of phase w, and assumes values $+1$ and -1 when connected to the positive and negative terminals of the dc source, respectively. Sliding mode control of the buck inverter is examined in greater detail in Chapter 5.

2.2.3 Boost Inverter

The boost inverter can be current reference programmed using the inductor current in a manner similar to that used for the flyback inverter. At the beginning of each switching cycle, energy is stored in the inductor by connecting both triple-throw switches to the same phase of the output voltage. During this interval dT_s, the inductor is connected directly across the dc source and the current ramps up. When the inductor current crosses the reference threshold value, the sinusoidal pulse width modulation is applied to the output switches and energy is released to the load. The duty ratios are

$$d'_{1w} = \frac{d'}{3} + \frac{d'}{3}\cos[\theta_m - (w-1)\frac{2\pi}{3}] \tag{2.3}$$

$$d'_{2w} = \frac{d'}{3} - \frac{d'}{3}\cos[\theta_m - (w-1)\frac{2\pi}{3}] \tag{2.4}$$

where

$$d' = 1 - d \quad , \quad \text{and} \quad 1 \leq w \leq 3 \tag{2.5}$$

and θ_m is the instantaneous phase of the modulation. This is analogous to the modulation used in the flyback inverter with d'_m set equal to d'. Subharmonic oscillations can occur in the current reference programmed boost inverter and a stabilizing ramp should be used.

2.3 Application of Current Programming to Rectifiers

Rectifiers are current programmed using various methods, depending on the topology of the converter. A general rectifier converts the balanced polyphase input power into a rectified dc output using many switches. In some topologies, there is an independent switch on the dc output side that can change the operation of the rectifier from energy storage to energy release mode. Such a switch can be used for current programming if its duty ratio is not modulated during normal steady-state operation. Again, the flyback and buck-boost topologies include such a switch. In the other topologies, all the switches have to be used in conjunction with each other to program one or more inductor currents.

2.3.1 Buck-boost Rectifier

The buck-boost rectifier is the easiest to current program because of the presence of independent switches on the ac and dc sides of the converter. The switch on the dc side can be current programmed while the duty ratios of the switches on the ac side are sinusoidally pulse width modulated. This converter also suffers from subharmonic oscillations, under certain operating conditions, which are discussed in greater detail in the following chapter.

2.3.2 Buck and Flyback Rectifiers

In both these converters, the switches on the ac side have to be used to rectify the ac source voltages and store energy in the inductor and also to release the stored energy into the load. In the buck rectifier, energy is released from the inductor when both the upper and lower triple-throw switches are connected to the same phase of the source. In the flyback rectifier, the inductor releases its stored energy when the switch on the dc side is ON. In both cases, the source currents are pulsating in nature, and it

is difficult to program the inductor current while maintaining the sinusoidal nature of the average source currents. A sliding mode approach is necessary and a simple fixed-frequency approach is not possible. In both these rectifiers, current programming does not provide a significant advantage as it is difficult to implement.

2.3.3 Boost Rectifier

The boost rectifier comprises three inductors on the source side and it is possible to program the inductor currents using an approach similar to that of the current programmed buck inverter. The magnitude and phase of the input currents can be programmed using sliding mode control, or by directly using the inductor current in each phase to control the double-throw switch of that phase.

Chapter 3

Dc-Three Phase, Current Reference Programmed Buck-Boost Converter

The dc-three phase, current reference programmed buck-boost converter is examined in this chapter. Section 3.1 reviews the topology and operation of the dc-three phase buck-boost converter and the motivation for using this topology. The modulation scheme and method of current programming are described and some of the advantages and disadvantages of this method of control discussed.

Section 3.2 considers the converter in the inverter mode of operation. The system is described in the inverter mode of operation and the steady-state response obtained. The stability of the current reference programmed loop is examined and conditions for stability found. The dynamic responses of the current reference programmed inverter are obtained in the dq reference frame. The theoretical predictions are compared with experimental measurements of the steady-state and dynamic responses. Measurements of the harmonic contents of the outputs are also presented.

The rectifier mode of operation is studied in Section 3.3 and the steady-state and dynamic responses found. Section 3.4 explores control strategies for the operation of the current programmed converter in the bidirectional mode. Methods to determine and control the direction of power flow are described.

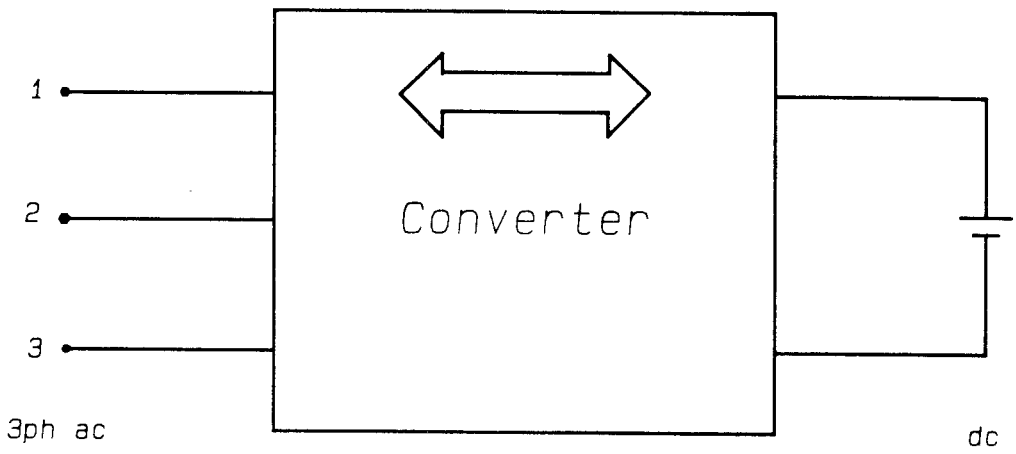

Figure 3.1: Three-phase ac-dc battery charger/UPS.

3.1 Dc-Three Phase Buck-Boost Converter

This section describes the topology and operation of the dc-three phase buck-boost converter. The motivations for deriving the topology and method of control are recounted. The six-segmented, sinusoidal pulse width modulation scheme used is detailed and compared with the continuous sinusoidal modulation scheme. Current programming of the converter in the inverter and rectifier modes of operation is considered.

3.1.1 Motivation

The choice of converter topology and the use of current programming was made with two important applications in mind: dc-three phase uninterruptable power supply (UPS), Fig. 3.1, and variable frequency ac motor drive, Fig. 3.2. Both of these applications require bidirectional power flow. In normal operation, the UPS charges the

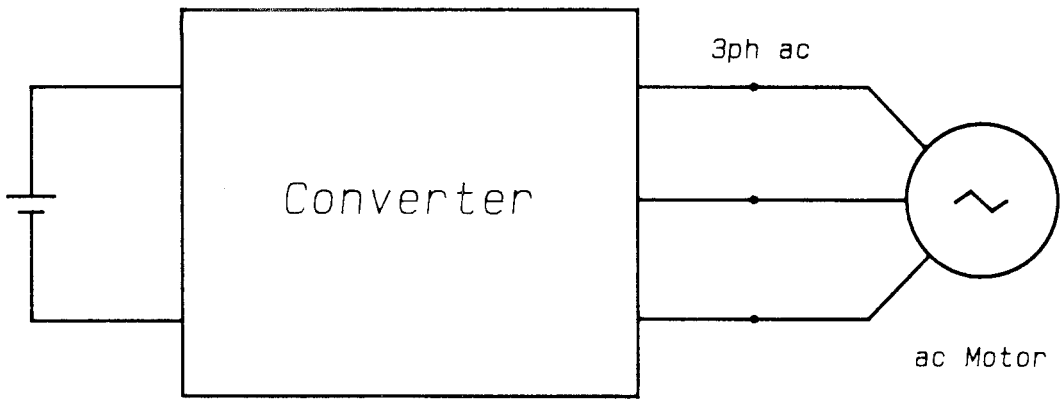

Figure 3.2: Variable frequency, variable voltage ac motor drive.

battery and power flows from the ac side to the dc battery. When the mains is absent, the dc battery supports the ac load and power flows from the dc battery to the ac side. In a variable frequency ac motor drive, the motor constitutes a regenerative load and power flows back to the dc battery when the motor is braking.

The buck-boost topology is used as bidirectional power flow is achieved with the use of eight current unidirectional active switches, as shown in Fig 3.3. The modification of the dc side of the buck-boost inverter into a bridge configuration enables bidirectional power flow *without* the use of *four-quadrant* switches. The UPS application also confronts the converter with stiff voltage sources at both ends of the converter. Current reference programming is chosen as a simple method for maintaining volt-second balance on the inductor in the presence of two stiff voltage sources.

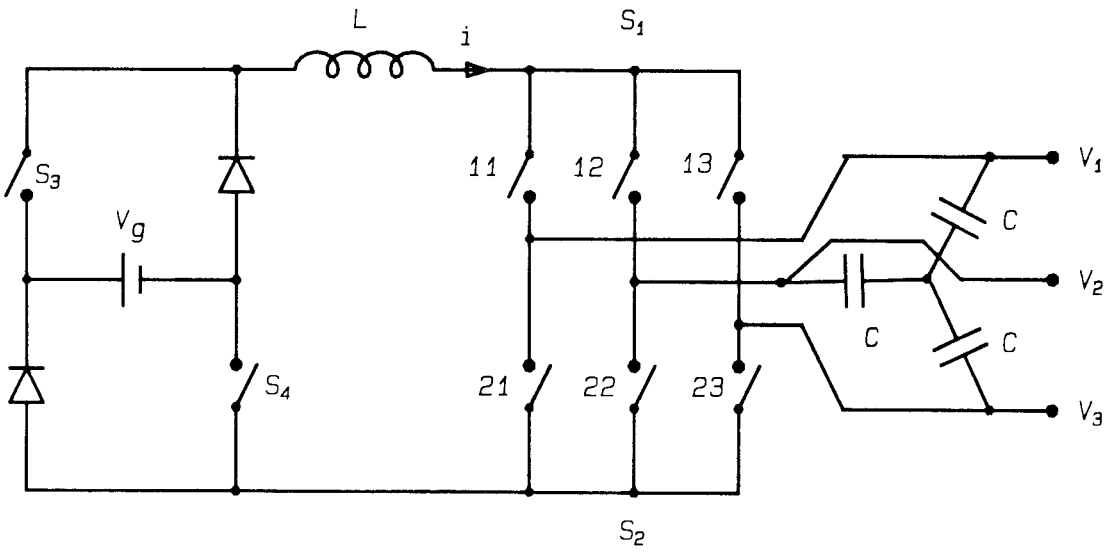

Figure 3.3: The dc-three phase buck-boost inverter modified to allow bidirectional power flow.

3.1.2 Converter Topology

The converter topology of Fig. 3.3 is derived from the buck-boost rectifier, Fig. 3.4 (buck rectifier followed by a boost dc-dc converter), and buck-boost inverter, Fig. 3.5 (buck dc-dc converter followed by a boost inverter). From the converters of Figs. 3.4 and 3.5, it is observed that bidirectional power flow can be accomplished by changing the polarity of the voltage on the dc side *without changing the direction* of the current in the switches on the ac side of the converter. Hence, a bridge configuration is used on the dc side of the converter as shown in Fig. 3.3.

All the switches in the converters shown are current unidirectional, voltage bidirectional, two-quadrant switches and can be implemented using a MOSFET in series with a diode. It is also noted that the direction of current in the inductor and switches is

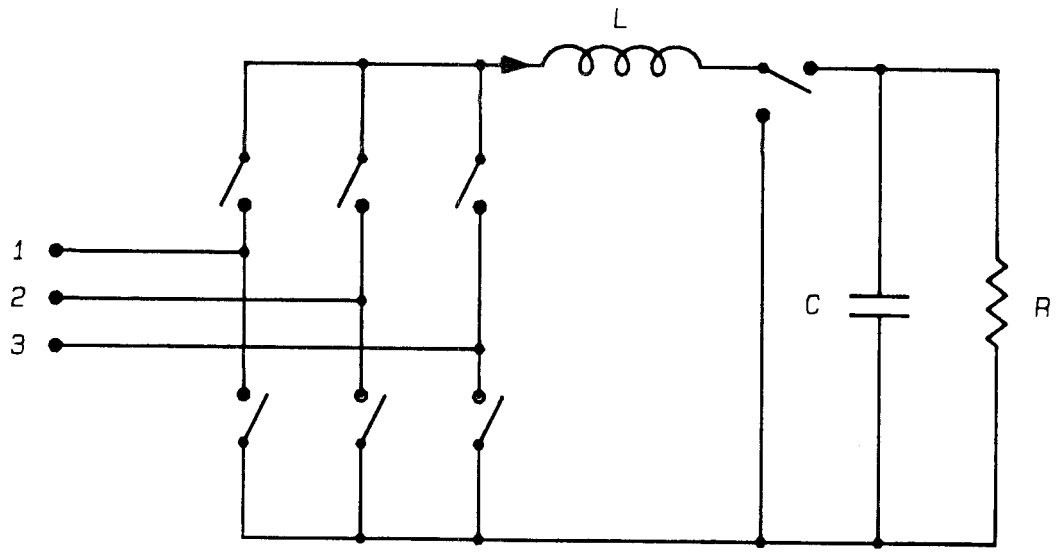

Figure 3.4: The three-phase buck-boost rectifier which is a cascade connection of a buck converter and a boost dc-dc converter.

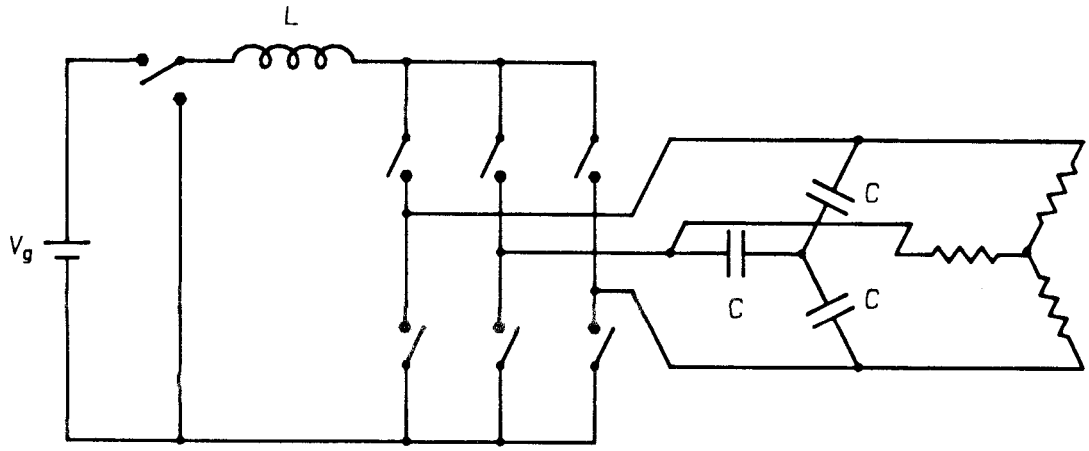

Figure 3.5: The dc-three phase buck-boost inverter, which can be interpreted as a buck dc-dc converter followed by a boost inverter.

the same regardless of the direction of power flow. For operation in the inversion mode, switch S_4 in Fig. 3.3 is maintained ON and switch S_3 is pulse width modulated. Switch S_3 is kept OFF and switch S_4 is pulse width modulated for operation in the rectifier mode. In both modes, the direction of the inductor current is the same and is as shown. If the converter is required to change the direction of power flow within one switching cycle, then both S_3 and S_4 can be pulse width modulated. This bidirectional mode of operation will result in higher losses in the converter, but is a price that has to be paid for the desired response. The switches on the ac side are modulated sinusoidally in all modes of operation and are not affected by the direction of power transfer.

3.1.3 Modulation Scheme

Any fast-switching pwm inverter or rectifier uses fast switching along with sinusoidal modulation to obtain effective duty ratios and ac waveforms that are sinusoidal in nature. Some modulation schemes achieve this by superposing a sinusoidal modulation over a dc level, as illustrated in Fig. 3.6. In Fig. 3.6, the x-axis employs the slow ac time scale to encompass all switching cycles within one modulation time period, while the switching instants and duty ratios are depicted along the y-axis using the fast-switching time scale. The numbers in the different regions represent the positions of switches S_1 and S_2 at those instants. However, this type of continuous modulation scheme results in many idling intervals during which no power is transferred to the load. The total idling time is proportional to the total area of the regions in which both switches are connected to the same phase (regions numbered 11, 22, and 33 in Fig. 3.6). Thus, if the average current in the inductor is I, the peak current on the ac side can only be $(2/3)I$. In comparison, a six-stepped current source inverter can provide a peak ac current of approximately $(1.1)I$.

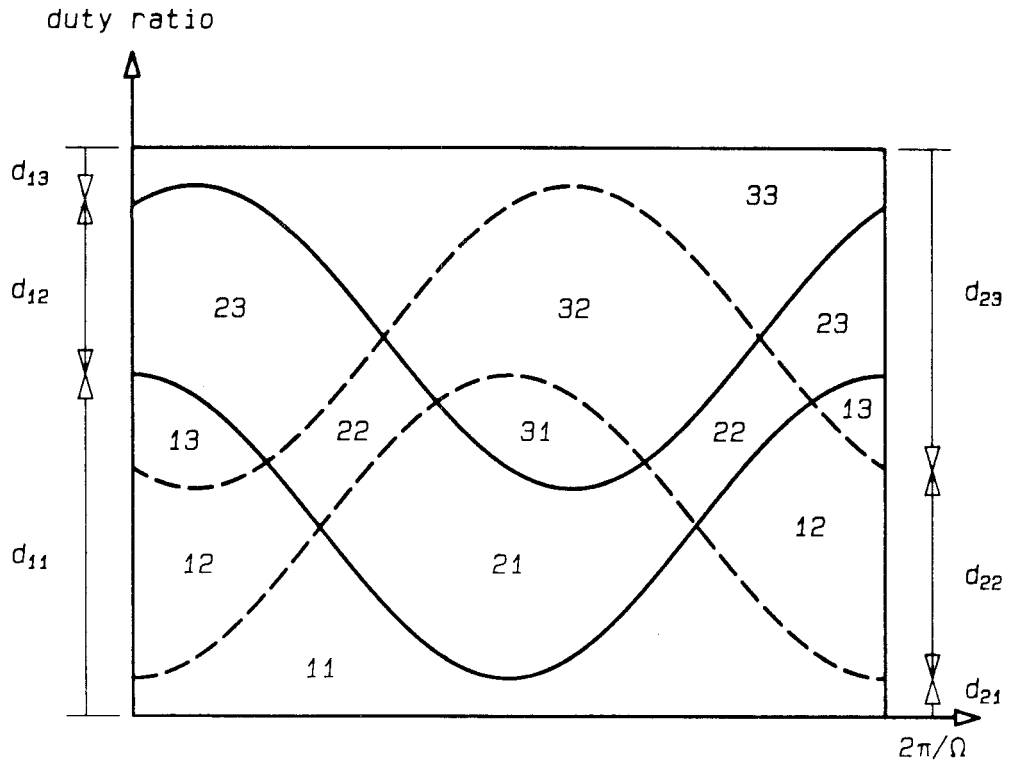

Figure 3.6: Illustration of the continuous, sinusoidal pwm scheme for the buck-boost dc-three phase converter. The x-axis uses the slow ac time scale and the y-axis the faster, switching time scale. The continuous line is the modulation of switch S_1, and the dashed line that of switch S_2. The numbers in the various regions represent the positions of the switches S_1 and S_2 at those instants.

A combination of the two modulation schemes is used to arrive at a more efficient pwm modulation in which the idling intervals are minimized. This hybrid scheme is referred to as the six-segmented sinusoidal pwm and is illustrated in Fig. 3.7. In this scheme, one of the switches S_1, S_2, remains in a fixed position for a sixth of the ac cycle, while the other is modulated. A peak ac current I can be obtained using this modulation scheme. Hence, it compares well with the six-stepped inverter in terms of device utilization and provides sinusoidal waveforns with low distortion.

The six-segmented sinusoidal pwm scheme results in better utilization of devices and higher efficiency than the continuous modulation scheme. The low frequency harmonic content of the ac waveforms is small because of fast switching and choice of

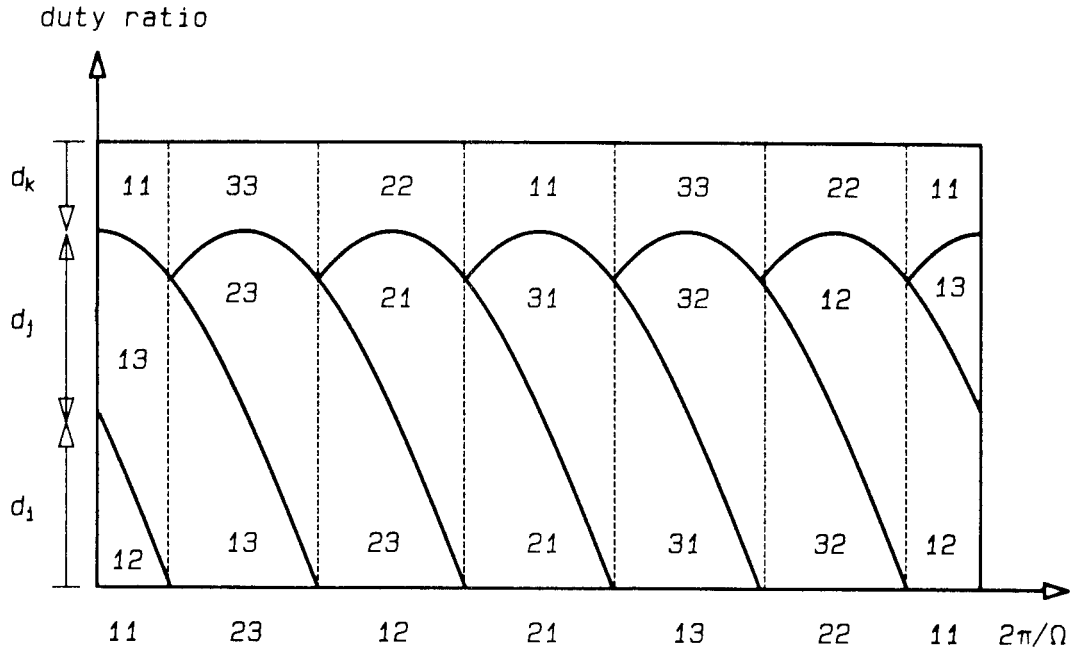

Figure 3.7: The six-segmented sinusoidal pwm scheme used for the buck-boost converter. The x-axis uses the slow ac time scale and the y-axis the fast-switching time scale. The numbers below the x-axis refer to the switch position that is ON during the corresponding sixth of the modulation cycle.

modulation. The disadvantage of this scheme lies in the necessity to keep active switches ON or OFF for long periods of time, depending on the ac time period. This can be overcome by using mosfet switches and the pulsed ON/OFF isolated drive scheme of Fig. 3.8. The switch is kept ON or OFF for extended periods of time by sending a stream of ON or OFF pulses for the required duration. The gate drive circuit of Fig 3.8 results in a very small drive transformer and can provide fast turn-ON or turn-OFF.

3.1.4 Current Programming

The technique of current reference programming can be applied to the switch that is not sinusoidally modulated and lies on the dc side of the converter. In the

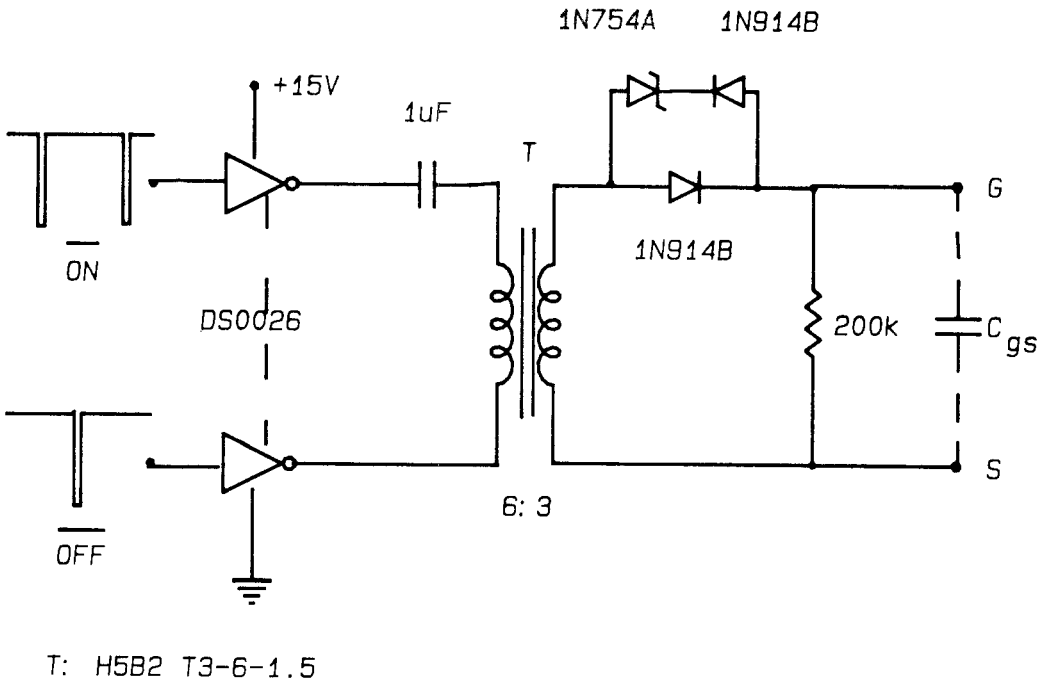

Figure 3.8: The pulsed ON/OFF gate drive used to drive the mosfet switches. The capacitance C_{gs} shown is the gate-source capacitance of the mosfet. The drive isolation transformer is wound on a very small toroidal ferrite core.

inversion mode of operation, switch S_3 is current reference programmed and consequently programs the inductor current. Switch S_4 is programmed in the rectifier mode. In the bidirectional mode of operation, the inductor current is programmed directly using switches S_3 and S_4. The phenomenon of subharmonic oscillations is present, under certain operating conditions, when the converter is operated in the current reference programmed mode. The stability of the converter in current reference programmed mode is discussed further in Section 3.2. Variable frequency current programming can also be used to program the inductor current.

The application of current reference programming results in lower harmonic distortion in the ac waveforms of the converter. It also essentially reduces the effective order of the system by one and improves the response of the converter. It also helps

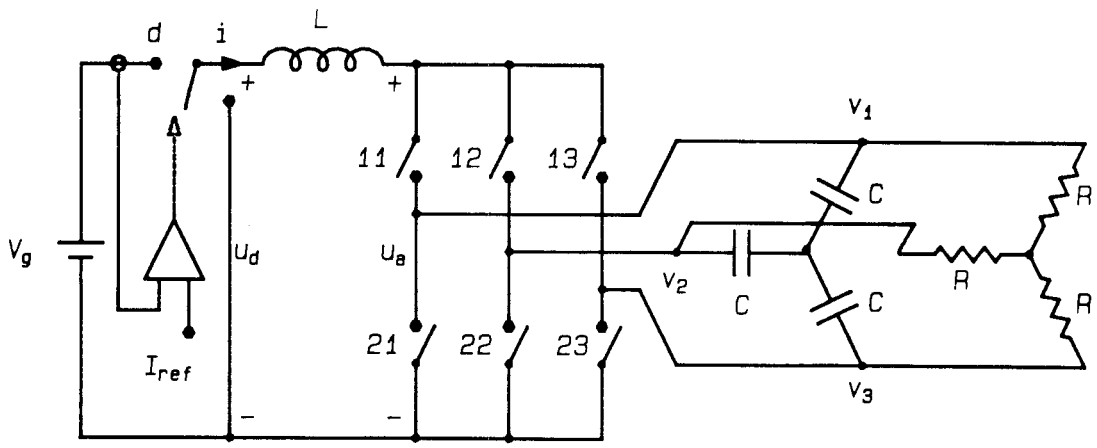

Figure 3.9: The current reference programmed dc-three phase buck-boost converter in the inversion mode of operation.

isolate source voltage variations from the output and provides inherent protection to the converter.

3.2 Inversion Mode of Operation

The converter is presumed to be in the inversion mode of operation and the load on the ac side is assumed to be a balanced, three phase load. The steady-state and dynamic behavior of the system depends on the dynamics of the converter and load, which is considered to be resistive in order to highlight the features of the converter. The system analyzed is shown in Fig. 3.9. The converter is considered to be ideal with perfect switches, sufficiently high switching frequency, etc. The converter is also assumed to satisfy the conditions required for the low frequency modelling of converters, as described

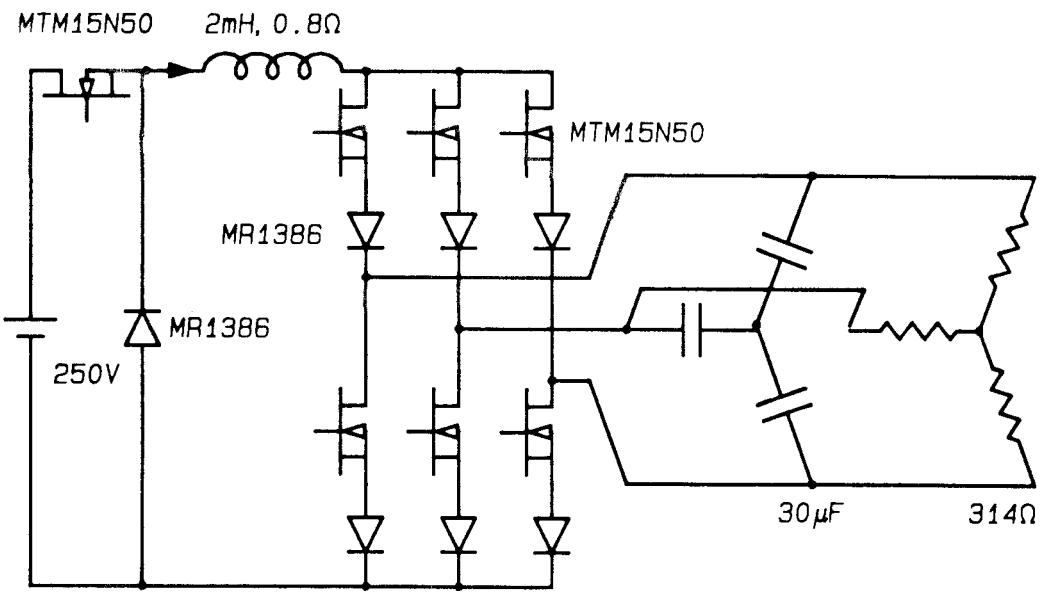

Figure 3.10: Circuit of the dc-three phase buck-boost inverter used for the experimental verification of predicted responses.

in Chapter 1.

3.2.1 Steady-State Analysis

The state space representation of the duty ratio programmed buck-boost inverter is derived in Section 1.2 of Chapter 1. The same description of the system holds for the converter of Fig. 3.9, when operated without current programming, with a few minor differences. The notation used to represent the duty ratios of the switches on the ac side of the converter is d_{1w} and d_{2w} instead of d'_{1w} and d'_{2w} used in Section 1.2. This is done as the converter considered is a bidirectional one and either side may be the load. The effective modulation amplitude provided by the six-segmented modulation scheme is D_m as opposed to $2D_m/3$ for the continuous sinusoidal modulation.

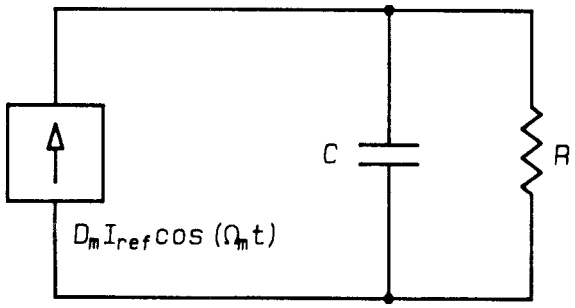

Figure 3.11: Equivalent circuit representing the steady-state behavior of the current reference programmed inverter (shown for phase 1).

The converter is presumed to operate properly in the current reference programmed mode; that is, V_g is large enough to enable the inductor current to reach I_{ref} and subharmonic oscillations do not occur. If the inductor current ripple is small compared to i_{ref}, then the average inductor current i can be approximated by i_{ref} itself. If the ripple is not small, it is necessary to find i as a function of i_{ref}. The current reference programming loop effectively moves the natural mode arising from the inductor higher in frequency, outside the bandwidth of interest. In a simplified form, the system can be represented in the *stationary* abc reference frame by the averaged description:

$$C\,\dot{v}_w = -\frac{1}{R}\left(v_w - \frac{1}{3}\sum_{z=1}^{3} v_z\right) + d_w\, i \quad ; \quad 1 \le w \le 3 \tag{3.1}$$

where

$$\begin{aligned} & i \approx i_{ref} \\ & d_w = d_m \cos[\theta_m - (w-1)\tfrac{2\pi}{3}] \quad ; \quad 1 \le w \le 3 \\ & d_m < 1 \quad , \quad \theta_m = \int_0^t \omega(\tau)\, d\tau + \phi_m \end{aligned} \tag{3.2}$$

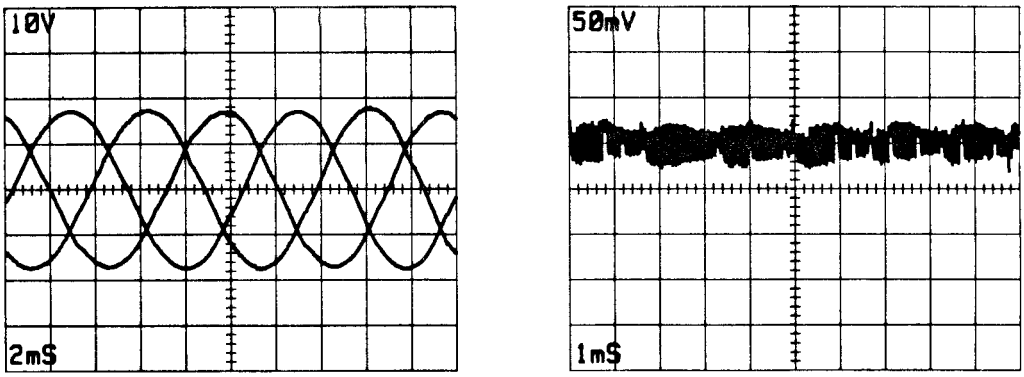

Figure 3.12: Steady-state output voltages (a) and inductor current (b) waveforms of the current reference programmed buck-boost inverter.

The steady-state solution of Eq. (3.1) is

$$V_w = V_m \cos[\theta_m + \phi - (w-1)\frac{2\pi}{3}] \quad , \quad 1 \leq w \leq 3 \tag{3.3}$$

where

$$\begin{aligned} V_m &= D_m R I \cos(\phi) \approx D_m R I_{ref} \cos(\phi) \\ \phi &= -\arctan(\Omega RC) \end{aligned} \tag{3.4}$$

in which capitals are used to represent steady-state quantities. The steady-state response of the converter can be modelled by the equivalent circuit of Fig. 3.11. The steady-state waveforms obtained from the experimental circuit of Fig. 3.10 are shown in the oscillograms of Fig. 3.12. The measured steady-state responses of the converter are plotted in Figs. 3.13 and 3.14. Figure 3.13 shows the magnitude of output voltage V_m as function of the modulation amplitude D_m, for different values of inversion frequency.

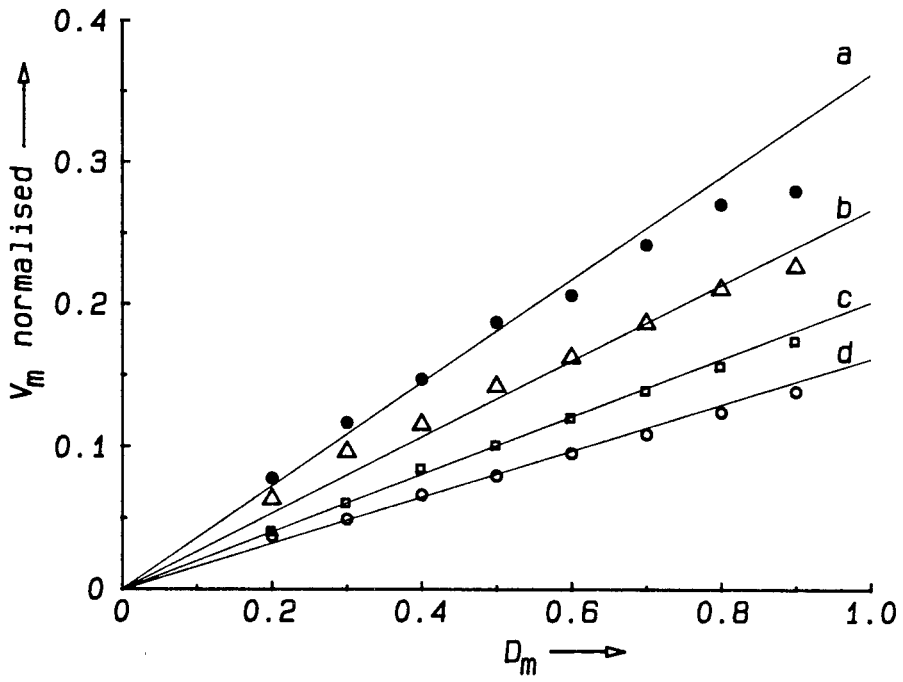

Figure 3.13: The predicted and measured steady-state response of the current reference programmed inverter for different values of inversion frequency: (a) 43 Hz, (b) 61 Hz, (c) 82 Hz, (d) 103 Hz. The values of the output voltage are normalized with respect to the zero frequency output voltage when D_m is equal to unity.

Figure 3.14 depicts the curves of V_m as a function of the inversion frequency Ω, with D_m as a parameter.

The distortion in the output voltages is lower when the converter is operated in the current reference programmed mode. In normal operation, any distortion in the output voltages results in harmonics in the inductor current, which in turn increases the distortion in the outputs. Current reference programming reduces the harmonics of the ac frequency present in the inductor current and results in low distortion of the outputs. The measured spectral content of the outputs is shown in Fig. 3.15. The plot of Fig. 3.15(a) is the low frequency spectral content, and Fig. 3.15(b) is the high frequency spectral content. The measured distortion in the output voltages was found to be less

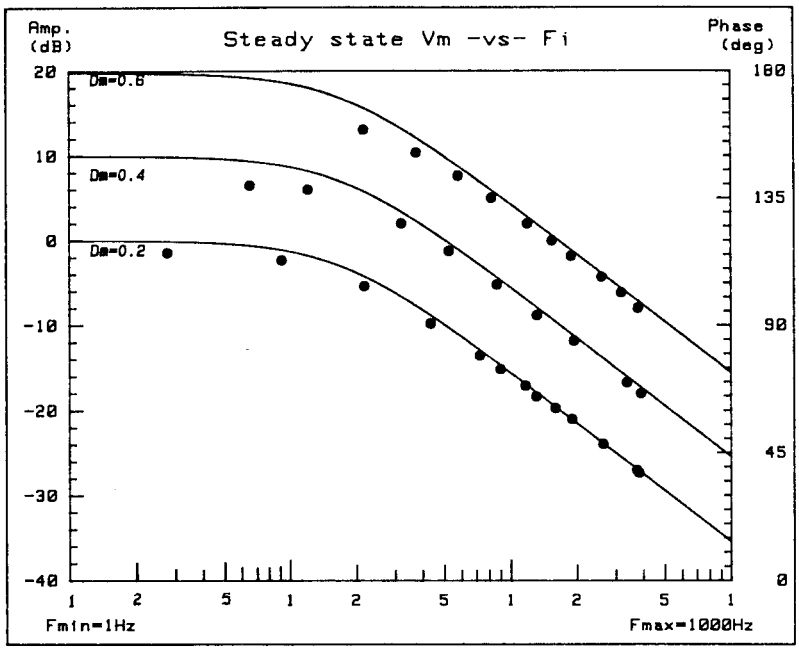

Figure 3.14: The predicted and experimental steady-state response of V_m as a function of F_i for various D_m. The y-axis is the output voltage normalized with respect to the zero frequency value at the corresponding D_m. The responses for $D_m = 0.4$ and $D_m = 0.6$ have been offset by 10db and 20db, respectively, for clarity.

than 5% THD, and harmonics of the inversion frequency were at least 50 dB lower than the fundamental.

3.2.2 Stability in Current Reference Programmed Mode

Subharmonic oscillations occur in the current reference programmed inverter in a manner similar to that observed in dc-dc converters. A close examination of the inductor current of the converter in current reference programmed mode, Fig. 3.16, reveals that the peak-to-peak ripple *varies* at six times the inversion frequency. The peak inductor current can be *higher* than I_{ref} for certain operating conditions and loads. Proper operation of the current reference programmed mode ensures that the duty ratio of the programmed

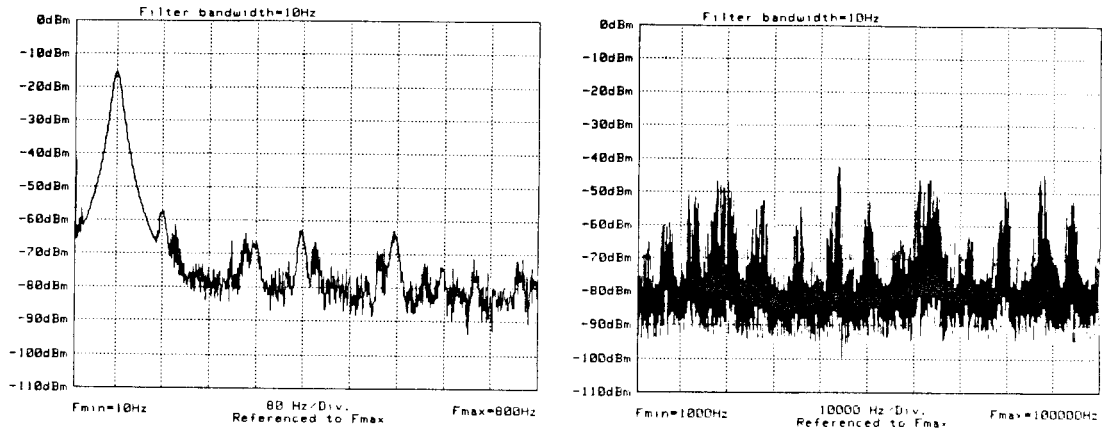

Figure 3.15: The low frequency (a) and high frequency (b) spectral content of the output voltages.

switch, at any instant of the inversion cycle, does not vary from one cycle to the next. The duty ratio of the programmed switch may vary by a small amount over the inversion time period (owing to second order effects and nonidealities), but does not vary by a noticeable extent over adjacent switching cycles. In the above discussion, it is assumed that the inversion frequency is well below the switching frequency.

The voltages $u_d(t)$ and $u_a(t)$ applied to the dc and ac ends of the inductor, respectively, result in the current waveform of Fig. 3.17. It is sufficient to examine the inductor current over a sixth of the inversion period owing to the six-fold symmetry present in the voltage applied to the inductor. It is noted that the voltage $u_a(t)$ can be less than zero during particular intervals of certain switching cycles depending on the value of the phase angle ϕ. If I_{ref} is required to be the peak value of the inductor

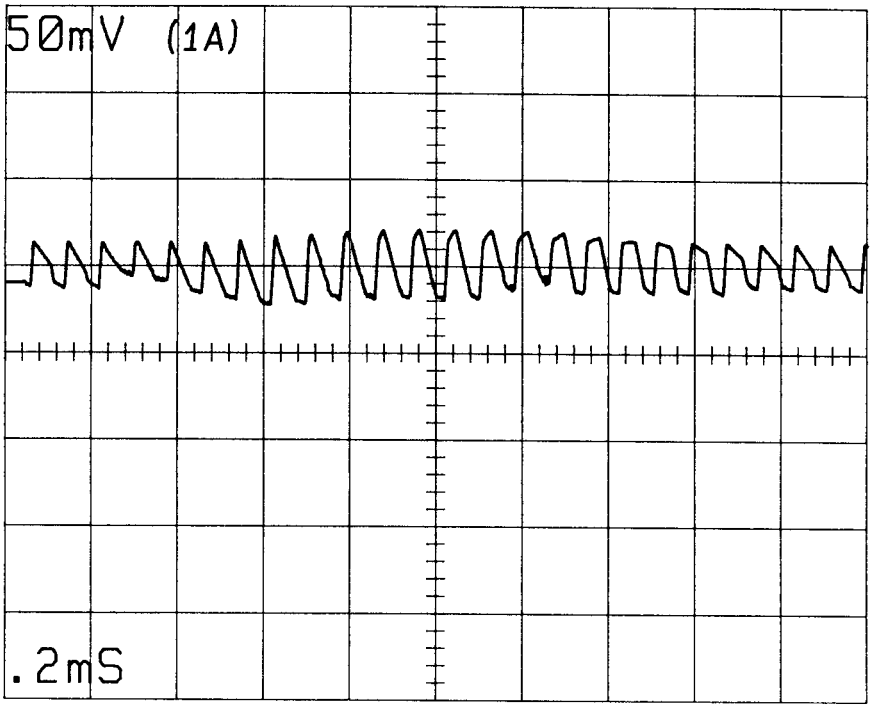

Figure 3.16: A closer view of the inductor current of the current reference programmed inverter to show the variation in peak-to-peak ripple with the modulation.

current, it is necessary to restrict $u_a(t)$ to be positive during $d'T_s$. It is noted, however, that the average value of $u_a(t)$, over any switching cycle, is positive and equal to DV_g. The inductor current ramps up towards I_{ref} only if the dc source V_g is greater than $u_a(t)$ during dT_s. Two possible cases can occur: d_{12} larger than d, and d_{12} smaller than d. Figure 3.18 examines the two cases mentioned.

The geometric method, utilizing knowledge of steady-state waveforms of the converter, is used to find the conditions for stability in the current reference programmed mode. The geometric method described in Chapter 2 is used as it provides the same information as the more rigorous discrete modelling technique but is easier to apply because of the foreknowledge of the waveforms of the converter. The gain of the current loop is found from Fig. 3.18 under the assumption that the inversion frequency is much

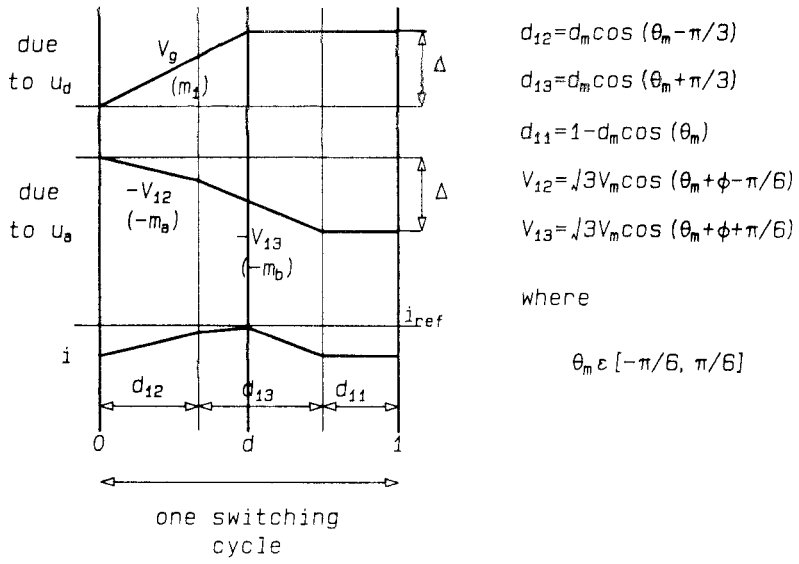

Figure 3.17: A detailed look at the effect of the voltages impressed at the two ends of the inductor to obtain the resultant current ripple.

lower than the switching frequency. This enables the ac voltages to be approximated as quasi-dc voltages for the purpose of stability analysis of the current loop. Thus, the gain k should be less than unity, over the inversion period, to ensure stable operation of the current reference programmed loop. The maximum values of k for various load angles, ϕ, are tabulated in Table 3.1.

A compensating ramp can be used to extend the region of stable operation in current reference programmed mode. If the converter is reconfigured as a flyback topology, which has the same low frequency behavior, the current reference programmed mode is stable for all operating conditions because of the presence of an independent idling interval.

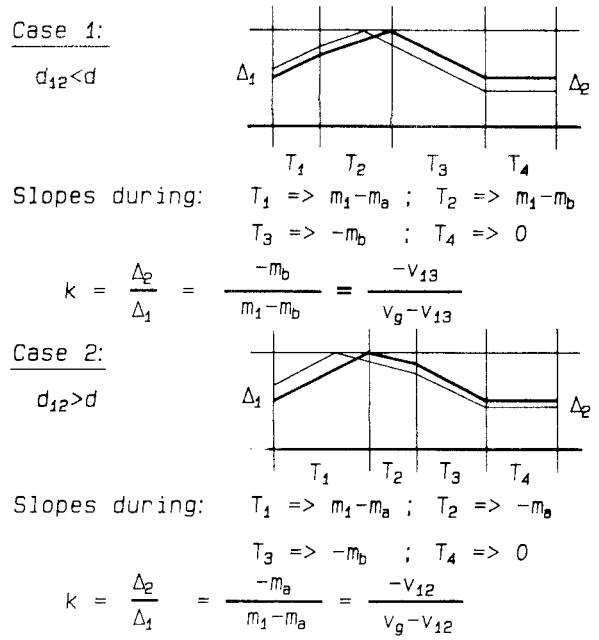

Figure 3.18: Propagation of a disturbance in the inductor current of a current reference programmed inverter. Stability in the current reference programmed mode depends on the values of k for the two cases: $d_{12} < d$ (a) and $d_{12} > d$ (b).

3.2.3 Dynamic Analysis

If the inductor current ripple is small and i is approximated by i_{ref}, the system is described by

$$C\,\dot{v}_w = -\frac{1}{R}(v_w - \frac{1}{3}\sum_{z=1}^{3} v_z) + d_w\, i_{ref} \quad , \quad 1 \leq w \leq 3 \tag{3.5}$$

where the effective duty ratios d_w are given by Eq. (3.2) and are time-varying. The time-varying coefficients in Eq. (3.5) are sinusoidal in nature and the system of equations can be transformed to the rotating dq reference frame in which the equations are time invariant. The system representation in the dq reference frame is obtained using the transformation described in Chapter 1.

LoadAngle ϕ	$\lvert k\rvert_{max}$
$\lvert\phi\rvert < \frac{\pi}{3}$	$\dfrac{1}{\frac{\sqrt{3}D_m}{2D}\cos\phi - 1}$
$\lvert\phi\rvert > \frac{\pi}{3}$	$\max\left\{ \dfrac{1}{\frac{\sqrt{3}D_m}{2D} - 1} \; , \; \dfrac{\cos(\pi/3 - \lvert\phi\rvert)}{\frac{\sqrt{3}D_m}{2D}\cos\phi - \cos(\pi/3 - \lvert\phi\rvert)} \right\}$

Table 3.1: Maximum magnitudes of k for various load angles in the current reference programmed inverter. The magnitude of k should be less than unity for stability.

In the dq reference frame, the system of Eq. (3.5) becomes

$$\tilde{\mathbf{P}}\,\dot{\tilde{\mathbf{x}}} = \tilde{\mathbf{A}}\,\tilde{\mathbf{x}} + \tilde{\mathbf{B}}\,\tilde{\mathbf{u}} \tag{3.6}$$

where

$$\tilde{\mathbf{P}} = \begin{bmatrix} C & 0 & 0 \\ 0 & C & 0 \\ 0 & 0 & C \end{bmatrix} \;,\; \tilde{\mathbf{A}} = \begin{bmatrix} -1/R & \omega C & 0 \\ -\omega C & -1/R & 0 \\ 0 & 0 & 0 \end{bmatrix}$$
$$\tilde{\mathbf{B}} = \begin{bmatrix} d_e \\ 0 \\ 0 \end{bmatrix} \;,\; \tilde{\mathbf{x}} = \begin{bmatrix} v_d \\ v_q \\ v_o \end{bmatrix} \;,\; \tilde{\mathbf{u}} = i_{ref} \;,\; d_e = \sqrt{\tfrac{3}{2}}\, d_m \tag{3.7}$$

and the phase ϕ_t of the transformation is chosen to be zero. In Eq. (3.6) it is noted that the component v_o, which represents the dc offset of the ac voltages, does not change and in practice will be zero. The component v_o is a trivial state and is dropped to give the

reduced order system

$$\mathbf{P}_r \dot{\tilde{\mathbf{x}}}_r = (\mathbf{A}_r + \mathbf{A}_\omega \omega)\tilde{\mathbf{x}}_r + \mathbf{B}_d d_e \tilde{\mathbf{u}} \tag{3.8}$$

in which the control parameters have been brought outside the matrices in order to show their effects on the operation of the converter. The system matrices are

$$\begin{aligned} \mathbf{P}_r &= \begin{bmatrix} C & 0 \\ 0 & C \end{bmatrix}, \quad \mathbf{A}_r = \begin{bmatrix} -1/R & 0 \\ 0 & -1/R \end{bmatrix} \\ \mathbf{A}_\omega &= \begin{bmatrix} 0 & C \\ -C & 0 \end{bmatrix}, \quad \mathbf{B}_d = \begin{bmatrix} 1 \\ 0 \end{bmatrix}, \quad \tilde{\mathbf{x}}_r = \begin{bmatrix} v_d \\ v_q \end{bmatrix} \end{aligned} \tag{3.9}$$

In steady state, i_{ref}, ω, d_m assume dc values I_{ref}, Ω, D_m, respectively, and the states in Eq. (3.8) are dc quantities. The steady-state and small signal linearized models are obtained from Eq. (3.8).

The steady-state solution is

$$\begin{aligned} V_d &= \frac{D_e R I_{ref}}{1 + (\Omega/\omega_p)^2} \\ V_q &= -\frac{D_e R I_{ref}(\Omega/\omega_p)}{1 + (\Omega/\omega_p)^2} \end{aligned} \tag{3.10}$$

where

$$\omega_p = \frac{1}{RC} \tag{3.11}$$

Standard notation, in which upper-case letters represent steady-state quantities and lower-case letters with carets indicate small signal perturbations, is used to describe the dynamic performance of the system. The quantities of interest are

$$\begin{aligned} \tilde{\mathbf{x}}_r &= \tilde{\mathbf{X}}_r + \hat{\tilde{\mathbf{x}}}_r \quad , \quad \omega = \Omega + \hat{\omega} \\ d_e &= D_e + \hat{d}_e \quad , \quad i_{ref} = I_{ref} + \hat{i}_{ref} \end{aligned} \tag{3.12}$$

The small signal linearized model is

$$\mathbf{P}_r \dot{\hat{\tilde{\mathbf{x}}}}_r = \mathbf{A}_o \hat{\tilde{\mathbf{x}}}_r + \mathbf{B}_o \hat{\tilde{\mathbf{u}}} + \mathbf{A}_\omega \tilde{\mathbf{X}}_r \hat{\omega} + \mathbf{B}_d \tilde{\mathbf{U}} \hat{d}_e \tag{3.13}$$

where

$$\mathbf{A}_o = \begin{bmatrix} -1/R & \Omega C \\ -\Omega C & -1/R \end{bmatrix} \quad , \quad \mathbf{B}_o = \begin{bmatrix} D_e \\ 0 \end{bmatrix}$$
$$\mathbf{A}_\omega \tilde{\mathbf{X}}_r = \begin{bmatrix} CV_q \\ -CV_d \end{bmatrix} \quad , \quad \mathbf{B}_d \tilde{\mathbf{U}} = \begin{bmatrix} I_{ref} \\ 0 \end{bmatrix} \tag{3.14}$$

The small signal transfer functions are found from Eq. (3.13) and all transfer functions have a common denominator $K(s)$. The system is a second order one as the pole arising from the inductor has been moved above the bandwidth of interest by the current loop. The zeros and dc gains of the various transfer functions are enumerated in Table 3.2.

Additional circuitry is necessary to transform the sinusoidal capacitor voltages to their equivalent dc descriptions in the dq reference frame for measurement of transfer functions. The transformation $\mathbf{T}$ is given by

$$\tilde{\mathbf{v}} = \mathbf{T}\,\mathbf{v} \tag{3.15}$$

where

$$\mathbf{T} = \sqrt{\frac{2}{3}} \begin{bmatrix} \cos(\theta_t) & \cos(\theta_t - 2\pi/3) & \cos(\theta_t + 2\pi/3) \\ -\sin(\theta_t) & -\sin(\theta_t - 2\pi/3) & -\sin(\theta_t + 2\pi/3) \\ 1/\sqrt{2} & 1/\sqrt{2} & 1/\sqrt{2} \end{bmatrix} \quad , \quad \theta_t = \theta_m - \phi_t \tag{3.16}$$

It is noted that v_q with ϕ_t equal to ϕ_o is the same as v_d with ϕ_t equal to ϕ_o plus $\pi/2$. Hence, the hardware used for measurements produces the output v_o given by

$$v_o = \sqrt{\frac{2}{3}} \sum_{z=1}^{3} v_z \cos[\theta_t - (z-1)\frac{2\pi}{3}] \tag{3.17}$$

and the desired v_d and v_q are obtained by proper choice of ϕ_t. Some of the predicted and measured transfer functions are plotted in Figs. 3.19 and 3.20. The Bode plots of Fig. 3.20 are for perturbations in the inversion frequency and include the dynamics of the phase locked loop present in the control circuit. The measurements are corrupted by

Function	DC Gain	Zeros
$\frac{\hat{v}_d}{\hat{d}_e}$	$\frac{RI_{ref}}{1+(\Omega/\omega_p)^2}$	$1+\frac{s}{\omega_p}$
$\frac{\hat{v}_q}{\hat{d}_e}$	$-\frac{RI_{ref}(\Omega/\omega_p)}{1+(\Omega/\omega_p)^2}$	1
$\frac{\hat{v}_d}{\hat{\omega}}$	$-\frac{2D_eRI_{ref}(\Omega/\omega_p)}{\omega_p\left[1+(\Omega/\omega_p)^2\right]^2}$	$1+\frac{s}{\omega_{z1}}$
$\frac{\hat{v}_q}{\hat{\omega}}$	$-\frac{D_eRI_{ref}[1-(\Omega/\omega_p)^2]}{\omega_p\left[1+(\Omega/\omega_p)^2\right]^2}$	$1+\frac{s}{\omega_{z2}}$
$\frac{\hat{v}_d}{\hat{i}_{ref}}$	$\frac{D_eR}{1+(\Omega/\omega_p)^2}$	$1+\frac{s}{\omega_p}$
$\frac{\hat{v}_q}{\hat{i}_{ref}}$	$-\frac{D_eR(\Omega/\omega_p)}{1+(\Omega/\omega_p)^2}$	1

Denominator $D(s) = 1 + \frac{s}{Q_o\omega_o} + \frac{s^2}{\omega_o^2}$

where $\omega_p = \frac{1}{RC}$; $\omega_o = \omega_p\sqrt{1+(\Omega/\omega_p)^2}$; $\omega_{z1} = 2\omega_p$

$\omega_{z2} = \omega_p\left[1-(\Omega/\omega_p)^2\right]$; $Q_o = \frac{1}{2}\sqrt{1+(\Omega/\omega_p)^2}$

Table 3.2: DC gains and zeros of some of the small signal transfer functions of the current programmed buck-boost inverter.

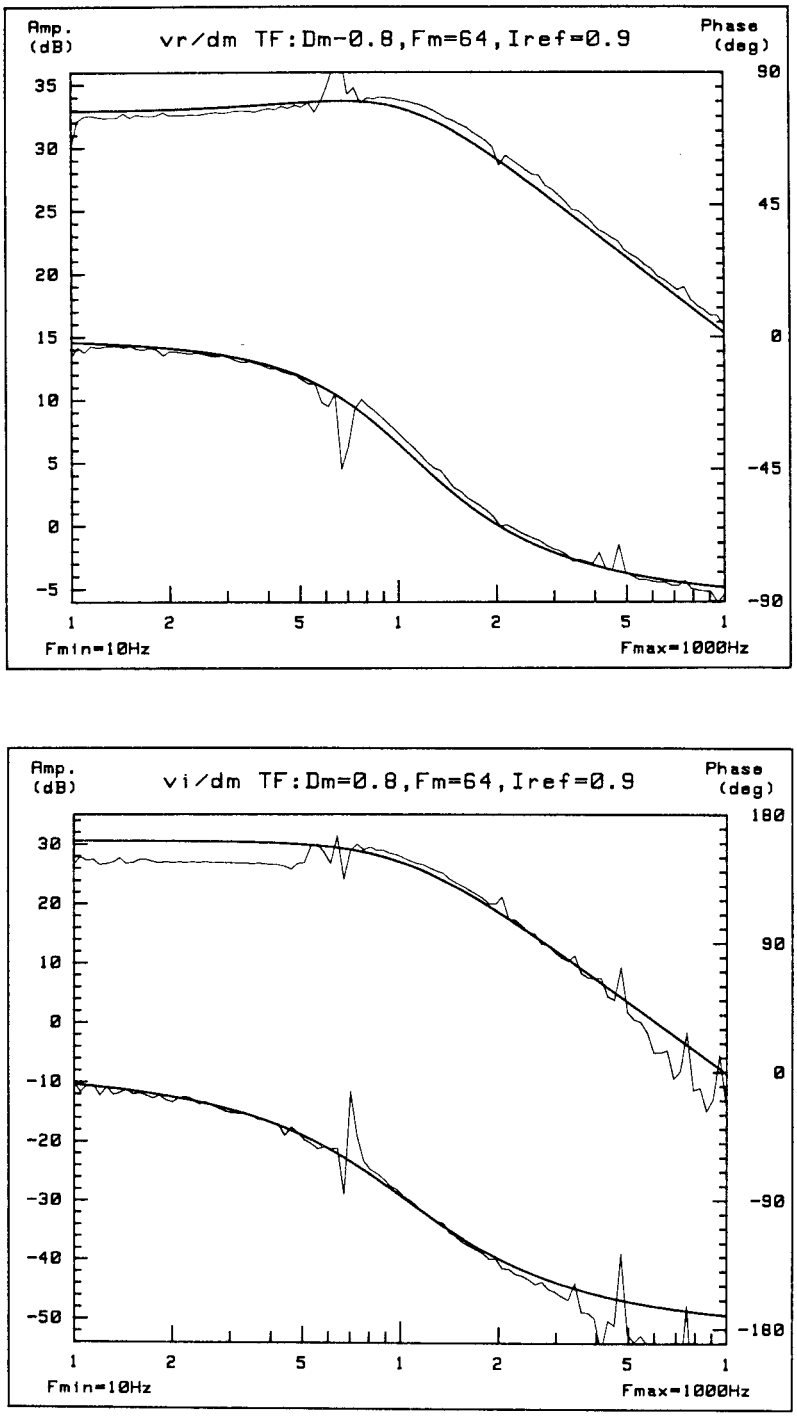

Figure 3.19: Predicted and measured small signal responses $\hat{v}_d/\hat{d}_m$ (a) and $\hat{v}_q/\hat{d}_m$ (b) for the converter of Fig. 3.10. Predictions are shown in thick lines and measured responses in thin lines.

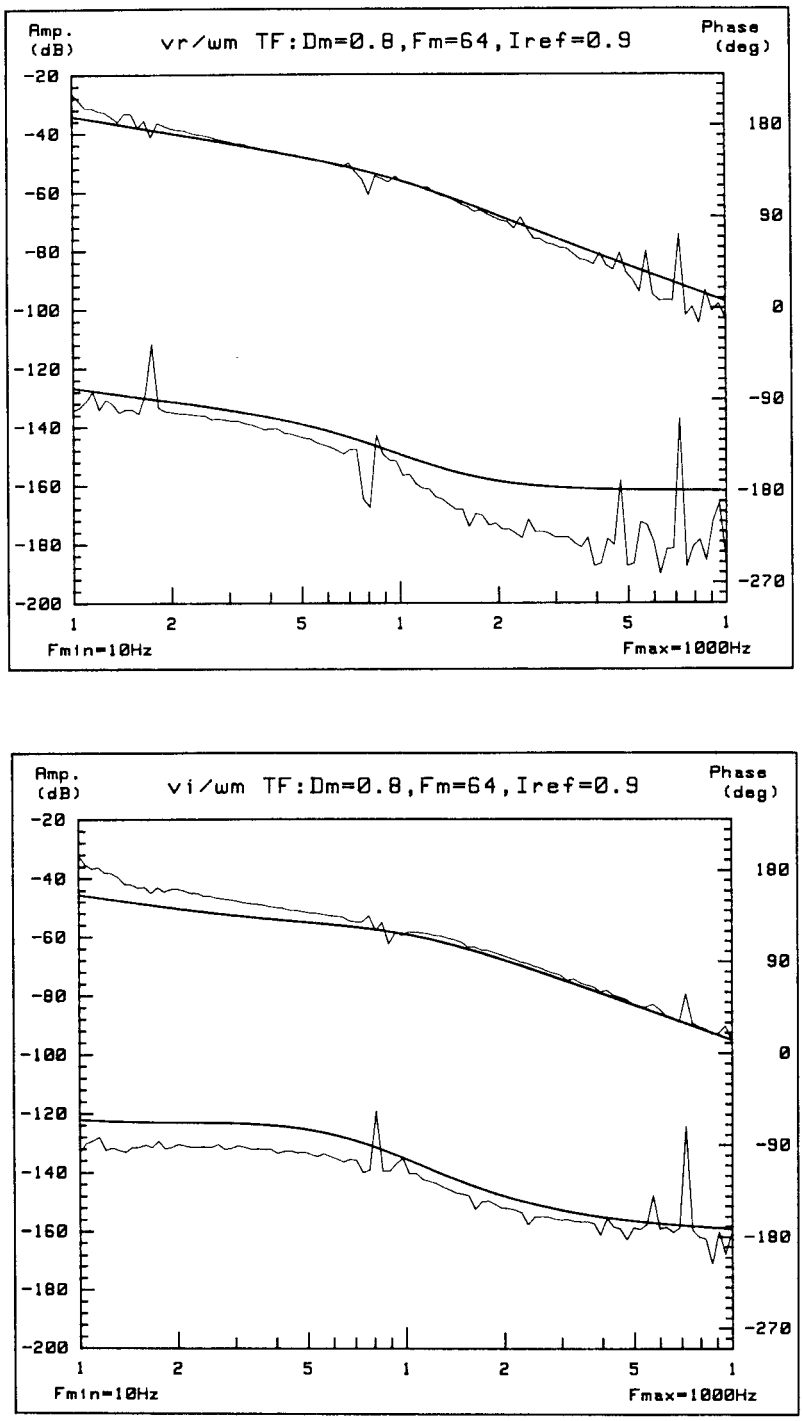

Figure 3.20: Predicted (thick lines) and measured (thinlines) small signal responses $\hat{v}_d/\hat{\omega}$ (a) and $\hat{v}_q/\hat{\omega}$ (b) for the converter of Fig. 3.10.

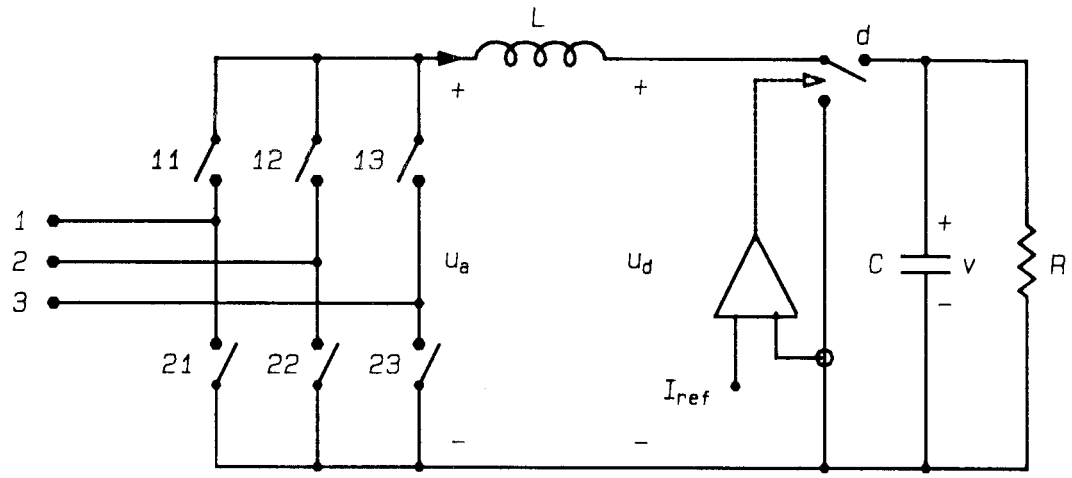

Figure 3.21: The current reference programmed dc-three phase buck-boost converter in the rectifier mode of operation.

the presence of harmonics of the inversion frequency, despite efforts to avoid them, as the signal injected for measuring responses is itself small in magnitude.

3.3 Rectifier Mode of Operation

The converter is presumed to be operating in the rectifier mode off a balanced three phase source. The steady-state and dynamic responses of the converter are discussed in the current reference programmed mode. The converter is considered to be ideal with lossless switches, sufficiently high switching frequency, etc., as shown in Fig. 3.21. The switch that is current programmed is on the output side in this case, for ease of implementation, even though it lacks the inherent isolation of source variations from the load that was present in the inversion mode. This converter can be considered to be

similar to a current reference programmed boost dc-dc converter. The switches on the ac side are instrumental in applying an average dc voltage to the input end of the inductor, while the switch on the output side is used for current programming in the same way as in a boost dc-dc converter. This feature reflects in the properties of the converter.

3.3.1 Steady-State Analysis

The converter is presumed to operate correctly in the current reference programmed mode without subharmonic oscillations. As in the case of the inverter, the average inductor current i can be approximated by the reference current i_{ref} if the inductor current ripple is small compared to i. The description of the system in the stationary abc reference frame is

$$\begin{aligned} L\,\dot{i} &= -d\,v + \sum_{z=1}^{3} d_z v_{gz} \\ C\,\dot{v} &= d\,i - \frac{v}{R} \end{aligned} \tag{3.18}$$

where

$$\begin{aligned} v_{gw} &= v_g \cos[\theta_m - (w-1)\frac{2\pi}{3} + \phi] \\ d_w &= d_m \cos[\theta_m - (w-1)\frac{2\pi}{3}] \quad , \quad 1 \le w \le 3 \end{aligned} \tag{3.19}$$

In the dq reference frame, the system of Eq. (3.19) is represented by

$$\tilde{\mathbf{P}}\,\dot{\tilde{\mathbf{x}}} = \tilde{\mathbf{A}}\,\tilde{\mathbf{x}} + \tilde{\mathbf{B}}_r\,\tilde{\mathbf{u}}_r \tag{3.20}$$

where

$$\begin{aligned} \tilde{\mathbf{P}} &= \begin{bmatrix} L & 0 \\ 0 & C \end{bmatrix} \quad , \quad \tilde{\mathbf{A}} = \begin{bmatrix} 0 & -d \\ d & -1/R \end{bmatrix} \quad , \quad \tilde{\mathbf{B}}_r = \begin{bmatrix} d_e & 0 \\ 0 & 0 \end{bmatrix} \\ \tilde{\mathbf{x}} &= \begin{bmatrix} i \\ v \end{bmatrix} \quad , \quad \tilde{\mathbf{u}}_r = \begin{bmatrix} v_{ge}\cos\phi \\ v_{ge}\sin\phi \end{bmatrix} \quad , \quad d_e = \sqrt{\tfrac{3}{2}}\,d_m \quad , \quad v_{ge} = \sqrt{\tfrac{3}{2}}\,v_g \end{aligned} \tag{3.21}$$

in which the "o" or dc component of the ac source voltages has been dropped from the equations as it is zero for a balanced three phase ac source. The steady-state solution

found from Eq. (3.20) is:

$$V = \frac{D_e}{D} V_{ge} \cos\phi$$
$$I_{ref} \approx I = \frac{V}{RD} \tag{3.22}$$

Thus, in terms of the controls I_{ref}, D_e, and ϕ, the steady-state output voltage is

$$V = \sqrt{R I_{ref} V_{ge} \cos\phi} \tag{3.23}$$

3.3.2 Stability in Current Reference Programmed Mode

Subharmonic oscillations occur in the current reference programmed rectifier, for certain operating conditions, in a manner similar to that observed in dc-dc converters and inverters. The peak-to-peak ripple of the inductor current varies at six times the ac frequency, as in the case of the inverter. The duty ratio of the switch on the dc output side does not vary from one switching cycle to the next when the current loop is functioning correctly. The switching frequency is assumed to be well above the ac source frequency.

The voltages $u_d(t)$ and $u_a(t)$ applied to the dc and ac ends of the inductor in the rectifier mode result in the current waveform of Fig. 3.22. In the rectifier, the inductor current ripple should increase during the interval when the active switch on the dc side is ON. This restricts $u_a(t)$ to being positive during $d'T_s$, and consequently imposes a limitation on the power factor that can be obtained at the input.

The gain of the current loop, k, is obtained from the waveforms of Fig. 3.23 and should be less than unity for stable operation of the current reference programmed loop. The maximum values of k for various input phase angles ϕ, are given in Table 3.3. A compensating ramp may be used to extend the region of stable operation.

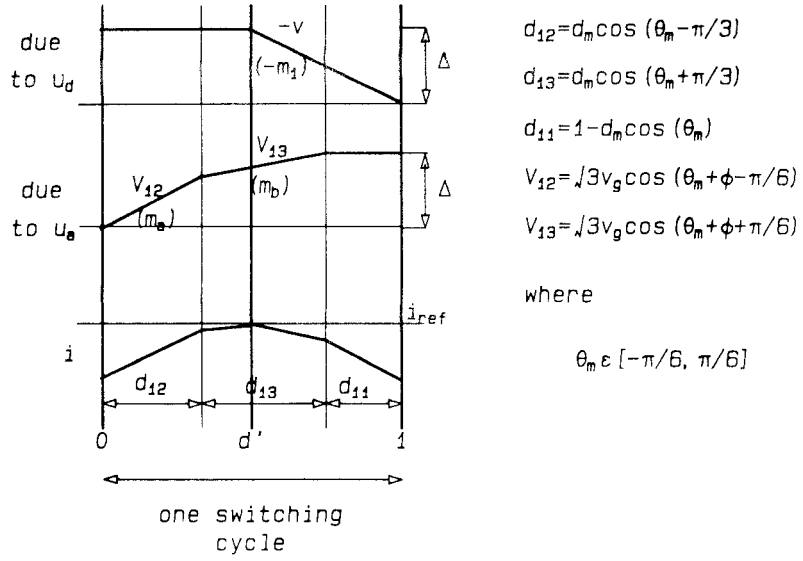

Figure 3.22: The effects of the voltages applied at the two ends of the inductor and the resulting current ripple.

3.3.3 Dynamic Analysis

The current ripple is assumed to be small and i is approximated by i_{ref}, to obtain the approximate dynamic model of the current programmed rectifier. The small signal model of the system is

$$L\,\dot{\hat{i}}_{ref} = -D\hat{v} - V\hat{d} + V_{ge}\cos\phi\hat{d}_e + D_e\cos\phi\hat{v}_{ge} \tag{3.24}$$

$$C\,\dot{\hat{v}} = D\hat{i}_{ref} + I_{ref}\hat{d} - \frac{\hat{v}}{R} \tag{3.25}$$

in which the terms with carets represent the small signal perturbations. The perturbation $\hat{d}$ is found in terms of $\hat{i}_{ref}$ from Eq. (3.24) and substituted into Eq. (3.25) to give

$$C\,\dot{\hat{v}} = -\frac{2}{R}\hat{v} + \frac{V}{IR}\hat{i}_{ref} - \frac{LI}{V}\dot{\hat{i}}_{ref} + \frac{D_eI\cos\phi}{V}\hat{v}_{ge} + \frac{V_{ge}I\cos\phi}{V}\hat{d}_e \tag{3.26}$$

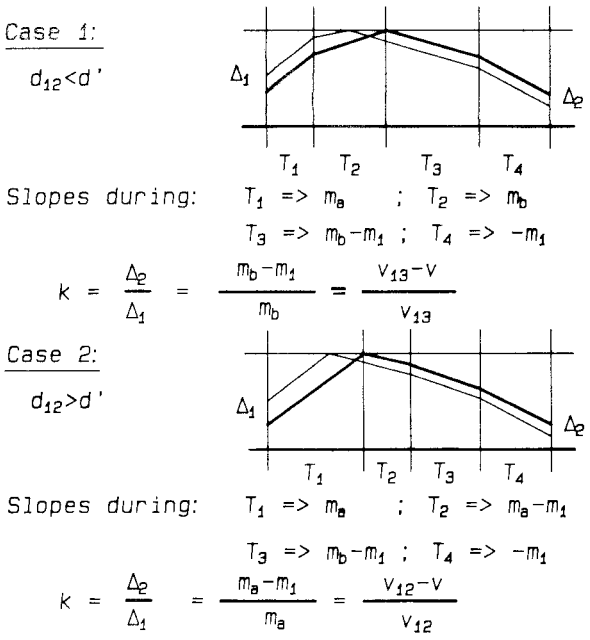

Figure 3.23: Propagation of a disturbance in the inductor current of the current reference programmed rectifier. The values of k for the two cases, $d' < d_{12}$ (a) and $d' > d12$ (b) are obtained.

The small signal responses are obtained from Eq. (3.26) and all responses have a common first order denominator $K(s)$. The right half-plane zero, that is inherent to the buck-boost toplogy, is present in the transfer function from $\hat{\imath}_{ref}$ to the output voltage $\hat{v}$. Thus, it is more advantageous to keep i_{ref} fixed and regulate the output voltage using d_e. Some of the small signal responses of interest are listed in Table 3.4.

3.4 Bidirectional Operation

The converter of Fig. 3.3 can be operated in the bidirectional mode by pulse width modulating switches S_3 and S_4, as described in Section 3.1.2. However, this results in a mode of operation that is inefficient in comparison with the inversion or rectifier mode of operation. Thus, it is advantageous to operate in the inversion mode when the steady-

Phase Angle ϕ	$\lvert k\rvert_{max}$
$\lvert\phi\rvert < \frac{\pi}{6}$	$\frac{\sqrt{3}D_m}{2D}\frac{\cos\phi}{\cos(\lvert\phi\rvert+\pi/3)} - 1$
$\lvert\phi\rvert > \frac{\pi}{6}$	$\lvert k\rvert_{max} > 1$

Table 3.3: Maximum magnitudes of k for various phase angles ϕ in the current reference programmed rectifier. The magnitude of k should be less than unity for stable operation in the CRP mode.

state power flow has to be from the dc to ac side, and in the rectifier mode when the steady-state power flow has to be from ac to dc side. The bidirectional mode need only be used when the direction of power flow changes. However, in order to be able to change modes of operation based on the direction of power flow, it is necessary to determine the instantaneous magnitude and direction of power flow through the converter.

Current programming can be applied to the bidirectional mode of operation by using a hysteretic or sliding mode control technique. The measured inductor current is compared with the reference current to generate the sign of the current error. The sign of the current error σ is used along with the sign of the power flow to determine the positions of switches S_3 and S_4 from a look-up table. Figure 3.24 depicts the waveforms and duty ratios on the dc side of the converter. The average value of the voltage u_d is proportional to the power flow and the sign indicates the direction of power flow. Thus, u_d is averaged over the switching frequency to determine the power flow and compared with two threshold values. If the average value of u_d lies within a narrow band around zero, the converter is operated in the bidirectional mode; otherwise, it is operated in the inversion or rectification modes depending on the sign of the average value. This

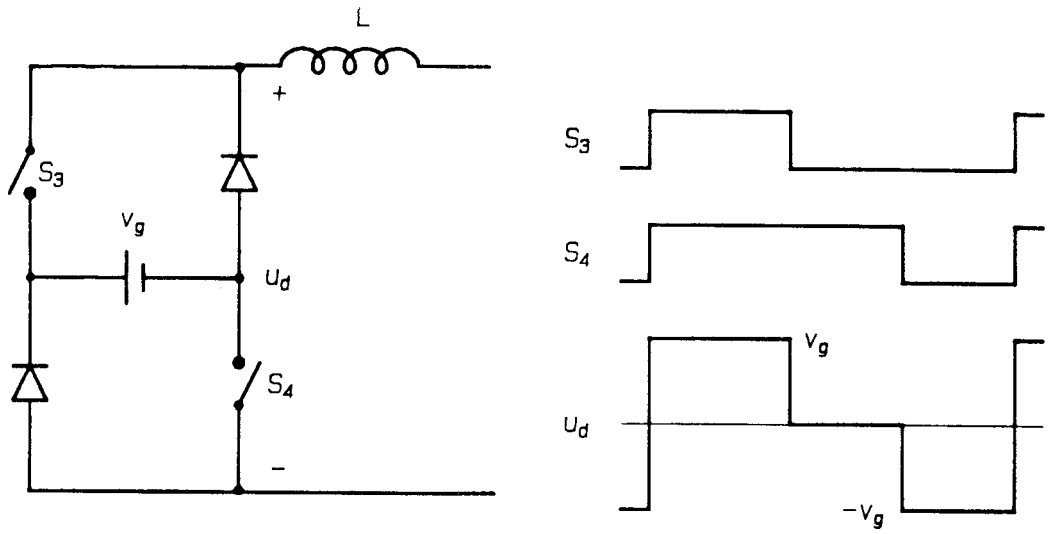

Figure 3.24: Waveforms and duty ratios at the dc end of the dc-three phase buck-boost converter.

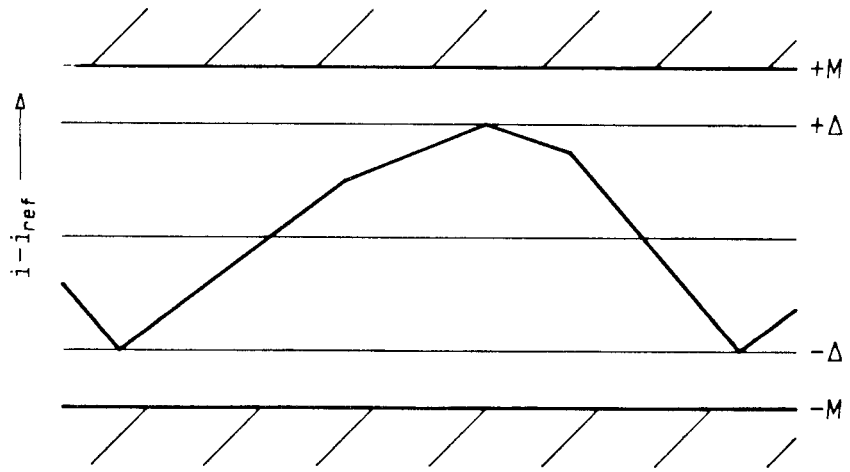

Figure 3.25: Fast detection of changes in the direction of power flow using the inductor current error signal.

Function	DC Gain	Zeros
$\frac{\hat{v}}{\hat{i}_{ref}}$	$\frac{V}{2I}$	$1 - \frac{s}{\omega_z}$
$\frac{\hat{v}}{\hat{d}_e}$	$\frac{V}{2D_e}$	1
$\frac{\hat{v}}{\hat{v}_{ge}}$	$\frac{V}{2V_{ge}}$	1
Denominator $D(s) = 1 + \frac{s}{\omega_o}$ where $\omega_o = \frac{2}{RC}$; $\omega_z = \frac{RD^2}{L}$		

Table 3.4: DC gains and zeros of some of the small signal transfer functions of the CRP rectifier.

method of choosing the duty ratios of switches S_3 and S_4 helps for proper operation in steady state and will not respond to sudden changes in the direction of power flow. Quick changes in the direction of power flow can be detected directly from the current as shown in Fig. 3.25. Thus, if the inductor current error exceeds a preset magnitude, the converter enters the bidirectional mode of operation.

Chapter 4

Review of Sliding Mode Control of DC-DC Converters

Dc-dc power conversion plays a pivotal role in many electric power systems and a multitude of converter topologies have been used to provide this function. All switched-mode dc-dc converters provide efficient conversion of power from one form to another by using reactive elements to transfer energy from the source to the load. This is achieved by the use of one or more semiconductor switches and reactive elements such as inductors and capacitors. Thus, the switched network assumed by the converter is different in the energy storage and energy release intervals. Consequently, any switched-mode power converter constitutes a *variable structure system* (VSS) and control is provided by the proper choice of switching structures and switching instants. The structures may occur periodically with a fixed switching frequency, or with a variable switching frequency.

Sliding mode control is a natural method of control for variable structure systems and is used to provide regulation in dc-dc converters. Section 4.1 reviews the sliding mode method of control, as applied to variable structure systems[20]. The conditions required for the existence of sliding mode are listed, as are the advantages and disadvantages of this method of control. Sections 4.2 through 4.4 describe the sliding mode control of the three basic dc-dc converters: the buck, boost, and flyback[21,22].

4.1 Sliding Mode Control of VSS

The sliding mode method of control of variable structure systems is reviewed in this section. The VSS is described in a form suitable for the application of sliding mode control. The existence conditions required and the equivalent control technique for analyzing sliding mode systems are discussed. The advantages and disdvantages that result from the use of sliding mode control are enumerated.

4.1.1 System Description

Variable structure systems are characterized by a time-varying structure that generally consists of two or more discrete structures. Control action is achieved by the choice of the structure and is discontinuous and results in a nonlinear plant. Switched-mode converters fall within this broad category of variable structure systems. Any variable structure system can be represented in the form:

$$\dot{\mathbf{x}} = \mathbf{f}(\mathbf{x}, \mathbf{u}, t) \tag{4.1}$$

where

$\mathbf{x}$ is the $N \times 1$ state vector,

$\mathbf{u}$ is the $M \times 1$ discontinuous control input,

$\mathbf{f}$ is a N-dimensional vector function.

In the case of dc-dc converters, the system can be represented in the form

$$\dot{\mathbf{x}} = \mathbf{A}\,\mathbf{x} + \mathbf{B}\,u + \mathbf{T} \tag{4.2}$$

in which the control u is a scalar and $\mathbf{B}$ may be a function of $\mathbf{x}$. The system state vector $\mathbf{x}$ and the matrices $\mathbf{A}$, $\mathbf{B}$, and $\mathbf{T}$ are all continuous functions while u is discontinuous.

4.1.2 Sliding Surface

The sliding surface is the surface on which the motion of the system is constrained when operating in sliding mode. The choice of the discontinuous control u is made depending on the value of the sliding function σ. The sliding surface in switched-mode dc-dc converters may be expressed as

$$\mathbf{G}\,\hat{\mathbf{x}} = 0 \tag{4.3}$$

where

$$\hat{\mathbf{x}} = \mathbf{x} - \mathbf{X}^* \tag{4.4}$$

is the error in the states from the desired operating point $\mathbf{X}^*$. The function σ given by

$$\sigma = \mathbf{G}\,\hat{\mathbf{x}} \tag{4.5}$$

is continuous and is referred to as the *sliding function*. The choice of control is made so as to maintain σ to be zero, thereby constraining the motion of the system along the surface of Eq. (4.3). In sliding mode, the dynamics of the system is dictated by the surface of Eq. (4.3), which is referred to as the *sliding surface* as the operating point moves on this surface. The sliding surface is normally chosen such that the error $\hat{\mathbf{x}}$ tends to zero with time, when the system is operating in the sliding mode.

4.1.3 Existence Conditions

The sliding function σ and the discontinuous control u have to satisfy certain conditions in order to assure that the system will reach the sliding surface and maintain the system on the surface. The existence condition[20] can be expressed as:

$$\lim_{\sigma \to 0^+} \dot{\sigma} < 0 \quad \text{and} \quad \lim_{\sigma \to 0^-} \dot{\sigma} > 0 \tag{4.6}$$

The system should also be able to reach the sliding surface from any initial condition within its domain of operation. The existence condition of Eq. (4.6) and the reaching condition can be expressed in the compact form:

$$\sigma\dot{\sigma} < 0 \tag{4.7}$$

The control u is chosen such that the inequality of Eq. (4.7) is satisfied over the domain of $\mathbf{x}$. Other factors that influence the choice of σ are the desired dynamic performance of the system and the stability of the sliding surface $\sigma = 0$. The choice of u in a dc-dc converter is made such that

$$u = \begin{cases} u^+ \;\; ; \;\; \sigma > 0 \\ u^- \;\; ; \;\; \sigma < 0 \end{cases} \tag{4.8}$$

satisfies

$$\mathbf{GA}\,\hat{\mathbf{x}} + \mathbf{GB}\,u^+ + \mathbf{GT} < 0 < \mathbf{GA}\,\hat{\mathbf{x}} + \mathbf{GB}\,u^- + \mathbf{GT} \tag{4.9}$$

4.1.4 Method of Equivalent Control

Although the control u is discontinuous, an equivalent continuous description of the system may be used to describe the low frequency behavior of the system, under sliding motion. In the equivalent description, the discontinuous control u is replaced by an equivalent continuous control u_{eq} given by

$$u_{eq} = -(\mathbf{GB})^{-1}[\mathbf{GA}\,\hat{\mathbf{x}} + \mathbf{GT}] \tag{4.10}$$

The low frequency or average motion of the system is characterized by

$$\dot{\hat{\mathbf{x}}} = [\mathbf{I} - \mathbf{B}(\mathbf{GB})^{-1}\mathbf{G}](\mathbf{A}\,\hat{\mathbf{x}} + \mathbf{T}) \tag{4.11}$$

Sliding mode ideally results in an infinite switching frequency, and Eq. (4.11) holds exactly. However, in all practical systems, the switching frequency is determined by the

hysteresis of the switching action and Eq. (4.11) is valid only for a fraction of the switching frequency. If $\sigma \neq 0$, the equivalent control can be expressed as

$$\tilde{u}_{eq} = -(\mathbf{GB})^{-1}[\mathbf{GA}\,\hat{\mathbf{x}} + \mathbf{GT}] + (\mathbf{GB})^{-1}\dot{\sigma} \tag{4.12}$$

and the system motion is given by

$$\dot{\hat{\mathbf{x}}} = [\mathbf{I} - \mathbf{B}(\mathbf{GB})^{-1}\mathbf{G}](\mathbf{A}\,\hat{\mathbf{x}} + \mathbf{T}) + \mathbf{B}(\mathbf{GB})^{-1}\dot{\sigma} \tag{4.13}$$

The first term signifies the average motion of the system and the last term signifies the switching ripple.

4.1.5 Advantages and Disadvantages of Sliding Mode Control

Sliding mode control results in several advantages in the design and control of the system. One of the most compelling reasons is that it is the more natural method of control for switching converters as they are inherently variable structured systems. Thus, sliding mode control is a way of ensuring large and small signal stability of a nonlinear plant such as the switching converter. Once the system reaches the sliding surface, the motion of the system is determined *exclusively* by the sliding surface (namely, the elements of $\mathbf{G}$) and is independent of the parameters of the system. Hence, the controller will be robust and guarantee stability as well as performance in the face of plant uncertainties.

The disadvantage of this method lies in the necessity to measure all the states of the system (in general). Hence, it requires that all the states be accessible. It also results in a variable switching frequency in the system, which may be undesirable in some applications.

4.2 Buck Converter

The sliding control of the buck dc-dc converter is reviewed in this section. The sliding function and controls used are identified and the existence conditions stated.

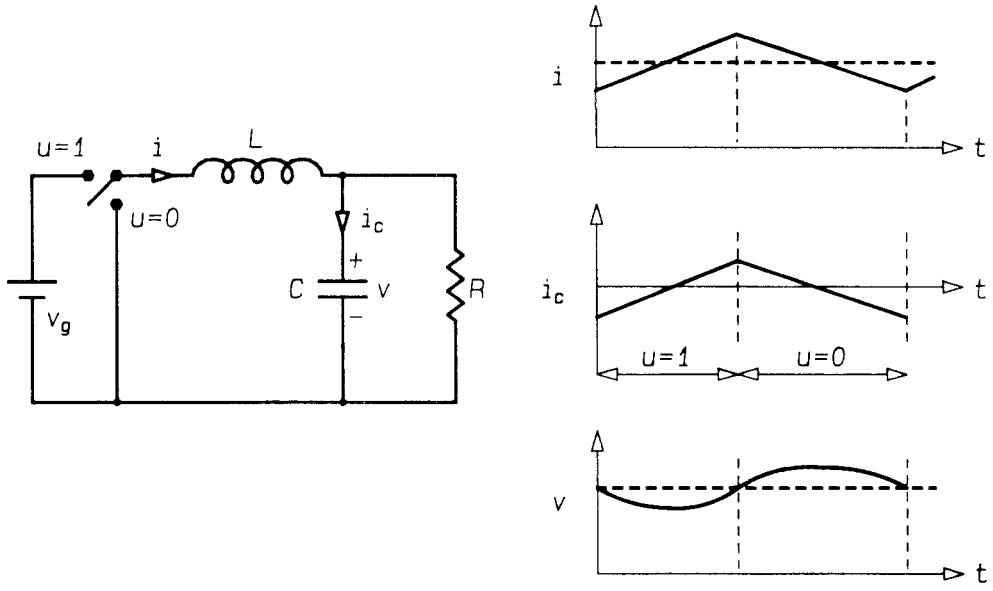

Figure 4.1: The buck dc-dc converter and the control u defined as a function of the switch position. The capacitor voltage and current are both continuous in this topology.

4.2.1 System Description

The buck dc-dc converter of Fig. 4.1 is represented by

$$\dot{\mathbf{x}} = \mathbf{A}\,\mathbf{x} + \mathbf{b}\,u + \mathbf{t} \tag{4.14}$$

where

$$\mathbf{x} = \begin{bmatrix} \hat{v} \\ \dot{\hat{v}} \end{bmatrix} \;;\; \mathbf{A} = \begin{bmatrix} 0 & 1 \\ -1/LC & -1/RC \end{bmatrix} \;;$$
$$\mathbf{b} = \begin{bmatrix} 0 \\ v_g/LC \end{bmatrix} \;;\; \mathbf{t} = \begin{bmatrix} 0 \\ -v^*/LC \end{bmatrix} \;;\; \hat{v} = v - v^* \tag{4.15}$$

in which v^* is the desired output voltage and u is the scalar control that assumes values 1 and 0.

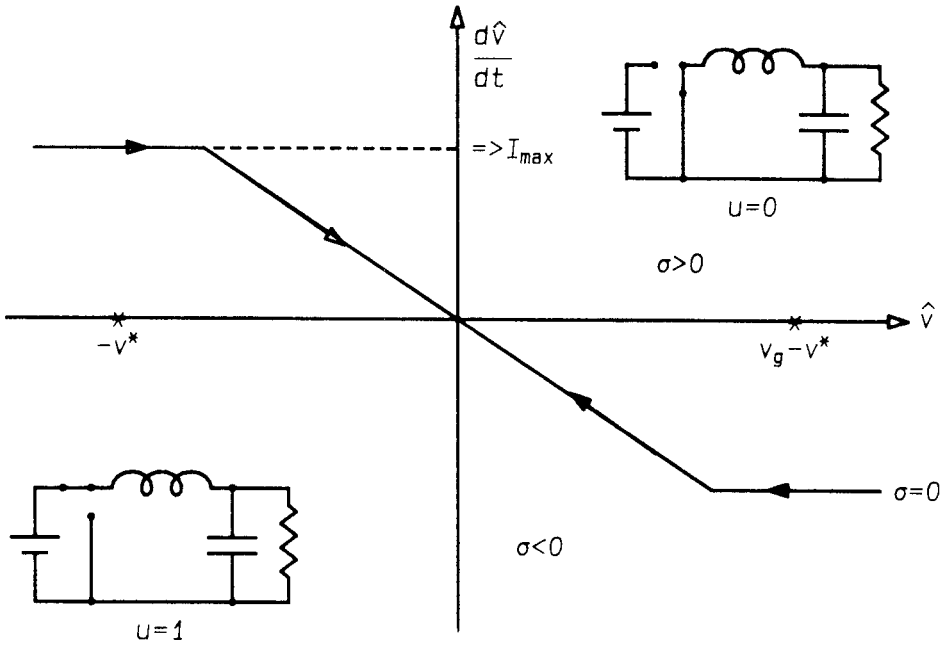

Figure 4.2: The sliding line for the buck converter in the phase plane defined in terms of the output voltage and its derivative. A current limiting segment is used to provide protection.

4.2.2 Sliding Surface

The buck dc-dc converter is a second order system with one control and the dynamic response that can be obtained using sliding control mode control is a first order one. The sliding surface is consequently a sliding line in this case, and is given by

$$\sigma = \hat{v} + \tau\dot{\hat{v}} = 0 = \mathbf{gx} \tag{4.16}$$

where

$$\mathbf{g} = [1 \quad \tau] \tag{4.17}$$

This sliding line represents a stable first order response with time constant τ and is shown in Fig. 4.2. The control u is chosen to be

$$u = \begin{cases} u^+ & ; \sigma > 0 \\ u^- & ; \sigma < 0 \end{cases} \tag{4.18}$$

where u^+ and u^- are selected as 0 and 1, respectively. The conditions required for existence of sliding mode on the given sliding line are

$$\begin{aligned} \tau &> RC \\ v_g &> v^* \end{aligned} \tag{4.19}$$

In a practical converter, a current limit segment is added to the sliding line in order to protect the devices in the converter.

4.3 Boost Converter

The sliding mode control of the boost dc-dc converter is discussed in brief in this section.

4.3.1 System Description

The boost dc-dc converter and its waveforms are shown in Fig. 4.3. The system cannot be described in terms of the output voltage and its derivative, as was done for the buck converter, because the derivative of the output voltage (which is proportional to the capacitor current) is discontinuous in this converter. Hence, the system is represented in terms of the inductor current and capacitor voltage by

$$\dot{\mathbf{x}} = \mathbf{A}\,\mathbf{x} + \mathbf{b}\,u + \mathbf{t} \tag{4.20}$$

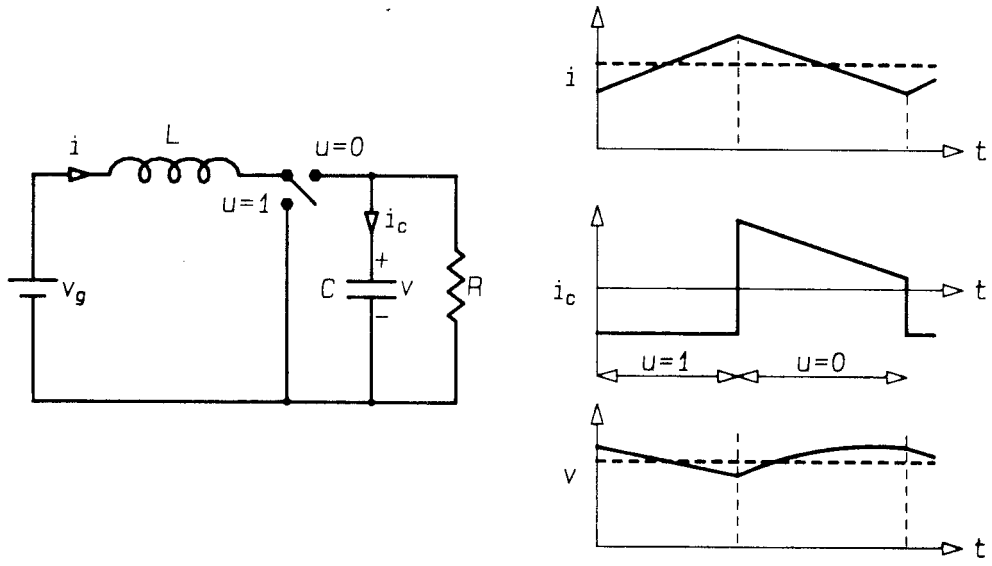

Figure 4.3: The boost dc-dc converter and its waveforms. The capacitor current is discontinuous at the switching instants.

where

$$\mathbf{x} = \begin{bmatrix} i \\ v \end{bmatrix} \; ; \; \mathbf{A} = \begin{bmatrix} 0 & -1/L \\ 1/C & -1/RC \end{bmatrix} \; ;$$
$$\mathbf{b} = \begin{bmatrix} v/L \\ -i/C \end{bmatrix} \; ; \; \mathbf{t} = \begin{bmatrix} v_g/L \\ 0 \end{bmatrix} \tag{4.21}$$

The control u is discontinuous and assumes the values 1 and 0 for the two positions of the switches.

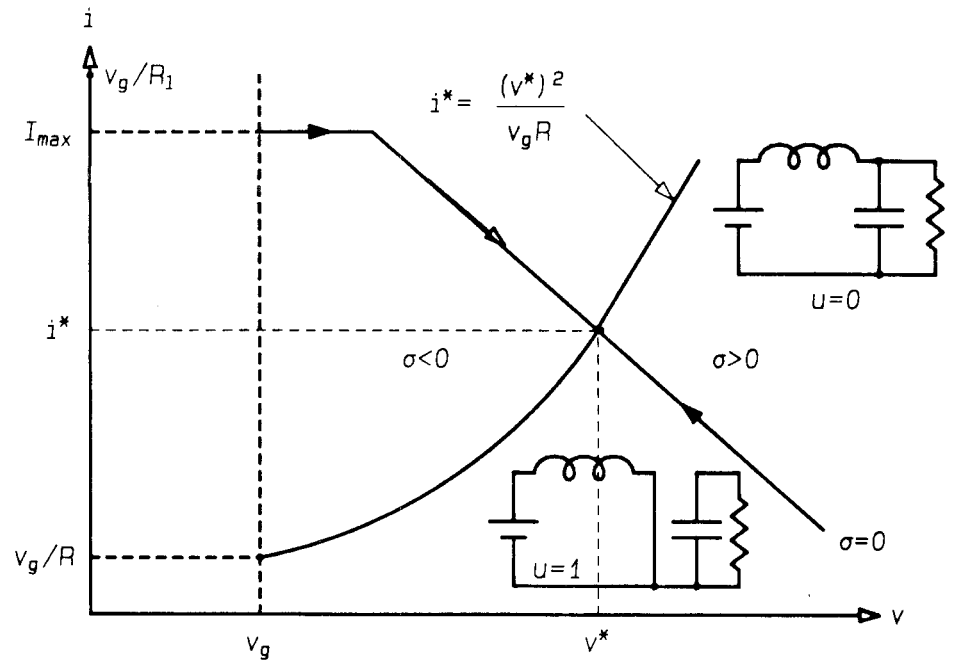

Figure 4.4: The sliding line of the boost converter in the phase plane consisting of the inductor current and capacitor voltage. The sliding line is piecewise linear in the phase plane and one segment is used to provide current limiting action.

4.3.2 Sliding Surface

For the boost converter, the sliding line is chosen in terms of the inductor current and capacitor voltage as shown in Fig. 4.4 and is given by

$$\sigma = \mathbf{g}\hat{\mathbf{x}} = R_s\hat{\imath} + \hat{v} \tag{4.22}$$

where

$$\begin{aligned} \hat{\imath} &= i - i^* \\ \hat{v} &= v - v^* \end{aligned} \tag{4.23}$$

and i^*, v^* represent the desired operating point. The parameter R_s is like the current sense resistor and is in practice much smaller than the load resistance R. The method of equivalent control is used to determine the stability of the system on the sliding line.

The relation between i and v found using the equivalent control is

$$v^2 + RCv\frac{dv}{dt} = Ri(v_g - L\frac{di}{dt}) \approx Riv_g \tag{4.24}$$

The sliding line can thus be expressed in terms of $\hat{v}$ by

$$\sigma = \hat{v} + \frac{2v^* R_s}{Rv_g}\hat{v} + \frac{Cv^* R_s}{v_g}\frac{d\hat{v}}{dt} + \frac{R_s}{Rv_g}\hat{v}^2 + \frac{CR_s}{2v_g}\frac{d(\hat{v}^2)}{dt} \tag{4.25}$$

and is stable if the relative error $\hat{v}/v^*$ is less than unity. The small and large signal responses can be obtained from Eq. (4.25). The existence conditions that need to be satisfied for sliding mode to exist on the given sliding line are:

$$\begin{aligned} L &< \frac{R_s C(v - v_g)}{I_{max}} \\ L &< \frac{R_s RCv_g}{v} \end{aligned} \tag{4.26}$$

4.4 Flyback Converter

The flyback converter is similar to the boost converter in that the derivative of the output voltage is discontinuous. Hence, sliding mode has to be applied using the inductor current and capacitor voltage.

4.4.1 System Description

The flyback converter shown in Fig. 4.5 is described in terms of the inductor current and capacitor voltage by

$$\dot{\mathbf{x}} = \mathbf{A}\,\mathbf{x} + \mathbf{b}\,u + \mathbf{t} \tag{4.27}$$

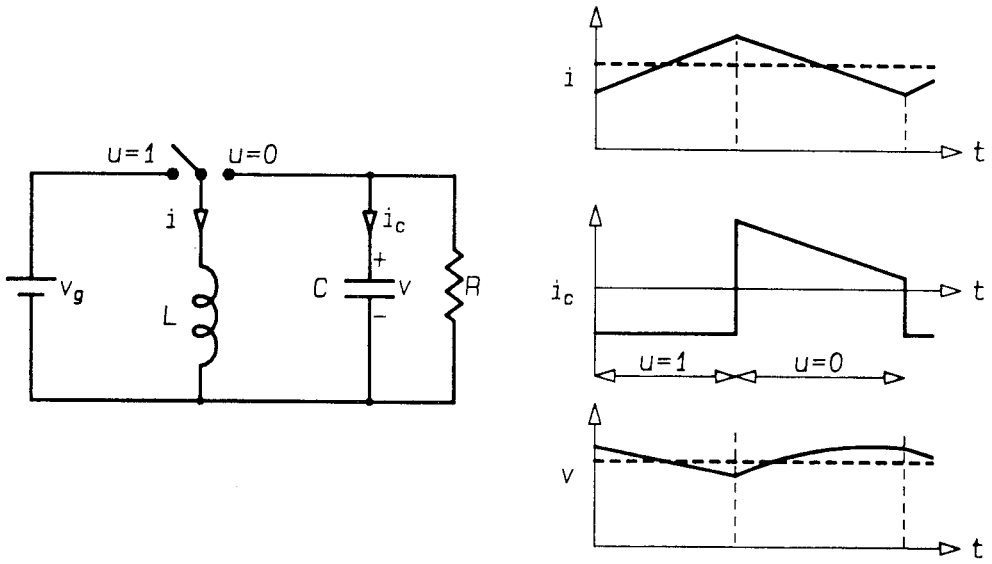

Figure 4.5: The flyback topology and waveforms showing the discontinuity in the capacitor current at the switching instants.

where

$$\mathbf{x} = \begin{bmatrix} i \\ v \end{bmatrix} \; ; \; \mathbf{A} = \begin{bmatrix} 0 & -1/L \\ 1/C & -1/RC \end{bmatrix} \; ;$$
$$\mathbf{b} = \begin{bmatrix} (v_g + v)/L \\ -i/C \end{bmatrix} \; ; \; \mathbf{t} = \begin{bmatrix} 0 \\ 0 \end{bmatrix} \tag{4.28}$$

4.4.2 Sliding Surface

The choice of sliding line in the flyback converter is similar to that of the boost converter. The function σ chosen is shown in Fig. 4.6 and is represented by

$$\sigma = \mathbf{g}\hat{\mathbf{x}} = R_s\hat{i} + \hat{v} \tag{4.29}$$

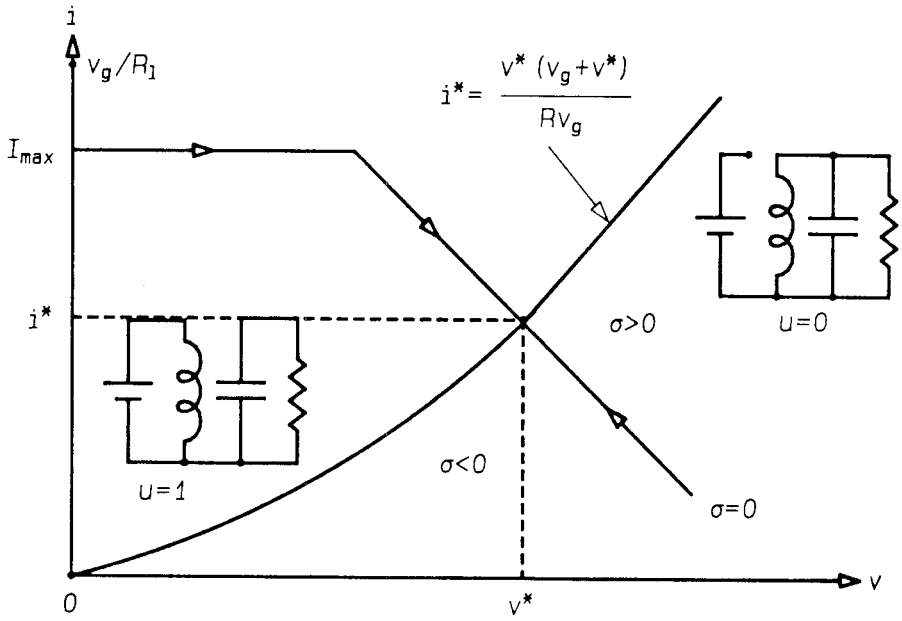

Figure 4.6: The sliding line of the flyback converter in the phase plane consisting of the inductor current and capacitor voltage. The current limiting segment is used to provide protection as well as to ensure that reaching conditions are satisfied.

where

$$\begin{aligned} \hat{\imath} &= i - i^* \\ \hat{v} &= v - v^* \end{aligned} \tag{4.30}$$

in terms of the desired operating point i^*, v^*. Again, i^* can be expressed in terms of v^* to find the conditions for σ to be stable. The constraint that has to be satisfied for stability of the response is

$$\frac{\hat{v}}{v^*} < 1 \tag{4.31}$$

and the condition for existence of sliding mode is

$$L < \min\left\{ \frac{R_s C R v_g}{v} \, , \, \frac{R_s C v}{I_{max} + v/R} \right\} \tag{4.32}$$

and reaching is assured using current limiting action.

Chapter 5

Sliding Mode Control of Inverters

In the preceding chapter, sliding mode control was seen to be a powerful method of control for switched-mode converters that results in many advantages when used in dc-dc regulators. In this chapter, this technique is applied to the three basic inverters to generate sinusoidal waveforms and to regulate the outputs. The ac load is assumed to be resistive for convenience, and the system performance is insensitive to the load provided the conditions for sliding mode are satisfied and the system is on the sliding surfaces. The methods described in this chapter may be applied to any balanced polyphase inverter; however, all details refer to the specific implementations for three phase systems.

The sliding mode control of inverters is complicated by the fact that inverters constitute multiple input, multiple output systems. The definition of sliding motion in systems with multiple discontinuous control inputs, and the necessary conditions for its existence, are described in Appendix A. It is noted that sliding motion can exist at the intersection of the sliding surfaces *without* existing on the individual surfaces themselves. However, if sliding motion exists on each individual surface, it will exist at their intersection. Consequently, for design purposes, it is necessary to reduce the system to the diagonal or dominant diagonal form when possible. In general, this is best achieved in the dq reference frame in which the desired quantities are dc in nature. However, for practical implementations of the controller, the hardware necessary increases

if dq transformations need to be performed. In certain cases the dq transformations can be approximated or eliminated altogether, as described in Section 5.1.5.

5.1 Buck Inverter

The buck inverter of Fig. 5.1 consists of three single-pole, double-throw switches and the control u_w takes values $+1$, -1, depending on the position of the switch S_w. Though the three switches can be operated independently, there are only two independent controls as the topology of the converter constrains the output voltages and currents to be balanced. The various values assumed by the controls are enumerated in Fig. 5.2.

In the stationary reference frame, the desired steady-state output phasor is represented by a circle and this average output voltage is achieved by switching rapidly between the various switch positions. Any average voltage phasor that lies within the hexagon $ABCDEF$ of Fig. 5.2 can be attained using the switch positions A through F. This is a feature of the buck topology and determines the domain over which the output voltage phasor can be controlled. Different switching strategies may be used to obtain the same steady-state output voltages: the choice of strategy is determined by the necessity to optimize efficiency, switching loss, or dynamic response.

5.1.1 System Description

The output capacitor voltages and their derivatives are continuous and differentiable functions, and the state equations are expressed in terms of these variables. In the stationary reference frame, the system is described by

$$\ddot{v}_w = -\frac{1}{RC}\dot{v}_w - \frac{1}{LC}\left\{v_w - \frac{1}{3}\sum_{z=1}^{3} v_z\right\} + \frac{v_g}{LC}\left\{u_w - \frac{1}{3}\sum_{z=1}^{3} u_z\right\} \quad ; \quad 1 \leq w \leq 3 \qquad (5.1)$$

in which the controls u_w assume values $+1$ and -1 depending on the positions of the switches. In the two phase $\alpha\beta$ reference frame, the reduced order state space representa-

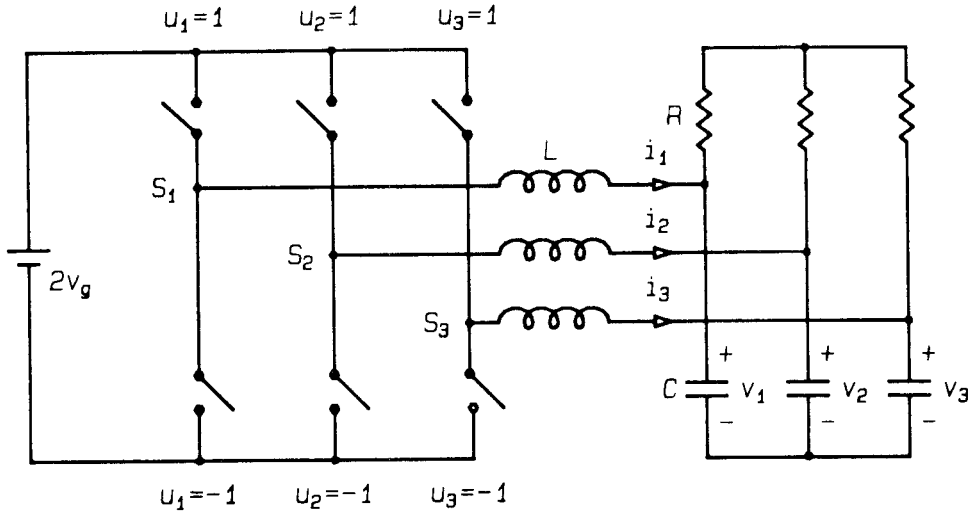

Figure 5.1: The buck inverter with three single-pole, double-throw switches. There are, however, only two independent controls that influence the output.

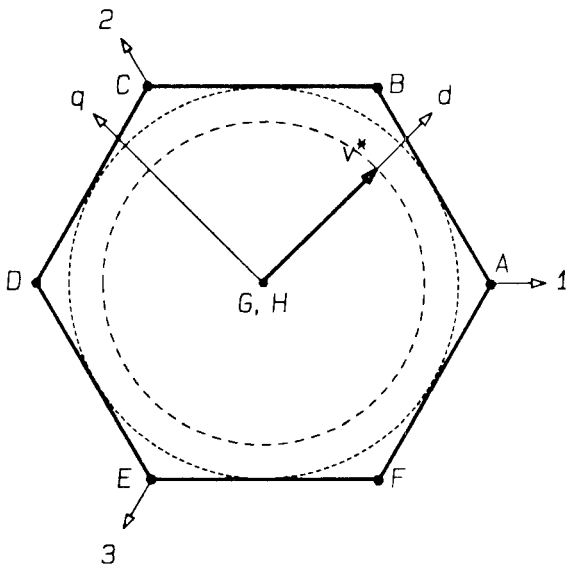

	u_1	u_2	u_3
A	1	−1	−1
B	1	1	−1
C	−1	1	−1
D	−1	1	1
E	−1	−1	1
F	1	−1	1
G	1	1	1
H	−1	−1	−1

Figure 5.2: The eight possible switch positions and corresponding steady-state output voltage phasors in the stationary abc reference frame. The outer circle in the phasor diagram represents the maximum output voltage amplitude that can be obtained.

tion in terms of the voltage error and its derivative is

$$\dot{\hat{\mathbf{x}}} = \mathbf{A}\,\hat{\mathbf{x}} + \mathbf{B}\,\mathbf{u} + \mathbf{T} \tag{5.2}$$

where

$$\mathbf{A} = \begin{bmatrix} 0 & 0 & 1 & 0 \\ 0 & 0 & 0 & 1 \\ -\omega_o^2 & 0 & -\omega_p & 0 \\ 0 & -\omega_o^2 & 0 & \omega_p \end{bmatrix} \quad , \quad \hat{\mathbf{x}} = \mathbf{x} - \mathbf{x}^* = \begin{bmatrix} \hat{v}_\alpha \\ \hat{v}_\beta \\ \dot{\hat{v}}_\alpha \\ \dot{\hat{v}}_\beta \end{bmatrix}$$

$$\mathbf{B} = \begin{bmatrix} 0 & 0 \\ 0 & 0 \\ \omega_o^2 v_g & 0 \\ 0 & \omega_o^2 v_g \end{bmatrix} \quad , \quad \mathbf{T} = \begin{bmatrix} 0 \\ 0 \\ (\omega_r^2 - \omega_o^2) v_d^* \cos(\theta_r) + \omega_r \omega_p v_d^* \sin(\theta_r) \\ (\omega_r^2 - \omega_o^2) v_d^* \cos(\theta_r) - \omega_r \omega_p v_d^* \sin(\theta_r) \end{bmatrix} \tag{5.3}$$

$$\mathbf{u} = \begin{bmatrix} u_\alpha \\ u_\beta \end{bmatrix} \quad , \quad \omega_o^2 = \frac{1}{LC} \quad , \quad \omega_p = \frac{1}{RC}$$

In the $\alpha\beta$ frame, the desired voltages v_α^*, v_β^* are cosine and sine functions with amplitude v_d^* and frequency ω_r.

In the dq axes, the system equations are

$$\dot{\tilde{\hat{\mathbf{x}}}} = \tilde{\mathbf{A}}\tilde{\hat{\mathbf{x}}} + \tilde{\mathbf{B}}\tilde{\mathbf{u}} + \tilde{\mathbf{T}} \tag{5.4}$$

where

$$\tilde{\mathbf{A}} = \begin{bmatrix} 0 & 0 & 1 & 0 \\ 0 & 0 & 0 & 1 \\ (\omega_r^2 - \omega_o^2) & \omega_r\omega_p & -\omega_p & 2\omega_r \\ -\omega_r\omega_p & (\omega_r^2 - \omega_o^2) & -2\omega_r & -\omega_p \end{bmatrix} \quad , \quad \hat{\tilde{\mathbf{x}}} = \tilde{\mathbf{x}} - \tilde{\mathbf{X}}^* = \begin{bmatrix} \hat{v}_d \\ \hat{v}_q \\ \dot{\hat{v}}_d \\ \dot{\hat{v}}_q \end{bmatrix}$$

$$\tilde{\mathbf{B}} = \mathbf{B} \quad , \quad \tilde{\mathbf{T}} = \begin{bmatrix} 0 \\ 0 \\ (\omega_r^2 - \omega_o^2)v_d^* \\ -\omega_r\omega_p v_d^* \end{bmatrix} \quad , \quad \tilde{\mathbf{u}} = \begin{bmatrix} u_d \\ u_q \end{bmatrix} \tag{5.5}$$

5.1.2 Sliding Surface

The sliding surfaces and controls can be implemented in either the $\alpha\beta$ or dq reference frame. The sliding surfaces are considered in the dq frame first as it is easier to see the similarity between the inverter and the corresponding dc-dc topology.

In the dq frame, the state space description of the system is seen to be similar to that of two cross-coupled dc-dc buck converters. Hence, sliding surfaces are chosen to be functions of the voltage errors and their derivatives. The two sliding surfaces used to determine the two independent controls are

$$\begin{aligned} \sigma_d &= \hat{v}_d + \tau\dot{\hat{v}}_d \\ \sigma_q &= \hat{v}_q + \tau\dot{\hat{v}}_q \end{aligned} \tag{5.6}$$

and are expressed in the more compact form

$$\tilde{\sigma} = \tilde{\mathbf{G}}\hat{\tilde{\mathbf{x}}} \tag{5.7}$$

where

$$\tilde{\mathbf{G}} = \begin{bmatrix} 1 & 0 & \tau & 0 \\ 0 & 1 & 0 & \tau \end{bmatrix} \quad , \quad \tilde{\sigma} = \begin{bmatrix} \sigma_d \\ \sigma_q \end{bmatrix} \tag{5.8}$$

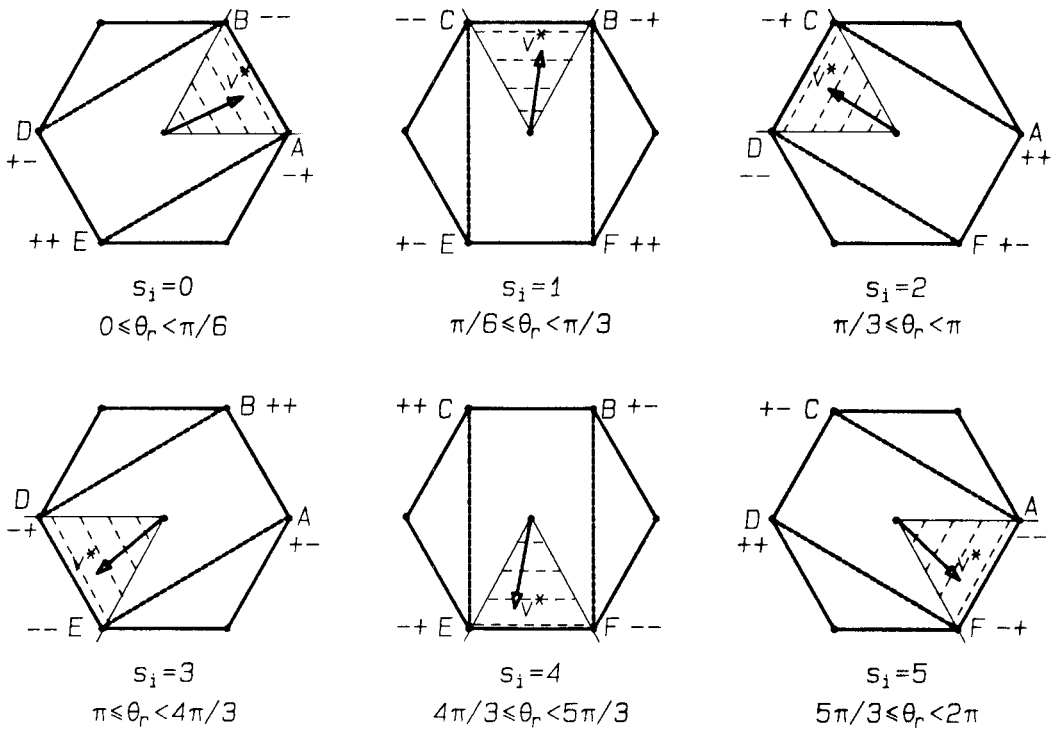

Figure 5.3: The choice of control input depends on the sector in which the desired reference voltage phasor lies, and on the signs of the functions σ_d and σ_q. The signs next to the switch position represent the signs of σ_d and σ_q for which it is chosen.

The signs of the error functions σ_d and σ_q are used to select the switch positions, as shown in Fig. 5.3. In the practical case, hysteresis is used to set the maximum switching frequency of the switches. The control inputs are

$$\tilde{\mathbf{u}} = \mathbf{Q}\mathbf{u}_s = \begin{bmatrix} \cos(\phi_r) & \sin(\phi_r) \\ -\sin(\phi_r) & \cos(\phi_r) \end{bmatrix} \begin{bmatrix} u_{sd} \\ u_{sq} \end{bmatrix} \tag{5.9}$$

where

$$u_{sd} = \begin{cases} +\sqrt{3/2} & ; \ \sigma_d < -\Delta_d \\ -\sqrt{3/2} & ; \ \sigma_d > +\Delta_d \end{cases}$$

$$u_{sq} = \begin{cases} +1/\sqrt{2} & ; \ \sigma_q < -\Delta_q \\ -1/\sqrt{2} & ; \ \sigma_q > +\Delta_q \end{cases} \tag{5.10}$$

$$\phi_r = \theta_r - [\pi/6 + (\pi/3)\, s_i] \ ; \ 0 \leq s_i \leq 5$$

The value of ϕ_r varies from $-\pi/6$ to $\pi/6$ for any sector s_i and consequently, the values of u_d and u_q are functions of time. The control input u_{sd} is determined by the sign of σ_d alone, and u_{sq} by σ_q alone, whereas, u_d and u_q are dependent on both σ_d and σ_q. For example, when the reference phasor lies in the sector BGA, the switch positions B, D, E, and A are used and the controls u_d and u_q are the projections of the corresponding control phasors on the d and q axes. The sliding surfaces described above are modified to provide protection by adding a current limiting segment to each sliding function.

Sliding functions of the same form can be used in the $\alpha\beta$ frame as well and are given by

$$\sigma = \mathbf{G}\hat{\mathbf{x}} \tag{5.11}$$

where

$$\sigma = \begin{bmatrix} \sigma_\alpha \\ \\ \sigma_\beta \end{bmatrix} \ , \ \mathbf{G} = \tilde{\mathbf{G}} \tag{5.12}$$

However, only four switch positions B, C, E, and F are used to obtain the control inputs u_α and u_β, as shown in Fig. 5.4. The control inputs are given by

$$\begin{aligned} u_\alpha &= \begin{cases} +1/\sqrt{2} & ; \ \sigma_\alpha < -\Delta_\alpha \\ -1/\sqrt{2} & ; \ \sigma_\alpha > +\Delta_\alpha \end{cases} \\ u_\beta &= \begin{cases} +\sqrt{3/2} & , \ \sigma_\beta < -\Delta_\beta \\ -\sqrt{3/2} & , \ \sigma_\beta > +\Delta_\beta \end{cases} \end{aligned} \tag{5.13}$$

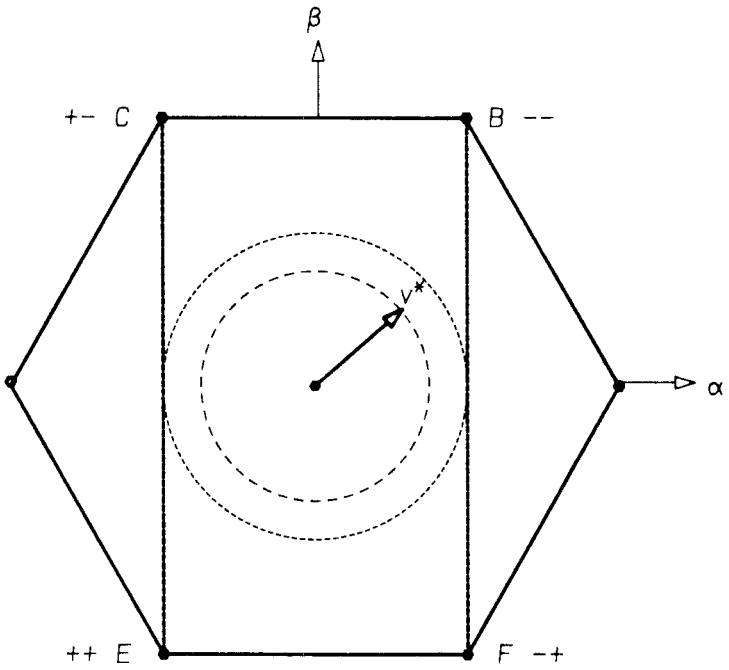

Figure 5.4: The choice of switch position depends on the signs of the error functions σ_α and σ_β. The control input does not depend on θ_r in this case. The outer circle represents the maximum output voltage amplitude possible using the four switch positions chosen.

The switch positions do not depend on θ_r, but as only four of the six outer positions are utilized, it is not possible to maintain sliding mode control for reference phasors that lie outside the inner circle. Thus, the output capabilities of the inverter will not be exploited to the full extent.

A third method is outlined that uses a combination of the above methods. This method is used in order to avoid the transformation of measured states to the dq frame, without forgoing the advantages available in the dq approach. The sliding surfaces are in terms of variables in the stationary two-phase $\alpha_i\beta_i$ co-ordinate frame, where $\alpha_i\beta_i$ depend on the sector s_i in which the reference phasor lies. The axes α_i, β_i, and the corresponding switch positions used, are shown in Fig. 5.5. Consequently, it is possible

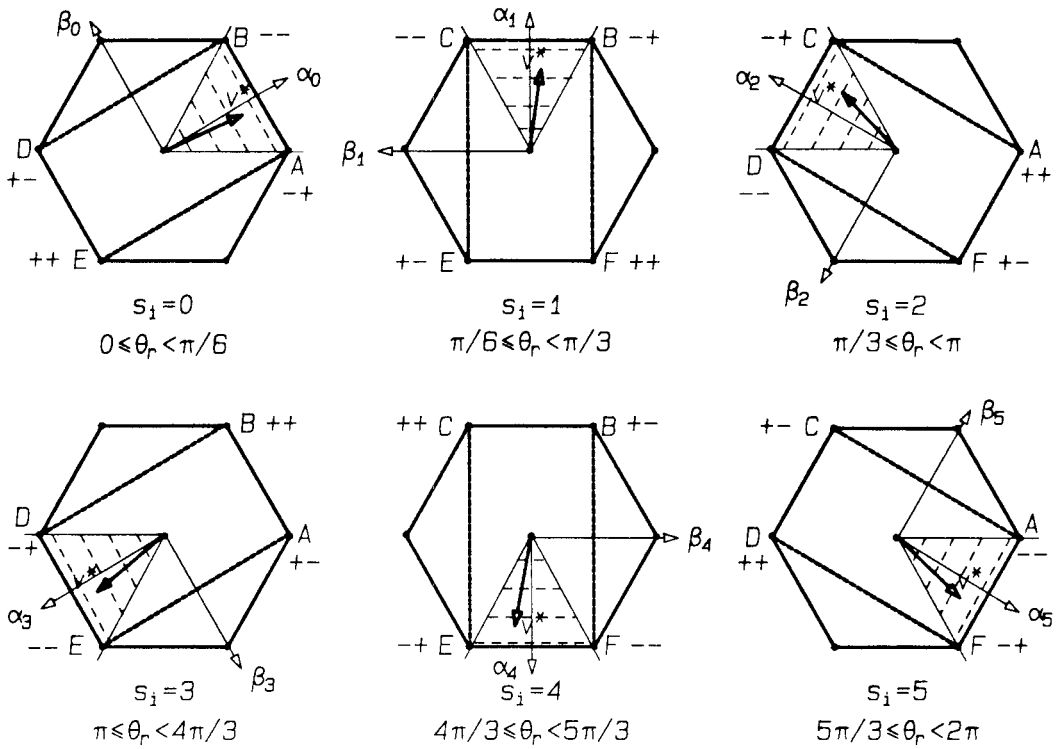

Figure 5.5: The $\alpha_i\beta_i$ axes and the control inputs which depend on the sector s_i in which the reference lies.

to maintain sliding mode control, under steady-state operation, over the operating range of the inverter.

5.1.3 Existence and Reaching Conditions

The conditions required for sliding motion to occur at the intersection of the discontinuity surfaces chosen are derived and the domain of sliding operation is obtained, in this subsection. The method of equivalent control provides a *necessary* condition that the sliding surfaces must satisy for sliding motion to occur. The *dq* axes method is considered first; the equivalent control $\tilde{\mathbf{u}}_{eq}$ is found from

$$\tilde{\sigma} = \mathbf{0} \quad \Rightarrow \quad \tilde{\mathbf{G}}\tilde{\mathbf{A}}\hat{\tilde{\mathbf{x}}} + \tilde{\mathbf{G}}\tilde{\mathbf{B}}\tilde{\mathbf{u}}_{eq} + \tilde{\mathbf{G}}\tilde{\mathbf{T}} = \mathbf{0} \tag{5.14}$$

Equation (5.14) can be used to find the domain of v_d^* over which the necessary condition is satisfied, for steady-state operation. If the inverter is in steady state at the desired operating point, then

$$\dot{\tilde{\mathbf{x}}} = \mathbf{0} \tag{5.15}$$

and the equivalent control must satisfy the inequalities

$$\begin{aligned} \min(u_{sd}^+, u_{sd}^-) \leq u_{sd_{eq}} \leq \max(u_{sd}^+, u_{sd}^-) \\ \min(u_{sq}^+, u_{sq}^-) \leq u_{sq_{eq}} \leq \max(u_{sq}^+, u_{sq}^-) \end{aligned} \tag{5.16}$$

Similar constraints exist for the other two methods as well. The constraints of Eq. (5.16) imply that the equivalent or average value of any control input must lie between the minimum and maximum instantaneous values that the control can assume. However, it only provides a *necessary* condition and cannot guarantee operation in the sliding mode. These conditions essentially represent the limitations set by the topology and correspond to the largest possible domain of outputs for the inverter. The best choice of sliding surfaces is one for which the above conditions are necessary and sufficient, and the sliding domain corresponds to the domain of operation of the converter.

It is not possible to obtain a *necessary and sufficient* condition in a general vector control system. However, it is possible to obtain sufficient conditions for certain special classes such as diagonal, or dominantly diagonal systems. The rate of change in the error function $\tilde{\sigma}$ is given by

$$\dot{\tilde{\sigma}} = \tilde{\mathbf{G}}\tilde{\mathbf{A}}\dot{\tilde{\mathbf{x}}} + \tilde{\mathbf{G}}\tilde{\mathbf{B}}\mathbf{Q}\mathbf{u}_s + \tilde{\mathbf{G}}\tilde{\mathbf{T}} \tag{5.17}$$

where

$$\begin{aligned} \tilde{\mathbf{G}}\tilde{\mathbf{A}} &= \begin{bmatrix} \tau(\omega_r^2 - \omega_o^2) & \tau\omega_r\omega_p & 1 - \tau\omega_p & 2\omega_r\tau \\ -\tau\omega_r\omega_p & \tau(\omega_r^2 - \omega_p^2) & -2\omega_r\tau & 1 - \omega_p\tau \end{bmatrix} \\ \tilde{\mathbf{G}}\tilde{\mathbf{B}}\mathbf{Q} &= \omega_o^2\tau v_g \begin{bmatrix} \cos(\phi_r) & \sin(\phi_r) \\ -\sin(\phi_r) & \cos(\phi_r) \end{bmatrix}, \quad \tilde{\mathbf{G}}\tilde{\mathbf{T}} = \begin{bmatrix} \tau(\omega_r^2 - \omega_o^2) \\ -\tau\omega_r\omega_p \end{bmatrix} \end{aligned} \tag{5.18}$$

It is noted that the matrix $\tilde{\mathbf{G}}\tilde{\mathbf{B}}\mathbf{Q}$ in Eq. (5.17) is not a diagonal one but is diagonally dominant, and sufficient conditions for the existence of sliding motion cannot be obtained easily from Eq. (5.17) without being unduly conservative. The sliding functions $\tilde{\sigma}$ are transformed to σ^* using the nonsingular linear transformation $\mathbf{Q}^T$:

$$\sigma^* = \mathbf{Q}^T\tilde{\sigma} \tag{5.19}$$

where $\mathbf{Q}$ is defined by Eq. (5.9). In the vicinity of the sliding manifold $\tilde{\sigma} = 0$, the system behavior can be expressed by

$$\dot{\sigma}^* = \mathbf{Q}^T\tilde{\mathbf{G}}\tilde{\mathbf{A}}\hat{\tilde{\mathbf{x}}} + \mathbf{Q}^T\tilde{\mathbf{G}}\tilde{\mathbf{T}} + \mathbf{Q}^T\tilde{\mathbf{G}}\tilde{\mathbf{B}}\mathbf{Q}\mathbf{u}_s + O(\sigma^*) \tag{5.20}$$

provided $\| \dot{\mathbf{Q}} \|$ is bounded. The matrix multiplying the control $\mathbf{u}_s$ is diagonal in this case, and *sufficient* conditions for the existence of sliding motion can be found by considering the system to be similar to two scalar input sliding mode problems.

Let $\mathbf{f}$ and $\mathbf{D}$ be defined by

$$\begin{aligned} \mathbf{f} &= \mathbf{Q}^T\tilde{\mathbf{G}}\tilde{\mathbf{A}}\hat{\tilde{\mathbf{x}}} + \mathbf{Q}^T\tilde{\mathbf{G}}\tilde{\mathbf{T}} \\ \mathbf{D} &= \mathbf{Q}^T\tilde{\mathbf{G}}\tilde{\mathbf{B}}\mathbf{Q} \end{aligned} \tag{5.21}$$

where

$$\mathbf{D} = \begin{bmatrix} \tau\omega_o^2 v_g & 0 \\ 0 & \tau\omega_o^2 v_g \end{bmatrix} \quad , \quad \mathbf{f} = \begin{bmatrix} f_d(\hat{\tilde{\mathbf{x}}}, v_d^*) \\ f_q(\hat{\tilde{\mathbf{x}}}, v_d^*) \end{bmatrix} \tag{5.22}$$

Sufficient conditions for sliding motion to exist in a domain S on the sliding manifold $\tilde{\sigma} = 0$ are given by

$$\begin{aligned} \tau\omega_o^2 v_g\, u_{sd}^+ &< -f_d(\hat{\tilde{\mathbf{x}}}, v_d^*) \\ \tau\omega_o^2 v_g\, u_{sd}^- &> -f_d(\hat{\tilde{\mathbf{x}}}, v_d^*) \\ \tau\omega_o^2 v_g\, u_{sq}^+ &< -f_q(\hat{\tilde{\mathbf{x}}}, v_d^*) \\ \tau\omega_o^2 v_g\, u_{sq}^- &> -f_q(\hat{\tilde{\mathbf{x}}}, v_d^*) \end{aligned} \tag{5.23}$$

The parameters of the sliding line, and the reference phasor, have to satisfy the conditions

$$\begin{aligned} & 1-\tau\omega_p > 0 \quad \Rightarrow \quad \tau > RC \\ & v_d^* < \frac{\sqrt{3/2}\, v_g}{H(\omega_r)|\cos\{\phi_r + \phi(\omega_r)\}|} \\ & v_d^* < \frac{\sqrt{1/2}\, v_g}{H(\omega_r)|\sin\{\phi_r + \phi(\omega_r)\}|} \end{aligned} \tag{5.24}$$

where

$$\begin{aligned} & -\pi/6 \le \phi_r \le \pi/6 \\ & H(\omega_r) = \sqrt{(1-\omega_r^2/\omega_o^2)^2 + (\omega_r\omega_p/\omega_o^2)^2} \\ & \phi(\omega_r) = \arctan\left\{\frac{\omega_r\omega_p/\omega_o^2}{1-\omega_r^2/\omega_o^2}\right\} \end{aligned} \tag{5.25}$$

The inequalities of Eq. (5.23) do not ensure that the system will reach the sliding manifold, from any arbitrary initial condition, because they were obtained using an approximation of Eq. (5.20) when the state of the system is in the vicinity of the sliding manifold. Knowledge of the physical structure of the system suggests that the system will be able to reach the sliding manifold from any point in the state space that lies within the operating range of the converter.

Methods two and three can be analyzed in a similar way . The transformed dq functions of Eq. (5.20) are identical to the system representation for the method using $\alpha_i\beta_i$ axes, with the last term $O(\sigma^*)$ equal to zero; i.e., the approximation used is now exact and the conditions of Eq. (5.23) ensure that the system reaches the sliding manifold. In the second method described only four switch positions are used and the existence and reaching conditions are

$$\begin{aligned} & \tau > RC \\ & v_d^* < \frac{\sqrt{1/2} v_g}{H(\omega_r)} \end{aligned} \tag{5.26}$$

5.1.4 Stability of System in Sliding Mode

The sliding manifold should be such that the system is asymptotically stable when the system is maintained on the sliding line. The stable operating point on the sliding surface should also correspond to the reference applied to the system. The stability and equilibrium points are determined by setting $\tilde{\sigma} = \mathbf{0}$ and finding the motion of the system under this constraint. In the general case, this is done by substituting $\tilde{\mathbf{u}}_{eq}$ obtained from Eq. (5.14) for $\tilde{\mathbf{u}}$ in Eq. (5.4) and analyzing the resulting system.

For the sliding surfaces chosen in Section 5.1.2, the stability of the system in sliding mode can be determined directly from the constraint $\tilde{\sigma} = \mathbf{0}$. This results in the following description for the system motion:

$$\begin{aligned} \hat{\tilde{v}}_d + \tau \dot{\hat{\tilde{v}}}_d &= 0 \\ \hat{\tilde{v}}_q + \tau \dot{\hat{\tilde{v}}}_q &= 0 \end{aligned} \tag{5.27}$$

The system of Eq. (5.27) is asymptotically stable for $\tau > 0$ and the origin is the stable equilibrium point. Hence, the system will reach the desired operating point set by reference v_d^*, if the sliding mode conditions are satisfied.

5.1.5 Practical Implementation of Sliding Surfaces

In Section 5.1.2 three sets of sliding surfaces and control strategies for the buck inverter were described. In all cases, the sliding function was expressed as a function of the error voltages and their derivatives. In practice, these sliding surfaces are implemented by measuring the output voltages and capacitor currents and are expressed in a more

suitable form.

Method 1 :

$$\sigma_d = v_d - v_d^* + \tau \dot{v}_d$$
$$\sigma_q = v_q + \tau \dot{v}_q \tag{5.28}$$

Method 2 :

$$\sigma_\alpha = v_\alpha - v_\alpha^* + \tau \dot{v}_\alpha - \tau \dot{v}_\alpha^*$$
$$\sigma_\beta = v_\beta - v_\beta^* + \tau \dot{v}_\beta - \tau \dot{v}_\beta^*$$

The derivative of the output voltages can be found by measuring the capacitor currents and tranforming to the desired reference frame. The function σ_d does not contain a term dependent on $\dot{v}_d^*$ because it is zero for steady-state operation. In the $\alpha\beta$ frame, the derivatives of the references are nonzero and cannot be omitted without affecting the performance of the closed loop system. However, it is possible to use the sliding functions

$$\sigma_\alpha = v_\alpha - v_\alpha^* + \tau \dot{v}_\alpha$$
$$\sigma_\beta = v_\beta - v_\beta^* + \tau \dot{v}_\beta \tag{5.29}$$

and the same existence conditions must be satisfied. In this case, however, the response from the reference to the output is

$$\frac{v_\alpha(s)}{v_\alpha^*(s)} = \frac{1}{1+s\tau}$$
$$\frac{v_\beta(s)}{v_\beta^*(s)} = \frac{1}{1+s\tau} \tag{5.30}$$

when the system is operating in sliding mode. This implies that there will be an amplitude error and phase offset between the reference and the output. This error can be made small if the inversion frequency is small compared to the bandwidth $1/\tau$ of the sliding mode system. However, it is difficult to ensure analytically that the system will remain in the sliding manifold, at all instants of the inversion cycle, as the reference voltages vary. Qualitatively, the above-mentioned constraint on the inversion frequency should be

i	Sector	$\sqrt{2}\,x_{\alpha_i}$	$\sqrt{3/2}\,x_{\beta_i}$
0	$0 \leq \theta_r < \pi/3$	$x_1 - x_3$	x_2
1	$\pi/3 \leq \theta_r < 2\pi/3$	$x_2 - x_3$	$-x_1$
2	$2\pi/3 \leq \theta_r < \pi$	$x_2 - x_1$	x_3
3	$\pi \leq \theta_r < 4\pi/3$	$x_3 - x_1$	$-x_2$
4	$4\pi/3 \leq \theta_r < 5\pi/3$	$x_3 - x_2$	x_1
5	$5\pi/3 \leq \theta_r < 2\pi$	$x_1 - x_2$	$-x_3$

Table 5.1: Approximation of dq method using components of the vector in the different $\alpha_i\beta_i$ frames depending on the sector, using phase and line components of the vector in the stationary reference frame.

sufficient to ensure that the system remains in the sliding manifold at all times, when in steady-state operation.

The third method described in Section 5.1.2 uses the different axes $\alpha_i\beta_i$ in each sector to approximate the dq components in each sector. The transformations to the $\alpha_i\beta_i$ reference frames are easy to implement as the components can be obtained by choosing the right phase and line voltages in the stationary reference frame, in each sector. Table 5.1 enumerates the choices of the line and phase voltages or currents that are used in the different sectors. In this way the transformation of the states to the dq axes is avoided and the controller is realized using less hardware. It is also possible to use the phase voltages and currents directly and to choose the inputs appropriately, depending on the sector in which the reference lies. Though approximate, this method is very easy to implement and results in reasonably good system performance. The reference voltages required are still sinusoidal in nature, and their derivatives can be obtained by passing the references through a high-pass prefilter, or be omitted from the sliding lines, as in

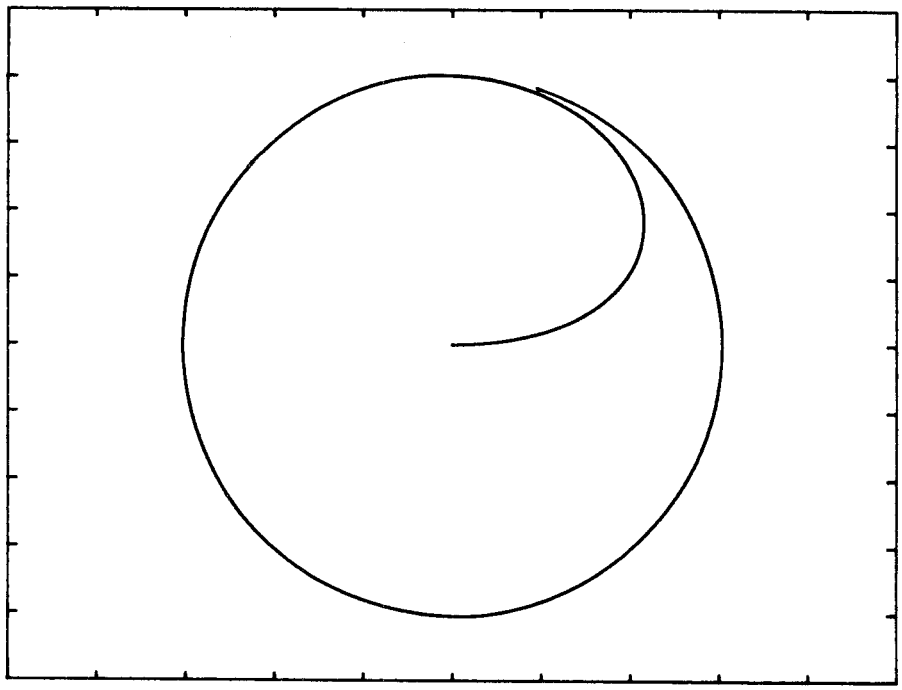

Figure 5.6: The output voltage phasor in the $\alpha\beta$ axes with sliding surfaces in the dq reference frame. In steady state, the locus of the vector is a circle.

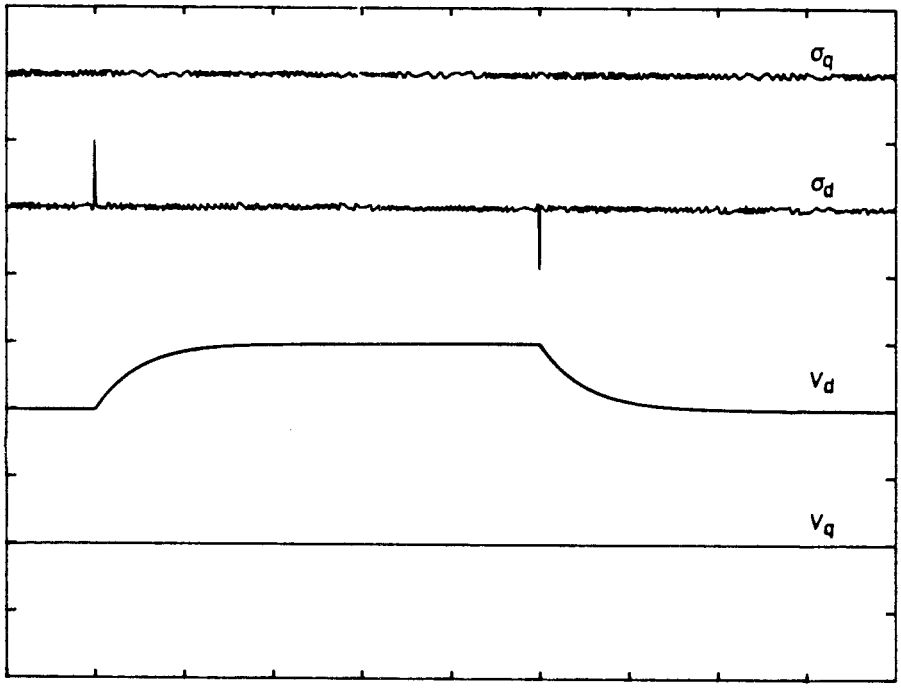

Figure 5.7: The step response of the components v_d and v_q to a change in the reference v_d^* for the system using sliding surfaces in the dq reference frame.

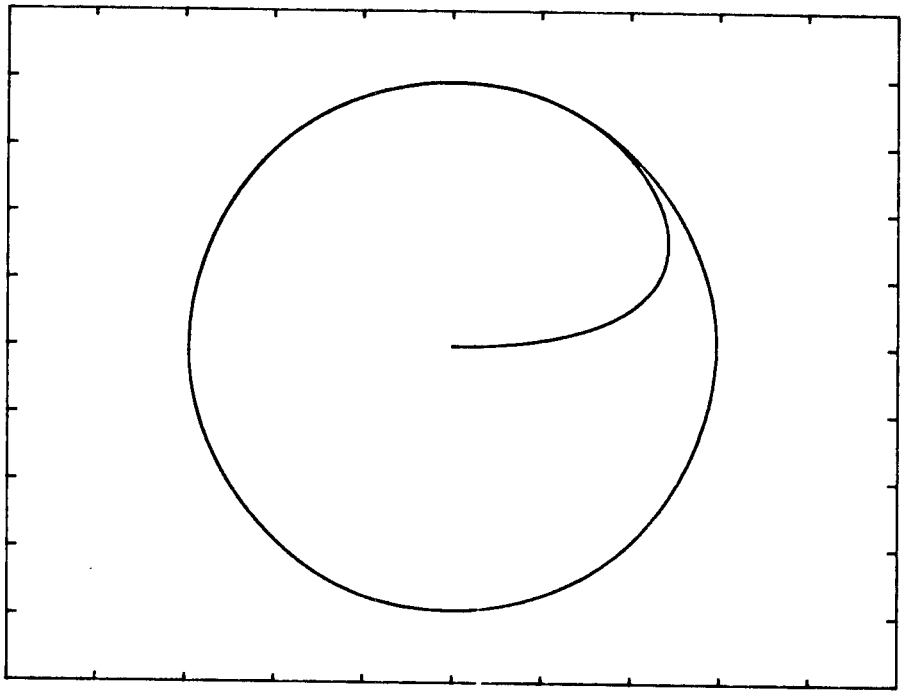

Figure 5.8: The output voltage phasor in the $\alpha\beta$ frame for the system using sliding surfaces in the stationary abc reference frame.

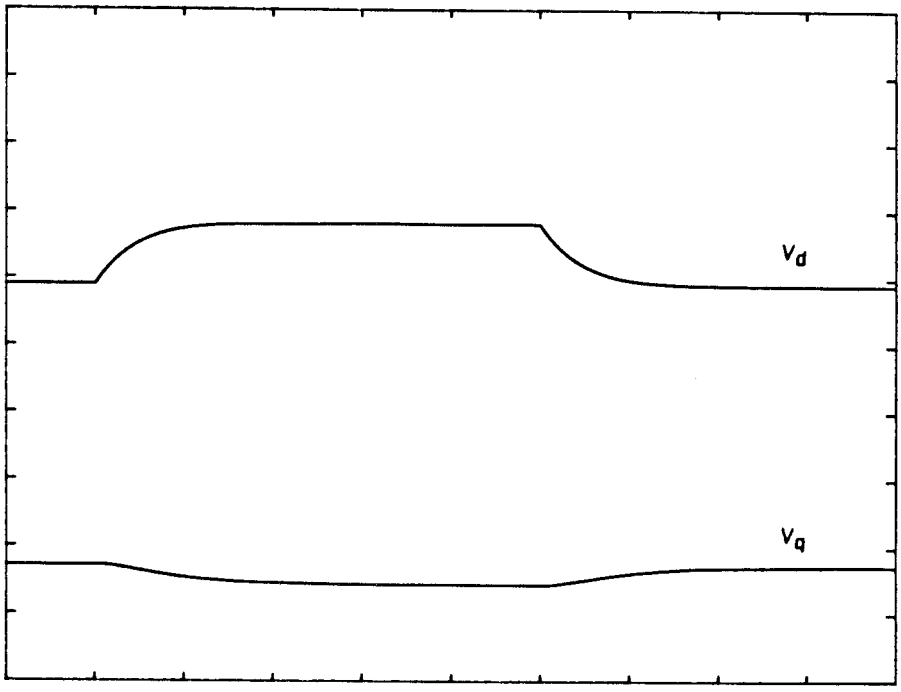

Figure 5.9: Response of the abc sliding mode system to a step change in the amplitude of the reference voltage.

the $\alpha\beta$ method.

5.1.6 Simulation Results

In this subsection, simulation results are presented for some of the methods of sliding mode control described for the buck inverter. The method utilizing the sliding lines in the dq frame and the approximate method using the stationary abc reference frame, are considered. Figure 5.6 shows the output voltage phasor in the $\alpha\beta$ frame, and Fig. 5.7 the response of the system to a step change in the reference v_d^*, for the system using sliding mode in the dq reference frame. Figures 5.8 and 5.9 show the corresponding results for the approximate method implemented in the stationary abc frame.

5.2 Boost Inverter

The boost inverter contains two single-pole, triple-throw switches as shown in Fig. 5.10, and the controls u_w assume values $+1$, -1, and 0 depending on the positions of the switches S_1 and S_2. The topology constrains the three controls to sum to zero; hence, there are only two independent controls available to control the balanced three phase outputs. The control inputs and the resultant current phasors are shown in Fig. 5.11.

The boost inverter is a current-fed topology and the switches control the current that is fed to the output section. The current phasor feeding the output phasor can assume seven discrete positions, the amplitude being determined by the magnitude of the inductor current. Any average current phasor that lies within the hexagon described by the six nonzero control positions can be attained by switching rapidly between these controls. The output current amplitude is consequently smaller than the inductor or input current, and the topology provides current step-down and voltage step-up. This determines the domain of operation of the inverter.

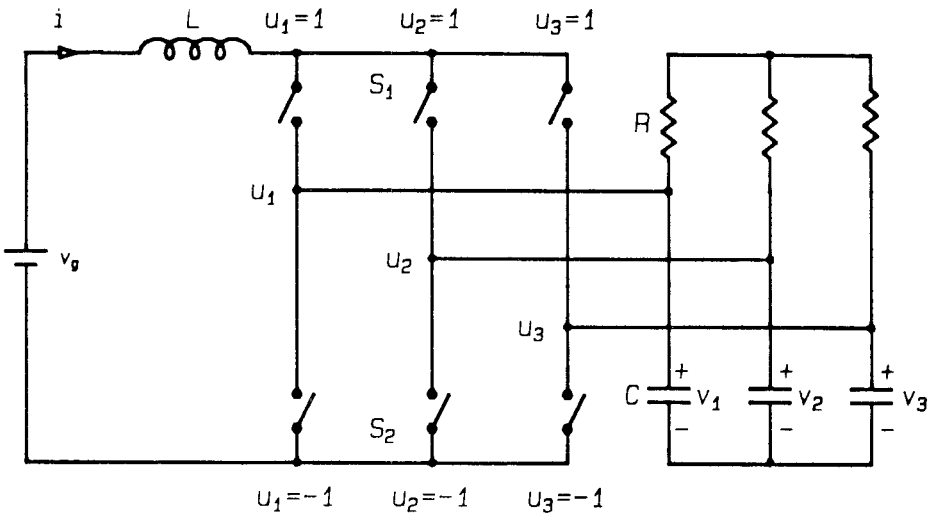

Figure 5.10: Three phase boost inverter with two single-pole, triple-throw switches.

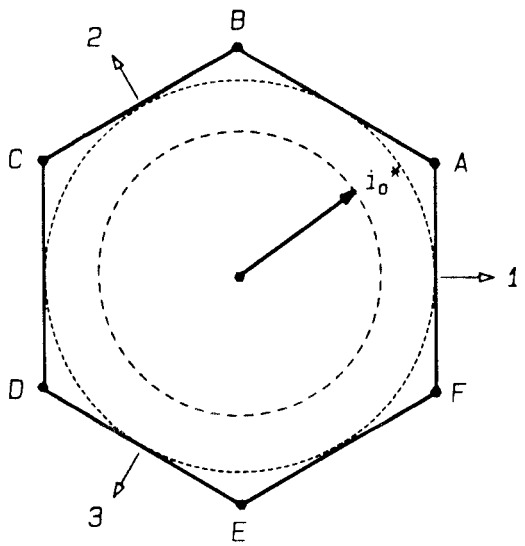

	u_1	u_2	u_3
A	1	0	-1
B	0	1	-1
C	-1	1	0
D	-1	0	1
E	0	-1	1
F	1	-1	0

Figure 5.11: The seven possible controls and the corresponding phasor of the current feeding the output sections. The amplitude of the phasors depends on the value of the inductor current.

5.2.1 System Description

The boost topology, being current-fed, results in pulsating currents in the output capacitors. The state space description of the system in the stationary reference frame is expressed in terms of the inductor current and capacitor voltages by

$$\begin{aligned} L\dot{i} &= v_g - \sum_{w=1}^{3} u_w v_w \\ C\dot{v}_w &= i\, u_w - \frac{1}{R} v_w + \frac{1}{3R} \sum_{z=1}^{3} v_z \end{aligned} \tag{5.31}$$

In the dq frame, the boost inverter is described by

$$\dot{\tilde{\mathbf{x}}} = \tilde{\mathbf{A}}\,\tilde{\mathbf{x}} + \tilde{\mathbf{B}}\,\tilde{\mathbf{u}} + \tilde{\mathbf{T}}_1 \tag{5.32}$$

where

$$\begin{aligned} \tilde{\mathbf{A}} &= \begin{bmatrix} 0 & 0 & 0 \\ 0 & -\omega_p & \omega_r \\ 0 & -\omega_r & -\omega_p \end{bmatrix} \quad , \quad \tilde{\mathbf{x}} = \begin{bmatrix} i \\ v_d \\ v_q \end{bmatrix} \\ \tilde{\mathbf{B}} &= \begin{bmatrix} -v_d/L & -v_q/L \\ i/C & 0 \\ 0 & i/C \end{bmatrix} \quad , \quad \tilde{\mathbf{T}}_1 = \begin{bmatrix} v_g/L \\ 0 \\ 0 \end{bmatrix} \\ \tilde{\mathbf{u}} &= \begin{bmatrix} u_d \\ u_q \end{bmatrix} \quad , \quad \omega_p = \frac{1}{RC} \end{aligned} \tag{5.33}$$

The desired outputs v_d^* and v_q^* determine the required operating point $\tilde{\mathbf{x}}^*$. In steady state, the desired operating point

$$\tilde{\mathbf{X}}^* = \begin{bmatrix} i^* \\ v_d^* \\ v_q^* \end{bmatrix} \tag{5.34}$$

consists of components that are dc in nature. The reference v_q^* is chosen to be zero by proper choice of θ_r and i^* is related to v_d^* by

$$i^* = \frac{v_d^{*2}}{v_g R} \tag{5.35}$$

Let $\hat{\tilde{\mathbf{x}}}$ represent the error in the states from the desired operating point $\tilde{\mathbf{X}}^*$. Then the system is described by

$$\dot{\hat{\tilde{\mathbf{x}}}} = \tilde{\mathbf{A}}\,\hat{\tilde{\mathbf{x}}} + \tilde{\mathbf{B}}\,\tilde{\mathbf{u}} + \tilde{\mathbf{T}} \tag{5.36}$$

where

$$\hat{\tilde{\mathbf{x}}} = \tilde{\mathbf{x}} - \tilde{\mathbf{X}}^* \quad , \quad \tilde{\mathbf{T}} = \begin{bmatrix} v_g/L \\ -\omega_p v_d^* \\ -\omega_r v_q^* \end{bmatrix} \tag{5.37}$$

The corresponding description in the $\alpha\beta$ reference frame is

$$\dot{\hat{\mathbf{x}}} = \mathbf{A}\,\hat{\mathbf{x}} + \mathbf{B}\,\mathbf{u} + \mathbf{T} \tag{5.38}$$

where

$$\mathbf{A} = \begin{bmatrix} 0 & 0 & 0 \\ 0 & -\omega_p & 0 \\ 0 & 0 & -\omega_p \end{bmatrix} \quad , \quad \hat{\mathbf{x}} = \begin{bmatrix} \hat{i} \\ \hat{v}_\alpha \\ \hat{v}_\beta \end{bmatrix} \quad , \quad \mathbf{u} = \begin{bmatrix} u_\alpha \\ u_\beta \end{bmatrix}$$

$$\mathbf{B} = \begin{bmatrix} -v_\alpha/L & -v_\beta/L \\ i/C & 0 \\ 0 & i/C \end{bmatrix} \quad , \quad \mathbf{T} = \begin{bmatrix} v_g/L \\ -\omega_p H(\omega_r) v_d^* \cos\{\theta_r + \phi(\omega_r)\} \\ -\omega_p H(\omega_r) v_d^* \sin\{\theta_r + \phi(\omega_r)\} \end{bmatrix} \tag{5.39}$$

$$\omega_p = \frac{1}{RC} \quad , \quad H(\omega_r) = \sqrt{1 + \omega_r^2/\omega_p^2} \quad , \quad \phi(\omega_r) = \arctan(\frac{\omega_r}{\omega_p})$$

5.2.2 Sliding Surface

Sliding mode control of the boost inverter can be implemented in the $\alpha\beta$ or dq reference frame. Sliding surfaces in the dq reference frame are considered first because of

the dc nature of all steady-state quantities in this reference frame. The sliding surfaces chosen are

$$\begin{aligned} \sigma_d &= \hat{v}_d + R_s \hat{i} \\ \sigma_q &= \hat{v}_q \end{aligned} \tag{5.40}$$

and written in the form

$$\tilde{\sigma} = \tilde{\mathbf{G}}\,\hat{\tilde{\mathbf{x}}} \tag{5.41}$$

where

$$\tilde{\sigma} = \begin{bmatrix} \sigma_d \\ \sigma_q \end{bmatrix} \quad , \quad \tilde{\mathbf{G}} = \begin{bmatrix} R_s & 1 & 0 \\ 0 & 0 & 1 \end{bmatrix} \tag{5.42}$$

In Eq. (5.36), it is noted that if u_q is chosen to constrain v_q to be small in magnitude, then the system effectively separates into two parts, which are linked by the inductor current alone. Hence, v_d and i can be controlled using u_d in a manner similar to a boost dc-dc converter, and v_q is like a disturbance to this loop. This loop also sets the necessary current in the inductor, which enables u_q to control v_q and reduce it to zero. Thus, the goal is to reduce the design of the system to the design of two single input sliding mode systems.

The switch positions are chosen using the signs of the errors in the sliding functions and the position θ_r of the reference phasor, as shown in Fig. 5.12. The control inputs are

$$\tilde{\mathbf{u}} = \mathbf{Q}\,\mathbf{u}_s = \begin{bmatrix} \cos(\phi_r) & \sin(\phi_r) \\ -\sin(\phi_r) & \cos(\phi_r) \end{bmatrix} \begin{bmatrix} u_{sd} \\ u_{sq} \end{bmatrix} \tag{5.43}$$

where

$$\begin{aligned} u_{sd} &= \begin{cases} +\sqrt{3/2} & ; \quad \sigma_d > +\Delta_d \\ -\sqrt{3/2} & ; \quad \sigma_d < -\Delta_d \end{cases} \\ u_{sq} &= \begin{cases} +1/\sqrt{2} & ; \quad \sigma_q < -\Delta_q \\ -1/\sqrt{2} & ; \quad \sigma_q > +\Delta_q \end{cases} \\ \phi_r &= \theta_r - (\pi/3)s_i \quad ; \quad 0 \le s_i \le 5 \end{aligned} \tag{5.44}$$

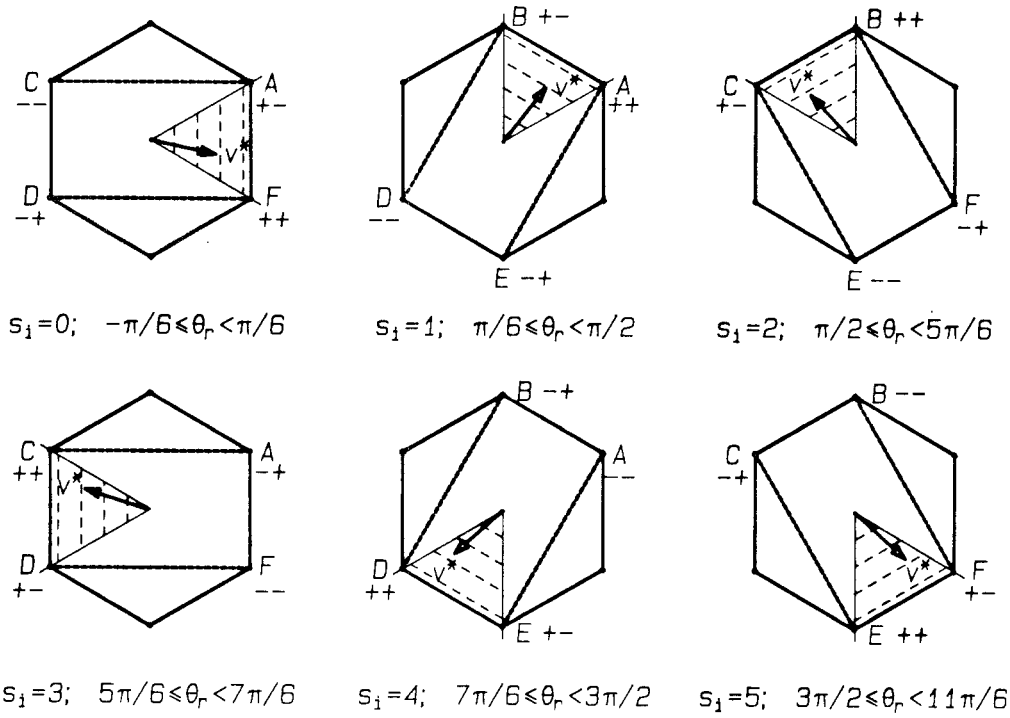

Figure 5.12: The choice of switch positions is based on the signs of the error functions σ_d, σ_q, and on the sector in which the reference voltage phasor lies.

This switching strategy is similar to that used for the buck inverter, except for the definition of the sectors. The magnitude of the control $|u_d|$ varies between $\sqrt{3/2}$ and $1/\sqrt{2}$ in each sector, while $|u_q|$ changes between $1/\sqrt{2}$ and 0.

Transformation to the dq reference frame can be avoided using $\alpha_i\beta_i$ reference frames for sliding control. The sliding functions in this method are obtained directly from measured quantities in the stationary three phase reference frame. The transformation to the $\alpha_i\beta_i$ frames is shown in Table 5.2. The sliding surfaces used in each sector are

$$\sigma_i = \mathbf{G}\,\hat{\mathbf{x}}_i \quad ; \quad 0 \leq s_i \leq 5 \tag{5.45}$$

i	Sector	$\sqrt{2/3}\,x_{\alpha_i}$	$\sqrt{2}\,x_{\beta_i}$
0	$-\pi/6 \leq \theta_r < \pi/6$	x_1	$x_2 - x_3$
1	$\pi/6 \leq \theta_r < \pi/2$	$-x_3$	$x_2 - x_1$
2	$\pi/2 \leq \theta_r < 5\pi/6$	x_2	$x_3 - x_1$
3	$5\pi/6 \leq \theta_r < 7\pi/6$	$-x_1$	$x_3 - x_2$
4	$7\pi/6 \leq \theta_r < 9\pi/6$	x_3	$x_1 - x_2$
5	$9\pi/6 \leq \theta_r < 11\pi/6$	$-x_2$	$x_1 - x_3$

Table 5.2: Components of a vector in the $\alpha_i\beta_i$ frames depending on the sector in which θ_r lies.

where

$$\sigma_i = \begin{bmatrix} \sigma_{\alpha_i} \\ \sigma_{\beta_i} \end{bmatrix} \quad ; \quad \hat{\mathbf{x}}_i = \begin{bmatrix} \hat{i} \\ \hat{v}_{\alpha_i} \\ \hat{v}_{\beta_i} \end{bmatrix} \quad ; \quad \mathbf{G} = \tilde{\mathbf{G}} \tag{5.46}$$

The $\alpha_i\beta_i$ axes and the switch positions utilized are depicted in Fig. 5.13. In each sector s_i the control u_{α_i} and u_{β_i} are chosen according to

$$u_{\alpha_i} = \begin{cases} +\sqrt{3/2} \; ; \; \sigma_{\alpha_i} > +\Delta_\alpha \\ -\sqrt{3/2} \; ; \; \sigma_{\alpha_i} < -\Delta_\alpha \end{cases}$$
$$u_{\beta_i} = \begin{cases} +1/\sqrt{2} \; ; \; \sigma_{\beta_i} < -\Delta_\beta \\ -1/\sqrt{2} \; ; \; \sigma_{\beta_i} > +\Delta_\beta \end{cases} \tag{5.47}$$

5.2.3 Existence and Reaching Conditions

The necessary conditions for the existence of sliding motion on the discontinuity surfaces of Eq. (5.41) are found using the conditions of Eq. (5.16) on the equivalent control calculated from Eq. (5.14). This results in the following necessary conditions for

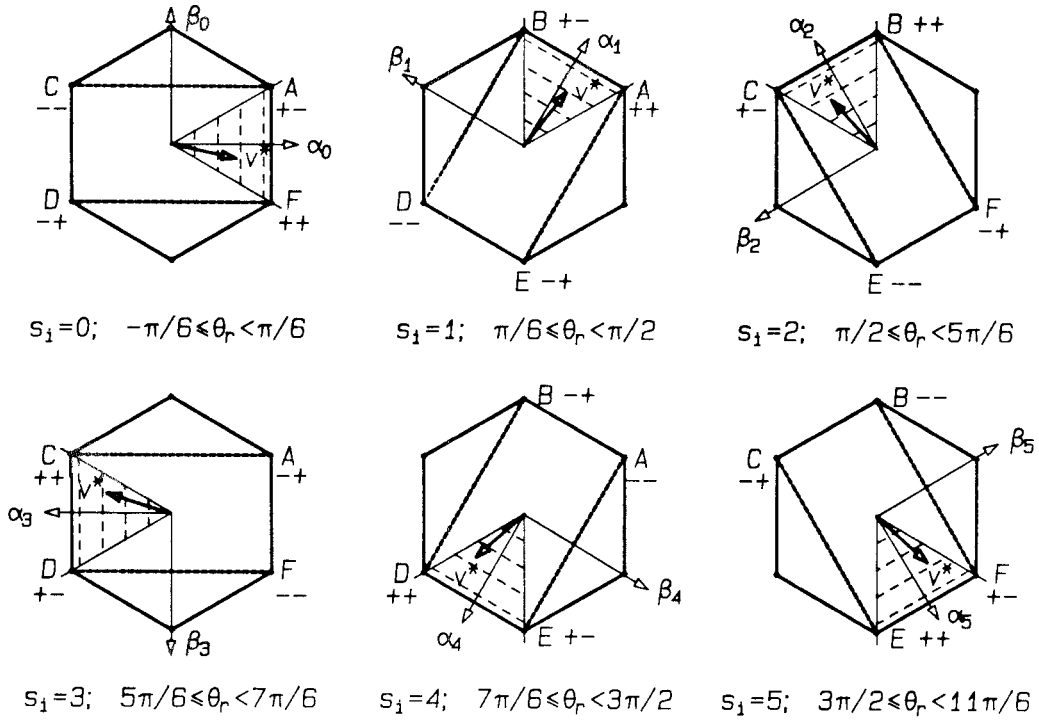

$s_i=0;\quad -\pi/6 \leq \theta_r < \pi/6$ $\qquad$ $s_i=1;\quad \pi/6 \leq \theta_r < \pi/2$ $\qquad$ $s_i=2;\quad \pi/2 \leq \theta_r < 5\pi/6$

$s_i=3;\quad 5\pi/6 \leq \theta_r < 7\pi/6$ $\qquad$ $s_i=4;\quad 7\pi/6 \leq \theta_r < 3\pi/2$ $\qquad$ $s_i=5;\quad 3\pi/2 \leq \theta_r < 11\pi/6$

Figure 5.13: The $\alpha_i\beta_i$ axes and the corresponding switch positions for the sliding mode control of the boost inverter.

the boost inverter:

$$\begin{aligned} v_d^* &> \sqrt{\tfrac{2}{3}}\, v_g \\ \frac{\omega_r}{\omega_p} &< \frac{1}{\sqrt{2}} \frac{v_d^*}{v_g} \end{aligned} \tag{5.48}$$

The same constraints are required if sliding control is implemented using the $\alpha_i\beta_i$ method.

The rate of change in the sliding functions is given by

$$\dot{\tilde{\sigma}} = \tilde{\mathbf{G}}\tilde{\mathbf{A}}\hat{\tilde{\mathbf{x}}} + \tilde{\mathbf{G}}\tilde{\mathbf{B}}\tilde{\mathbf{u}} + \tilde{\mathbf{G}}\tilde{\mathbf{T}} \tag{5.49}$$

where

$$\tilde{\mathbf{G}}\tilde{\mathbf{A}} = \begin{bmatrix} 0 & -\omega_p & \omega_r \\ 0 & -\omega_r & -\omega_p \end{bmatrix}$$

$$\tilde{\mathbf{G}}\tilde{\mathbf{B}} = \begin{bmatrix} i/C - R_s v_d/L & -R_s v_q/L \\ 0 & i/C \end{bmatrix} \quad , \quad \tilde{\mathbf{G}}\tilde{\mathbf{T}} = \begin{bmatrix} R_s v_g/L - \omega_p v_d^* \\ -\omega_r v_d^* \end{bmatrix} \tag{5.50}$$

The matrix $\tilde{\mathbf{G}}\tilde{\mathbf{B}}$ in Eq. (5.49) is an upper triangular one, and the method of hierarchy of controls[20] is used to examine the existence and reaching conditions for sliding motion on the surfaces of Eq. (5.41). The term dependent on u_q, in the equation describing $\dot{\sigma}_d$, is like a disturbance to the sliding motion along σ_d. However, if the magnitude of v_q is small, the control u_d can ensure sliding motion on σ_d regardless of the instantaneous value assumed by u_q. Consequently, the sliding motion along σ_d is very similar to that of a dc-dc boost converter in the presence of a disturbance. The control u_d establishes the required current in the inductor and u_q utilizes it to provide sliding motion along σ_q. However, at the boundary of each sector, $|u_q|$ goes to zero for two of the switch positions used, and sliding motion does not occur on σ_q when θ_r is in the vicinity of the sector boundary. Hence, sliding motion does not exist on each individual surface at all times. However, in practice, sliding motion occurs at the intersection of the sliding surfaces even when θ_r is in the vicinity of the sector boundary, but sufficient conditions for its existence cannot be obtained easily.

The time derivatives of the sliding functions in the $\alpha_i\beta_i$ axes are given by

$$\dot{\sigma} = \mathbf{GA}\hat{\mathbf{x}} + \mathbf{GBu} + \mathbf{GT} \tag{5.51}$$

where

$$\mathbf{GA} = \begin{bmatrix} 0 & -\omega_p & 0 \\ 0 & 0 & -\omega_p \end{bmatrix} \quad , \quad \mathbf{GB} = \begin{bmatrix} i/C - R_s v_\alpha/L & -R_s v_\beta/L \\ 0 & i/C \end{bmatrix}$$

$$\mathbf{GT} = \begin{bmatrix} R_s v_g/L - \omega_p H(\omega_r) v_d^* \cos\{\phi_r + \phi(\omega_r)\} \\ -\omega_p H(\omega_r) v_d^* \sin\{\phi_r + \phi(\omega_r)\} \end{bmatrix} \quad , \quad -\pi/6 \le \phi_r \le \pi/6 \tag{5.52}$$

$$H(\omega_r) = \sqrt{1 + \omega_r^2/\omega_p^2} \quad , \quad \phi(\omega_r) = \arctan(\omega_r/\omega_p)$$

Any single sector alone needs to be examined because of the sixfold symmetry present in the control scheme. Hence, sector s_0 is chosen and the axes $\alpha_0\beta_0$ correspond to $\alpha\beta$ axes and the subcript i is dropped in Eq. (5.51). The method of hierarchy of controls is used and the conditions for sliding motion to exist on the chosen sliding manifold are

$$\begin{aligned} &\left\{ \frac{i}{C} - \frac{R_s v_\alpha}{L} \right\} u_\alpha^+ < -f_\alpha + \frac{R_s v_\alpha}{L} u_\beta^\pm \\ &\left\{ \frac{i}{C} - \frac{R_s v_\alpha}{L} \right\} u_\alpha^- > -f_\alpha + \frac{R_s v_\alpha}{L} u_\beta^\pm \\ &\frac{i}{C} u_\beta^+ < -f_\beta \\ &\frac{i}{C} u_\beta^- > -f_\beta \end{aligned} \tag{5.53}$$

where

$$\mathbf{f} = \mathbf{GA}\hat{\mathbf{x}} + \mathbf{GT} = \begin{bmatrix} f_\alpha \\ f_\beta \end{bmatrix} \tag{5.54}$$

and $u_\beta^\pm$ is used to represent the two values that the control u_β assumes. The conditions of Eq. (5.53) result in the following inequalities:

$$\begin{aligned} &L < \frac{R_s RC}{a + \sqrt{3}M} \quad ; \quad a > 0 \\ &M > \sqrt{2} + \frac{1}{a}\sqrt{\frac{3}{2}} + \frac{1}{a\sqrt{2}} \frac{\omega_r}{\omega_p} \\ &M > \sqrt{2}\sqrt{1 + \omega_r^2/\omega_p^2} \end{aligned} \tag{5.55}$$

where M is the voltage gain v_d^*/v_g. Reaching is assured using current limiting action. The current limit I_m is chosen higher than i^* and u_{sd} and u_α are chosen to be $-\sqrt{3/2}$ when i exceeds I_m.

5.2.4 Stability of System in Sliding Mode

The stability of the system under sliding motion is determined using the method of equivalent control, as described in Section 5.1.4. The relation between $\hat{i}$ and $\hat{v}_d$ can be found using

$$v_g i = \frac{v_d^2}{R} + \frac{v_q^2}{R} + \frac{d}{dt}\left(\frac{1}{2}Cv_d^2\right) + \frac{d}{dt}\left(\frac{1}{2}Cv_d^2\right) + \frac{d}{dt}\left(\frac{1}{2}Li^2\right) \tag{5.56}$$

which represents the conservation of power in the converter. When the system is on the surface σ_q, $\hat{i}$ is related to $\hat{v}$ by

$$\hat{i} \approx \left\{\frac{2v_d^*}{Rv_g} + \frac{\hat{v}_d}{Rv_g}\right\}\hat{v}_d + \left\{\frac{C\hat{v}_d}{v_g} + \frac{Cv_d^*}{v_g}\right\}\dot{\hat{v}}_d \tag{5.57}$$

The motion of the system in the sliding manifold is described by

$$\left\{1 + \frac{2R_s v_d^*}{Rv_g} + \frac{R_s\hat{v}_d}{Rv_g}\right\}\hat{v}_d + \left\{\frac{\hat{v}_d}{v_g} + \frac{v_d^*}{v_g}\right\}R_s C\,\dot{\hat{v}}_d = 0 \tag{5.58}$$

The necessary condition for stability of the system on the intersection of the sliding surfaces is

$$\begin{aligned} \hat{v}_d &> -v_d^* \\ R_s &> 0 \end{aligned} \tag{5.59}$$

For the $\alpha_i\beta_i$ method, the conditions for stability are

$$\begin{aligned} \hat{v}_{\alpha_i} &> -v_{\alpha_i}^* \\ R_s &> 0 \\ \omega_r &< \sqrt{3}\,\omega_p + \frac{2v_g}{v_d^* R_s C} \end{aligned} \tag{5.60}$$

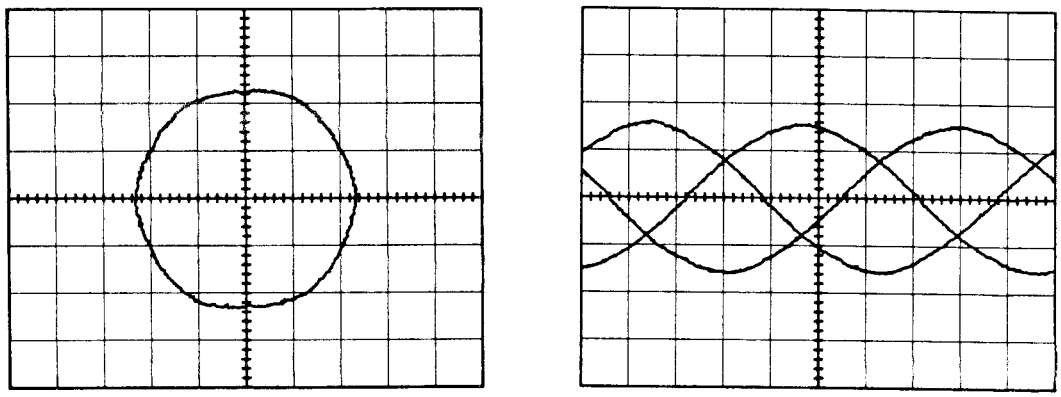

Figure 5.14: (a) The steady-state output voltage phasor in the $\alpha\beta$ frame for the system using sliding surfaces in the rotating dq reference frame. The scales on the x and y axes are 15 V/div and the inversion frequency is 100 Hz. (b) Steady-state three phase output voltages. The scale on the y-axis is 20 V/div.

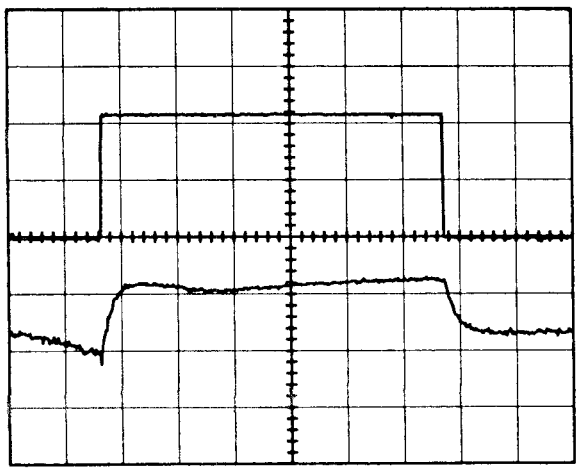

Figure 5.15: Response of the dq sliding mode system to a step change in the amplitude of the reference voltage. The scale on the x-axis is 8 ms/div while v_d is plotted on a scale of 6 V/div.

5.2.5 Experimental Results

In the practical implementation of the sliding surfaces described, the voltage error signals are obtained by direct measurement of output voltages and comparison with the desired reference voltages. However, the current error has to be obtained by measuring the inductor current and passing it through a high pass filter, and is given by

$$\hat{i}(s) = \frac{i(s)}{1+\omega_1/s} \quad ; \quad \omega_1 \ll \omega_p \tag{5.61}$$

Results shown are for the system implemented using sliding surfaces in the dq reference frame. Figure 5.14 portrays the measured output voltage phasor in the $\alpha\beta$ reference frame and Fig. 5.15 the response to a step change in the reference v_d. The parameters of the converter used for experimental measurements are:

$$\begin{aligned} &\mathrm{L} = 0.4 \text{ mH} \;\; ; \;\; \mathrm{C} = 31 \;\mu\mathrm{F} \;\; ; \;\; \mathrm{R} = 64\;\Omega \\ &\mathrm{V_g} = 20 \text{ V} \;\; ; \;\; \mathrm{R_s} = 10\;\Omega \;\; ; \;\; \mathrm{V_d^*} = 40 \text{ V} \end{aligned} \tag{5.62}$$

5.3 Flyback Inverter

The three phase flyback inverter consists of one triple-throw, and one quadruple-throw, current unidirectional, voltage bidirectional switch. The controls take values $+1$, -1, and 0 depending on the positions of the switches, as shown in Fig. 5.16. When the input control $u = 1$, then the output controls u_1, u_2, and u_3 have to be zero. Again, there are only two independent inputs that control the current that is fed to the output section. The current phasor feeding the output section can assume the seven dicrete positions shown in Fig. 5.17 with the amplitude of the phasor set by the inductor current. In this inverter, the average input current is lower than the inductor current, and the current gain of the inverter can be less than or greater than unity. Hence, the topology can provide voltage step-up or step-down.

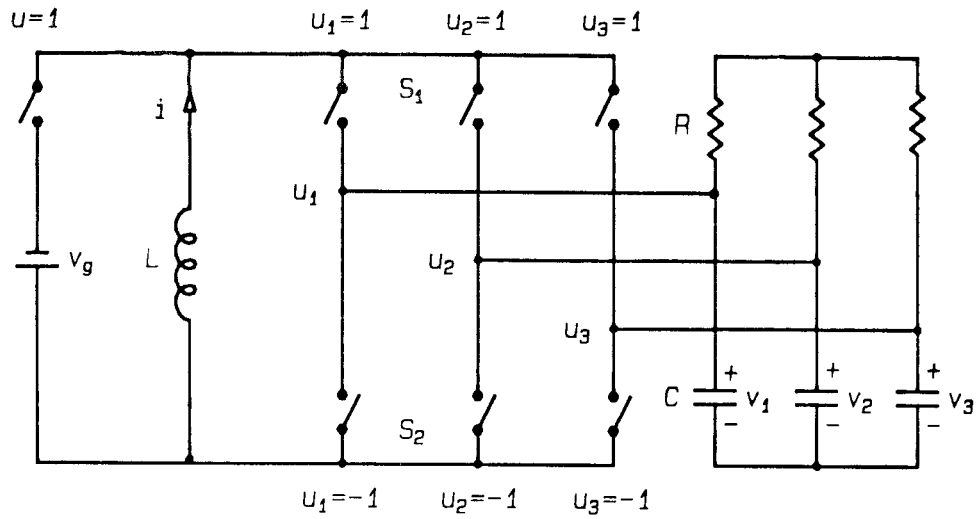

Figure 5.16: Three phase flyback inverter with one single-pole triple-throw switch and one quadruple-throw.

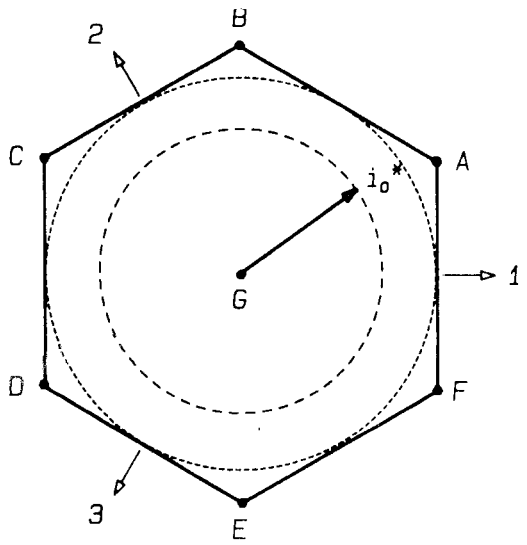

	u_1	u_2	u_3	u
A	1	0	−1	0
B	0	1	−1	0
C	−1	1	0	0
D	−1	0	1	0
E	0	−1	1	0
F	1	−1	0	0
G	0	0	0	1

Figure 5.17: The seven possible controls and the corresponding phasor of the current feeding the output sections. The amplitude of the phasors depends on the value of the inductor current.

5.3.1 System Description

The outputs of the flyback inverter are current-fed and the capacitor currents are discontinuous. The state space descripiton of the flyback inverter in the stationary reference frame is

$$\begin{aligned} L\dot{i} &= u\, v_g - \sum_{w=1}^{3} u_w v_w \\ C\dot{v}_w &= i\, u_w - \frac{1}{R} v_w + \frac{1}{3R} \sum_{z=1}^{3} v_z \end{aligned} \tag{5.63}$$

In the dq reference frame, the system is represented in terms of the state errors from the desired steady-state point $\tilde{\mathbf{x}}^*$ by

$$\dot{\tilde{\mathbf{x}}} = \tilde{\mathbf{A}}\,\tilde{\mathbf{x}} + \tilde{\mathbf{B}}\,\tilde{\mathbf{u}} + \tilde{\mathbf{T}} \tag{5.64}$$

where

$$\tilde{\mathbf{A}} = \begin{bmatrix} 0 & 0 & 0 \\ 0 & -\omega_p & \omega_r \\ 0 & -\omega_r & -\omega_p \end{bmatrix} \quad , \quad \tilde{\mathbf{x}} = \begin{bmatrix} \hat{i} \\ \hat{v}_d \\ \hat{v}_q \end{bmatrix}$$

$$\tilde{\mathbf{B}} = \begin{bmatrix} v_g/L & -v_d/L & -v_q/L \\ 0 & i/C & 0 \\ 0 & 0 & i/C \end{bmatrix} \quad , \quad \tilde{\mathbf{T}} = \begin{bmatrix} 0 \\ -\omega_p v_d^* \\ -\omega_r v_d^* \end{bmatrix} \tag{5.65}$$

$$\tilde{\mathbf{u}} = \begin{bmatrix} u \\ u_d \\ u_q \end{bmatrix} \quad , \quad \tilde{\mathbf{x}}^* = \begin{bmatrix} i^* \\ v_d^* \\ 0 \end{bmatrix} \quad , \quad \omega_p = \frac{1}{RC}$$

in which the reference v_q^* has been assumed to be zero. The steady-state values i^* and v_d^* are in accordance with

$$i^* = \frac{v_d^{*2}}{v_g R} + \frac{1}{\sqrt{2}} \frac{v_d^*}{R} \sqrt{1 + \frac{\omega_r^2}{\omega_p^2}} \tag{5.66}$$

In the $\alpha\beta$ frame, the system representation is

$$\dot{\hat{\mathbf{x}}} = \mathbf{A}\,\hat{\mathbf{x}} + \mathbf{B}\,\mathbf{u} + \mathbf{T} \tag{5.67}$$

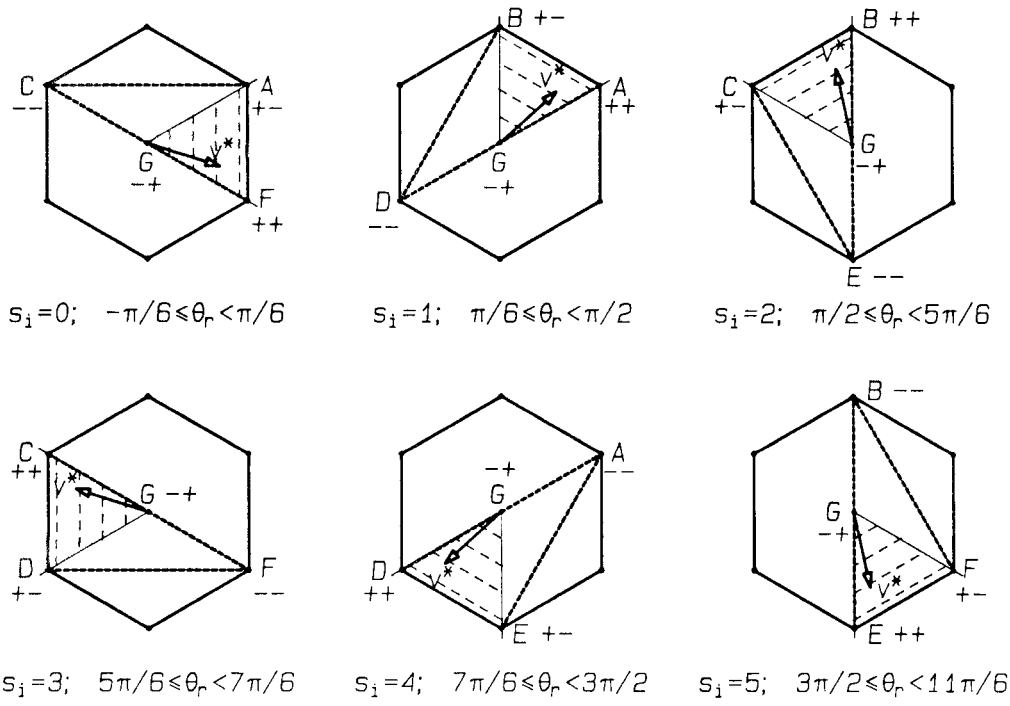

Figure 5.18: The switch positions used to control the flyback inverter depend on the signs of the functions σ_d, σ_q, and on the position of the reference phasor v^*.

where

$$\mathbf{A} = \begin{bmatrix} 0 & 0 & 0 \\ 0 & -\omega_p & 0 \\ 0 & 0 & -\omega_p \end{bmatrix} \quad , \quad \hat{\mathbf{x}} = \begin{bmatrix} \hat{i} \\ \hat{v}_\alpha \\ \hat{v}_\beta \end{bmatrix} \quad , \quad \mathbf{u} = \begin{bmatrix} u \\ u_\alpha \\ u_\beta \end{bmatrix}$$

$$\mathbf{B} = \begin{bmatrix} v_g/L & -v_\alpha/L & -v_\beta/L \\ 0 & i/C & 0 \\ 0 & 0 & i/C \end{bmatrix} \quad , \quad \mathbf{T} = \begin{bmatrix} 0 \\ -\omega_p H(\omega_r) v_d^* \cos\{\theta_r + \phi(\omega_r)\} \\ -\omega_p H(\omega_r) v_d^* \sin\{\theta_r + \phi(\omega_r)\} \end{bmatrix} \tag{5.68}$$

$$\omega_p = \frac{1}{RC} \quad , \quad H(\omega_r) = \sqrt{1 + \omega_r^2/\omega_p^2} \quad , \quad \phi(\omega_r) = \arctan(\frac{\omega_r}{\omega_p})$$

5.3.2 Sliding Surface

The flyback inverter is a current-fed topology like the boost inverter and similar sliding functions are used. However, the choice of controls has to be made in a different manner owing to the presence of a switch throw on the dc side of the converter. The sliding surfaces in the dq frame are given by

$$\tilde{\sigma} = \tilde{\mathbf{G}}\,\hat{\tilde{\mathbf{x}}} \tag{5.69}$$

where

$$\tilde{\sigma} = \begin{bmatrix} \sigma_d \\ \\ \sigma_q \end{bmatrix} \quad , \quad \tilde{\mathbf{G}} = \begin{bmatrix} R_s & 1 & 0 \\ \\ 0 & 0 & 1 \end{bmatrix} \tag{5.70}$$

The switch positions are chosen using the signs of the error functions σ_d, σ_q and the position θ_r of the reference phasor as shown in Fig. 5.18. The control inputs are given by

$$\tilde{\mathbf{u}} = \mathbf{Q}\,\mathbf{u}_s = \begin{bmatrix} 1 & 0 & 0 \\ 0 & \cos(\phi_r) & \sin(\phi_r) \\ 0 & -\sin(\phi_r) & \cos(\phi_r) \end{bmatrix} \begin{bmatrix} u \\ u_{sd} \\ u_{sq} \end{bmatrix} \tag{5.71}$$

where

$$\mathbf{u}_s^T = \begin{cases} [0, \quad \sqrt{3/2}, \quad -1/\sqrt{2}] & \text{for } \sigma_d > +\Delta_d \ , \ \sigma_q > +\Delta_q \\ [0, \quad \sqrt{3/2}, \quad 1/\sqrt{2}] & \text{for } \sigma_d > +\Delta_d \ , \ \sigma_q < -\Delta_q \\ [0, \quad -\sqrt{3/2}, \quad 1/\sqrt{2}] & \text{for } \sigma_d < -\Delta_d \ , \ \sigma_q < -\Delta_q \\ [1, \quad 0, \quad 0] & \text{for } \sigma_d < -\Delta_d \ , \ \sigma_q > +\Delta_q \end{cases} \tag{5.72}$$

$$\phi_r = \theta_r - (\pi/3)\, s_i \quad ; \quad 0 \le s_i \le 5$$

The $\alpha_i\beta_i$ reference frames shown in Table 5.2 can be used and sliding motion achieved using surfaces in these reference frames.

$$\sigma_i = \mathbf{G}\,\hat{\mathbf{x}}_i \quad ; \quad 0 \le s_i \le 5 \tag{5.73}$$

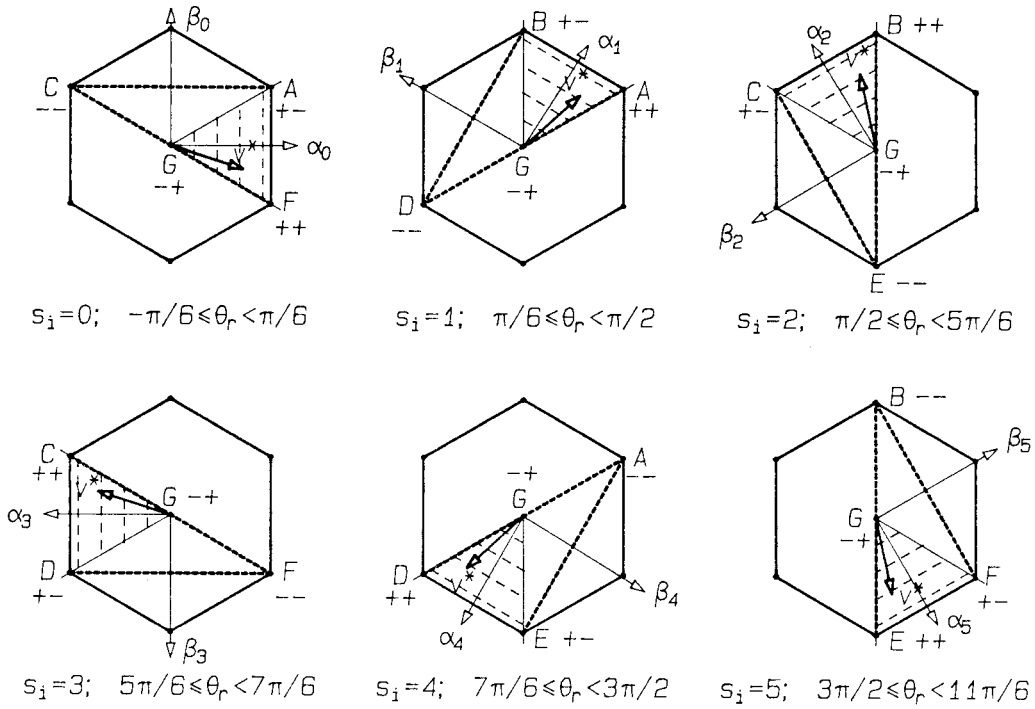

Figure 5.19: The $\alpha_i\beta_i$ axes and the corresponding switch positions for the sliding mode control of the flyback inverter.

where

$$\sigma_i = \begin{bmatrix} \sigma_{\alpha_i} \\ \sigma_{\beta_i} \end{bmatrix} \quad ; \quad \hat{\mathbf{x}}_i = \begin{bmatrix} \hat{i} \\ \hat{v}_{\alpha_i} \\ \hat{v}_{\beta_i} \end{bmatrix} \quad ; \quad \mathbf{G} = \tilde{\mathbf{G}} \tag{5.74}$$

The switch positions and axes used in each sector are shown in Fig. 5.19. In each sector the control input is described by

$$\mathbf{u}_i^T = \begin{cases} [0, \quad \sqrt{3/2}, \quad -1/\sqrt{2}] & \text{for } \sigma_{\alpha_i} > +\Delta_\alpha \ , \ \sigma_{\beta_i} > +\Delta_\beta \\ [0, \quad \sqrt{3/2}, \quad 1/\sqrt{2}] & \text{for } \sigma_{\alpha_i} > +\Delta_\alpha \ , \ \sigma_{\beta_i} < -\Delta_\beta \\ [0, \quad -\sqrt{3/2}, \quad 1/\sqrt{2}] & \text{for } \sigma_{\alpha_i} < -\Delta_\alpha \ , \ \sigma_{\beta_i} < -\Delta_\beta \\ [1, \quad 0, \quad 0] & \text{for } \sigma_{\alpha_i} < -\Delta_\alpha \ , \ \sigma_{\beta_i} > +\Delta_\beta \end{cases} \tag{5.75}$$

5.3.3 Existence and Reaching Conditions

The sliding conditions cannot be obtained by separating into two separate single input systems, as the inputs depend on both the error functions. However, sliding motion on each discontinuity surface can be checked by checking for sliding conditions for any control input that occurs. In the dq method, the condition for existence of sliding motion on σ_d is

$$L < \frac{R_s RC}{M + \sqrt{\frac{2}{3}} + \frac{1}{\sqrt{2}}\sqrt{1 + \frac{\omega_r^2}{\omega_p^2}}} \tag{5.76}$$

However, it is not possible to obtain sufficient conditions to ensure sliding motion on σ_q for θ_r in the vicinity of the boundaries of the sector. However, in practice, sliding motion exists at the intersection of the discontinuity surfaces for all θ_r if ω_r is small compared to ω_p. Reaching is ensured using current limiting action, as was done in the boost inverter. The current limit i_m should be higher than i^* and and L should be chosen to satisfy

$$L < \frac{R_s RC}{\sqrt{\frac{2}{3}} + \frac{i_m R}{v_d^*}} \tag{5.77}$$

In the $\alpha_i\beta_i$ method, the sufficient conditions for sliding motion to exist on each individual surface are

$$\begin{aligned} L &< \frac{R_s RC}{\sqrt{3}\,(M + 1/\sqrt{2}) + \sqrt{3/2}\sqrt{1 + \omega_r^2/\omega_p^2}} \\ M &> 1/\sqrt{2}\sqrt{1 + \omega_r^2/\omega_p^2} \\ \omega_r &> \sqrt{2/3}\,\omega_p \end{aligned} \tag{5.78}$$

The latter two inequalities in Eq. (5.78) are highly restrictive and may be very conservative. Reaching is ensured using current limiting action.

5.3.4 Stability of System in Sliding Mode

The stability of the flyback inverter in the sliding manifold is determined using the method of equivalent control. The relation between $\hat{i}$ and $\hat{v}_d$ is

$$\hat{i} \approx \hat{v}_d \left\{ \frac{2v_d^*}{v_g R} + \frac{\hat{v}_d}{v_g R} + \frac{1}{\sqrt{2}\,R} \right\} + \frac{\dot{\hat{v}}_d}{\omega_p} \left\{ \frac{v_d^*}{v_g R} + \frac{\hat{v}_d}{v_g R} + \frac{1}{\sqrt{2}\,R} \right\} \tag{5.79}$$

for $\omega_r^2 \ll \omega_p^2$. The motion of the system in sliding mode is described by

$$\left\{ 1 + \frac{2R_s v_d^*}{R v_g} + \frac{R_s \hat{v}_d}{R v_g} + \frac{R_s}{\sqrt{2}\,R} \right\} \hat{v}_d + \left\{ \frac{v_d^*}{v_g} + \frac{\hat{v}_d}{v_g} + \frac{1}{\sqrt{2}} \right\} R_s C \dot{\hat{v}}_d = 0 \tag{5.80}$$

and the conditions for stability are

$$\begin{aligned} R_s &> 0 \\ \hat{v}_d &> -v_d^* - \frac{v_g}{\sqrt{2}} \end{aligned} \tag{5.81}$$

The conditions for stable motion in the sliding manifold using the $\alpha_i\beta_i$ method are

$$\begin{aligned} R_s &> 0 \\ \hat{v}_{\alpha_i} &> -v_{\alpha_i}^* - \frac{v_g}{\sqrt{2}} \\ \omega_r/\omega_p &< \sqrt{3} + 2/M \end{aligned} \tag{5.82}$$

5.3.5 Simulation Results

The sliding surfaces are implemented by measuring the output voltages and inductor current of the inverter. The current error $\hat{i}$ is obtained by passing the measured current signal through a high pass filter, as in the case of the boost inverter. The simulation results for the dq method are shown in Figs. 5.20 and 5.21, which portray the output voltage phasor in the $\alpha\beta$ frame, and the response of the system to a step change in the reference v_d^*.

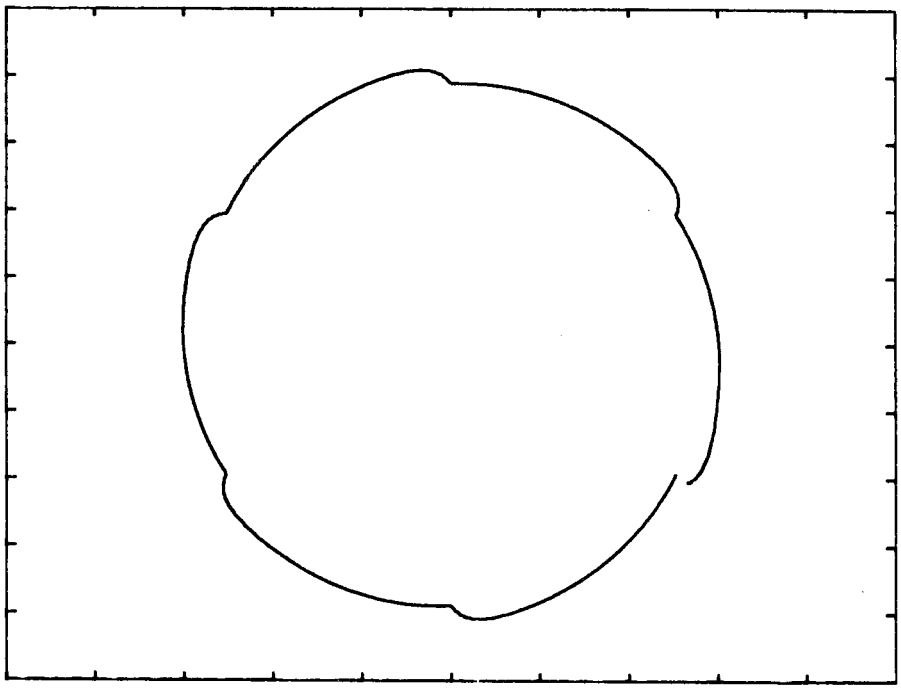

Figure 5.20: The output voltage phasor in the $\alpha\beta$ frame for the flyback inverter using sliding surfaces in the rotating dq reference frame.

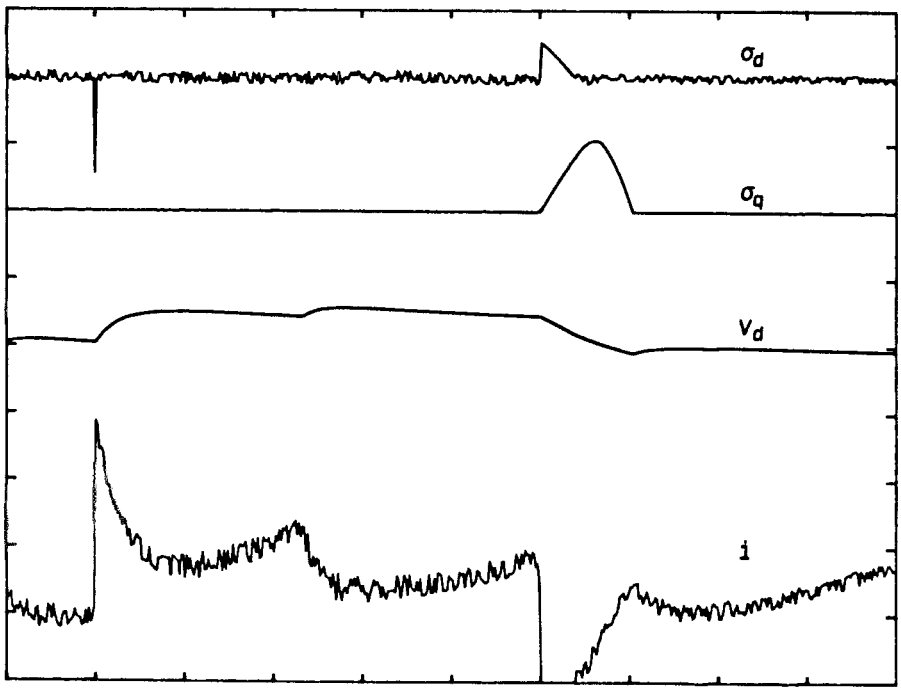

Figure 5.21: Response of the dq sliding mode system to a step change in the amplitude of the reference voltage.

Chapter 6

Sliding Mode Control of Rectifiers

The sliding mode control of balanced polyphase rectifiers is considered in this chapter. The control is used to regulate the desired dc output voltage, as well as to produce desired input waveforms and draw power from the ac source at unity power factor. The three basic topologies are considered and illustrated using three phase versions of these topologies.

The three phase rectifier has two independent controls which can be used to regulate the dc output and reduce the low frequency harmonic distortion of the input ac currents. The input ac current may be pulsating (at the switching frequency) or smooth depending on the converter topology. If the input currents are pulsating, it is necessary to obtain their average value from the duty ratios of the switches in order to control the low frequency ac harmonics in the input currents. Often, this feature may already be present in the power circuit in the form of an ac input filter.

6.1 Buck Rectifier

The three phase buck rectifier, Fig. 6.1, consists of two triple-throw switches that apply any one of the three ac line voltages to the ac end of the inductor. The control inputs u_k can assume values $+1$, -1, or 0, and the the possible combinations for the different positions of the switches are shown in Fig. 6.2. When in normal steady-state operation, the inductor current and output voltage are dc (with a switching ripple) and

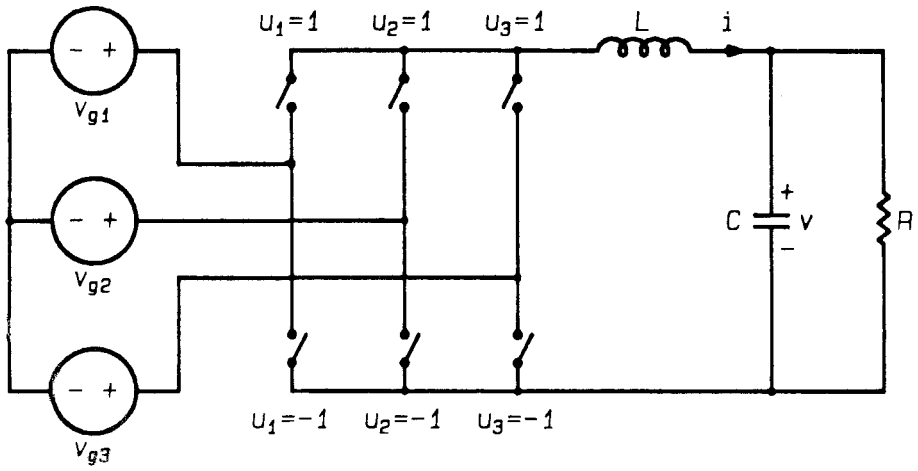

Figure 6.1: Three phase buck rectifier with two two triple-throw switches and two independent controls. The input currents are pulsating in nature.

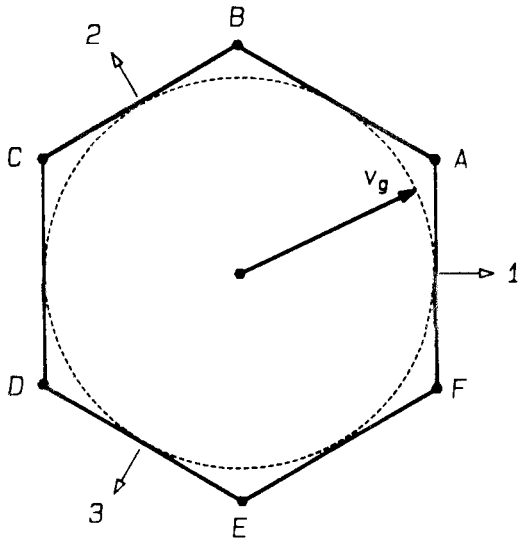

	u_1	u_2	u_3
A	1	0	-1
B	0	1	-1
C	-1	1	0
D	-1	0	1
E	0	-1	1
F	1	-1	0

Figure 6.2: The possible switch positions and corresponding control inputs shown in the stationary abc reference frame.

the input currents are pulsating. The control positions of the switches are chosen so as to maintain the average input current sinusoidal and with the desired phase. In this case, the average ac input currents cannot be measured directly from the power stage and have to be obtained in the control circuit.

6.1.1 System Description

The output capacitor voltage and its derivative are continuous and differentiable functions and the state space description of the system can be put in the control canonical form. In the *abc* reference frame, the system is described by

$$\ddot{v} = -\frac{1}{RC}\dot{v} - \frac{1}{LC}v + \frac{1}{LC}\sum_{k=1}^{3} u_k v_{gk} \tag{6.1}$$

where

$$v_{gk} = v_{gm}\cos\{\theta_r - (k-1)\frac{2\pi}{3}\} \quad ; \quad 1 \le k \le 3 \tag{6.2}$$

In the moving *dq* reference frame, the system is described in terms of the voltage error and its derivative by

$$\dot{\tilde{\mathbf{x}}} = \tilde{\mathbf{A}}\,\tilde{\mathbf{x}} + \tilde{\mathbf{B}}\,\tilde{\mathbf{u}} + \tilde{\mathbf{T}} \tag{6.3}$$

where

$$\tilde{\mathbf{A}} = \begin{bmatrix} 0 & 1 \\ -\omega_o^2 & -\omega_p \end{bmatrix} \quad ; \quad \tilde{\mathbf{B}} = \begin{bmatrix} 0 & 0 \\ \omega_o^2 v_{gd} & 0 \end{bmatrix}$$

$$\tilde{\mathbf{T}} = \begin{bmatrix} 0 \\ -\omega_o^2 v^* \end{bmatrix} \quad ; \quad \tilde{\tilde{\mathbf{x}}} = \tilde{\mathbf{x}} - \tilde{\mathbf{x}}^* = \begin{bmatrix} \hat{v} \\ \dot{\hat{v}} \end{bmatrix} \quad ; \quad \tilde{\mathbf{u}} = \begin{bmatrix} u_d \\ u_q \end{bmatrix} \tag{6.4}$$

$$\omega_o^2 = \frac{1}{LC} \quad ; \quad \omega_p = \frac{1}{RC}$$

in which the transformation has been chosen in phase with $\mathbf{v}_g$ such that the component v_{gq} is zero. The system of Eq. (6.4) is similar to a buck dc-dc converter with the control input u_d. The ac source currents, however, depend on both u_d and u_q, and the controller must

use u_q to provide average input currents that are sinusoidal in the stationary reference frame.

6.1.2 Sliding Surfaces

The system of Eq. (6.4) is similar to the buck dc-dc converter and consequently a sliding surface of the form

$$\sigma_d = \hat{v} + \tau \dot{\hat{v}} \tag{6.5}$$

can be utilized with u_d chosen depending on the position θ_r of the source phasor $\mathbf{v}_g$. This will, however, control the output voltage only and will not provide the desired average input current waveforms. Consequently, the system is augmented using the average value of the control input u_q given by

$$\dot{x}_{uq} = u_q \tag{6.6}$$

The sliding surface

$$\sigma_q = x_{uq} \tag{6.7}$$

is then used to maintain the average value of control u_q as zero and thus provide average ac source currents that are sinusoidal and in phase with the source voltage. If a power factor different from unity is desired, the average value of u_q can be regulated to be equal to a constant value that is determined by the desired input power factor.

The sliding mode control of the augmented system reduces to the control of two single input, single output systems using the above-mentioned sliding surfaces. The control inputs are chosen depending on the sector s_i in which the source vector $\mathbf{v}_g$ lies, as shown in Fig. 6.3, and are given by

$$\tilde{\mathbf{u}} = \mathbf{Q}\,\mathbf{u}_s = \begin{bmatrix} \cos(\phi_r) & \sin(\phi_r) \\ -\sin(\phi_r) & \cos(\phi_r) \end{bmatrix} \begin{bmatrix} u_{sd} \\ u_{sq} \end{bmatrix} \tag{6.8}$$

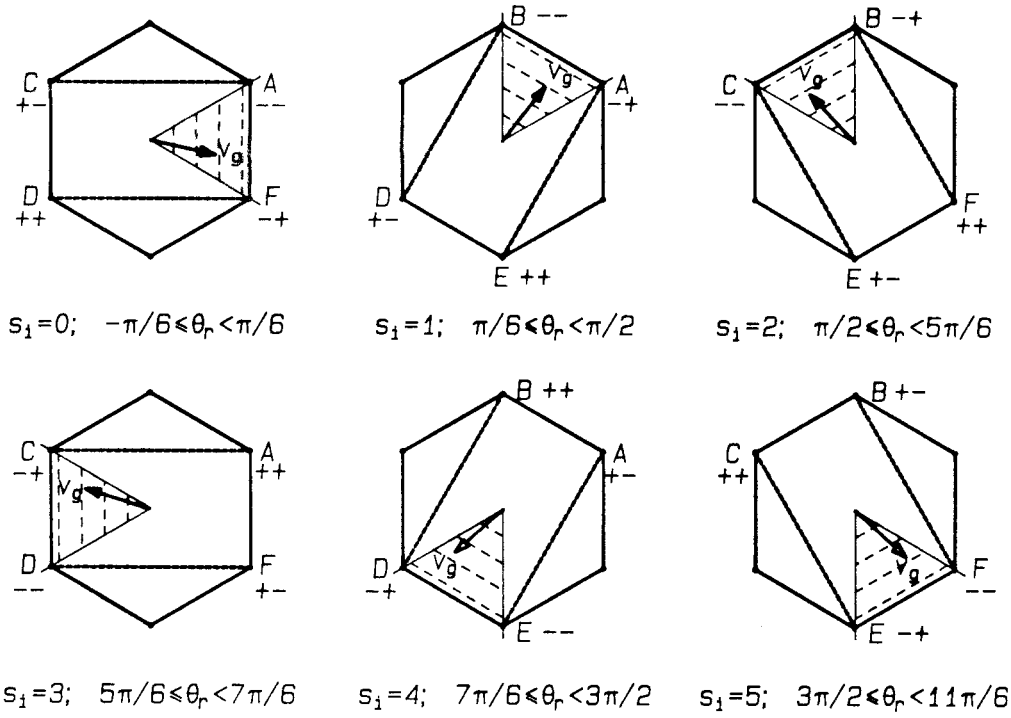

Figure 6.3: The switch position is chosen using the position of the source phasor $\mathbf{v}_g$ *and the signs of the* σ_d, σ_q.

where

$$u_{sd} = \begin{cases} +\sqrt{3/2} & ; \ \sigma_d < -\Delta_d \\ -\sqrt{3/2} & ; \ \sigma_d > +\Delta_d \end{cases}$$

$$u_{sq} = \begin{cases} +1/\sqrt{2} & ; \ \sigma_q < -\Delta_q \\ -1/\sqrt{2} & ; \ \sigma_q > +\Delta_q \end{cases} \tag{6.9}$$

$$\phi_r = \theta_r - (\pi/3)\, s_i \ ; \ 0 \leq s_i \leq 5$$

6.1.3 Existence and Reaching Conditions

Sufficient conditions for the existence of sliding motion on the surfaces σ_d and σ_q can be obtained by considering the dependence of u_d on u_{sq}, u_q on u_{sd} to be like disturbances to two single input, single output sliding mode systems. The time

derivatives of the sliding functions are given by

$$\begin{aligned} \dot{\sigma}_d &= (1 - \omega_p \tau)\, \dot{\hat{v}} - \omega_o^2 \tau \hat{v} - \omega_o^2 \tau v^* + \omega_o^2 \tau v_{gd}\, u_d \\ \dot{\sigma}_q &= u_q \end{aligned} \tag{6.10}$$

The magnitude of the control $|u_d|$ varies between $\sqrt{3/2}$ and $1/\sqrt{2}$ depending on u_{sq} and θ_r, while the sign of u_d is set by the sign of the σ_d. Similarly, the magnitude of control $|u_q|$ changes between $1/\sqrt{2}$ and 0.

The existence and reaching conditions for sliding motion on σ_q are automatically satisfied by the chosen controls for all θ_r, except at the boundary of the sectors. The conditions for existence of sliding motion on σ_d and reaching are

$$\begin{aligned} v &< \frac{\sqrt{3}}{2}\, v_{gm} \\ \tau &> RC \end{aligned} \tag{6.11}$$

6.1.4 Stability of System in Sliding Mode

The motion of the system on the sliding surfaces can be found using the method of equivalent control. In sliding mode, the system motion is described by

$$\hat{v} + \tau\, \dot{\hat{v}} = 0 \tag{6.12}$$

and the sliding mode system is asymptotically stable for $\tau > 0$. The origin is the stable equilibrium point and the system operates at the desired steady-state operating point set by the reference v^*.

6.1.5 Simulation Results

The sliding surface σ_d is implemented using the measured output capacitor voltage and capacitor current. The function σ_q is found directly from the switch controls u_1, u_2, and u_3, by transforming to find u_q and then passing through an integrator. The circuitry necessary for implementing the transformation is of the same order of complexity

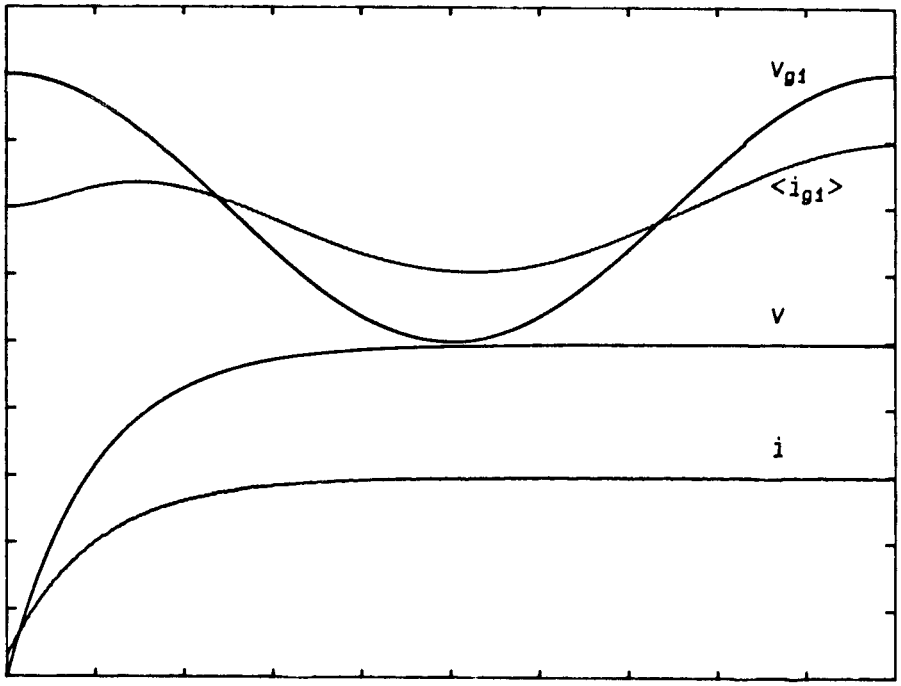

Figure 6.4: Starting transient of the three phase buck rectifier. The top two traces depict the ac source voltage v_{g1} and average source current $< i_{g1} >$ of phase 1 while the bottom traces show the output voltage v and the inductor current i. The ac source frequency was set at 100 Hz.

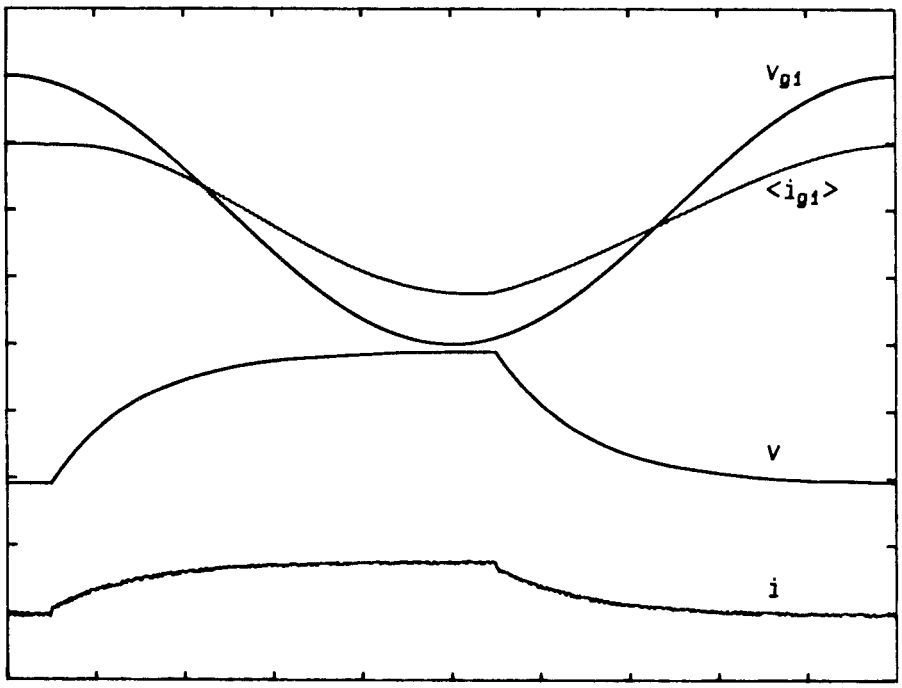

Figure 6.5: The response of the system to a step change in the voltage reference v^* from $15V$ *to* $17V$.

as that used for pulse-width modulated schemes as only one-half of the dq transformation is involved.

The simulation results of the three phase buck rectifier are shown in Figs. 6.4 and 6.5. The scale and origin used for each variable plotted is different and is not marked for clarity. Figure 6.4 shows the starting transient of the sliding mode system. The starting transient consists of two segments: first, reaching of the sliding manifold; second, moving along the sliding surface to the desired steady-state operating point. In the buck rectifier, the reaching segment of the transient is very short and corresponds to the initial fast rise in the inductor current. The average steady-state ac input currents are sinusoidal and the small phase difference between the source voltage and current is due to the low pass filter used to calculate the average source current. The response of the sliding mode system to a step change in the reference voltage v^* is plotted in Fig. 6.5. The system leaves the sliding surface owing to the step change, but returns to the surface rapidly and proceeds towards steady state along the sliding surface. The converter and sliding mode parameters of the system used in the simulation are

$$\begin{aligned} &\mathrm{L} = 1\ \mathrm{mH} \quad ; \quad \mathrm{C} = 10\ \mu\mathrm{F} \quad ; \quad \mathrm{R} = 10\ \Omega \\ &\mathrm{V_g} = 30\ \mathrm{V} \quad ; \quad \mathrm{V}^* = 15\ \mathrm{V} \quad ; \quad \tau = 10^{-3}\,\mathrm{sec} \end{aligned} \tag{6.13}$$

6.2 Boost Rectifier

The boost rectifier of Fig. 6.6 consists of three single-pole, double throw switches. The inductors at the source end enable the converter to provide smooth input currents, while the output capacitor current is pulsating in nature, as is characteristic of the boost topology. The controls u_k can assume values $+1$ and -1 depending on the positions of the switches. The eight possible switch positions and the corresponding control inputs are depicted in the phasor diagram of Fig. 6.7. There are only two independent

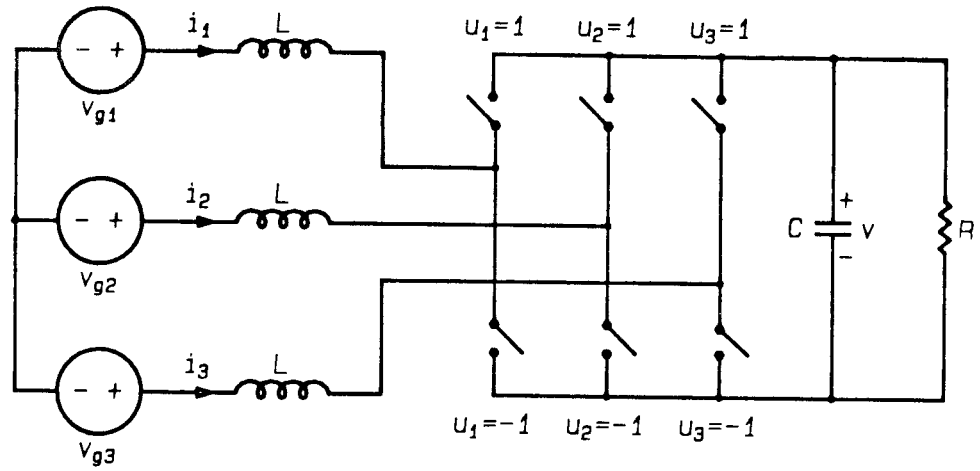

Figure 6.6: The boost rectifier with three single-pole, double-throw switches. The ac input currents are smooth, but the output current is pulsating in this topology.

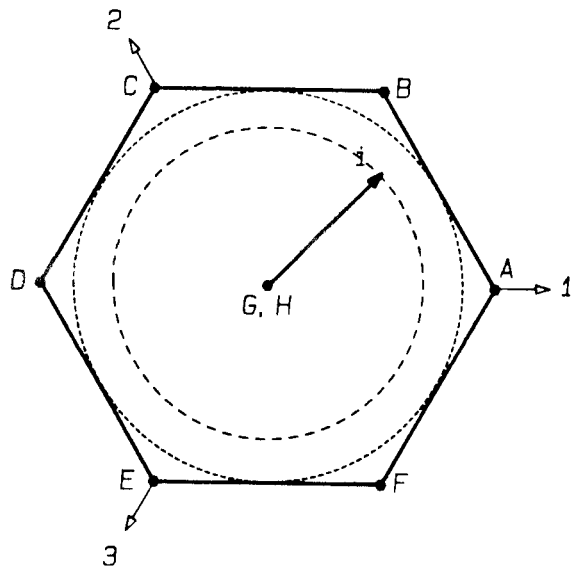

	u_1	u_2	u_3
A	1	-1	-1
B	1	1	-1
C	-1	1	-1
D	-1	1	1
E	-1	-1	1
F	1	-1	1
G	1	1	1
H	-1	-1	-1

Figure 6.7: The eight possible switch positions and corresponding control inputs for the boost rectifier.

controls, as the topology constrains the inductor currents to be balanced. In steady state, the desired inductor currents are balanced sinusoidal currents and the output capacitor voltage is a constant dc voltage.

6.2.1 System Description

Owing to the pulsating nature of the output capacitor current, the boost rectifier cannot be put in the controllable canonical form in terms of the output voltage and its derivatives. The state space description of the system in terms of the inductor currents and capacitor voltage is given by

$$\begin{aligned} L\dot{i}_k &= v_{gk} - u_k\frac{v}{2} + \frac{v}{2}\sum_{z=1}^{3} u_z \quad ; \quad 1 \le k \le 3 \\ C\dot{v} &= \frac{1}{2}\sum_{k=1}^{3} i_k u_k - \frac{v}{R} \end{aligned} \tag{6.14}$$

where the balanced ac source voltages v_{gk} are as described by Eq. (6.2). The system representation in the dq reference frame is

$$\dot{\tilde{\hat{\mathbf{x}}}} = \tilde{\mathbf{A}}\,\tilde{\hat{\mathbf{x}}} + \tilde{\mathbf{B}}\,\tilde{\mathbf{u}} + \tilde{\mathbf{T}} \tag{6.15}$$

where

$$\begin{aligned} \tilde{\mathbf{A}} &= \begin{bmatrix} 0 & \omega_r & 0 \\ -\omega_r & 0 & 0 \\ 0 & 0 & -\omega_p \end{bmatrix} \quad ; \quad \tilde{\mathbf{B}} = \begin{bmatrix} v/2L & 0 \\ 0 & v/2L \\ i_d/2C & i_q/2C \end{bmatrix} \quad ; \quad \tilde{\mathbf{T}} = \begin{bmatrix} v_{gd}/L \\ -\omega_r i_d^* \\ -\omega_p v^* \end{bmatrix} \\ \tilde{\hat{\mathbf{x}}} &= \tilde{\mathbf{x}} - \tilde{\mathbf{x}}^* = \begin{bmatrix} \hat{i}_d \\ \hat{i}_q \\ \hat{v} \end{bmatrix} \quad ; \quad \tilde{\mathbf{u}} = \begin{bmatrix} u_d \\ u_q \end{bmatrix} \quad ; \quad \omega_p = \frac{1}{RC} \end{aligned} \tag{6.16}$$

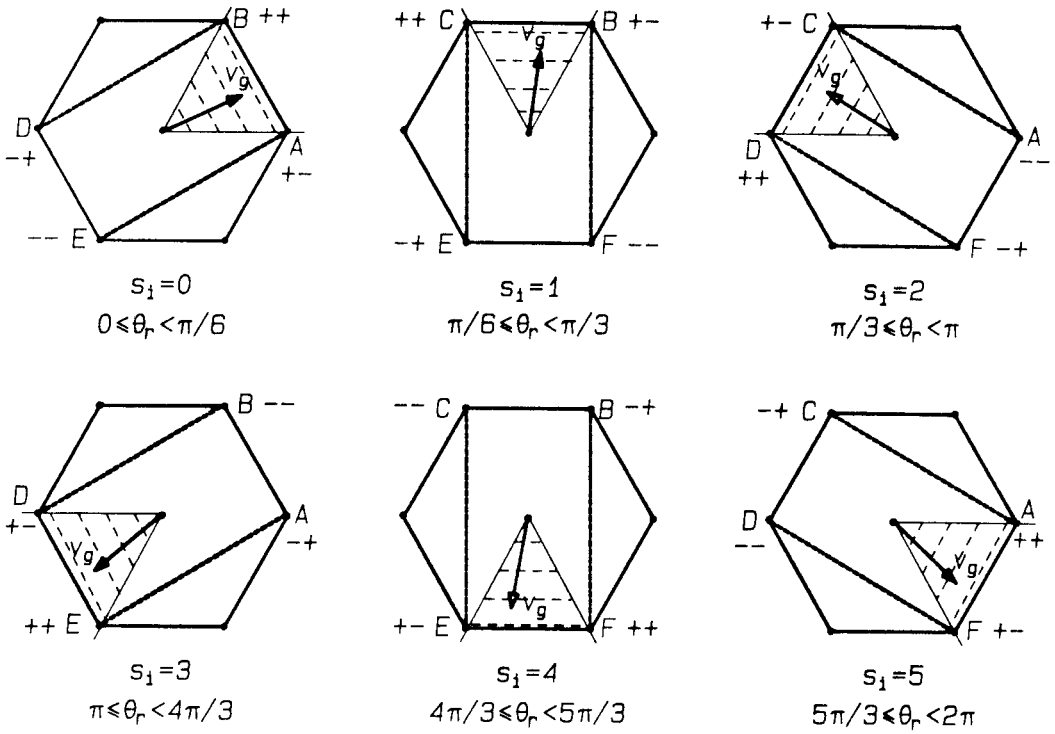

Figure 6.8: The switch positions used to control the boost rectifier depend on the the signs of σ_d, σ_q, and the sector in which the source voltage phasor lies.

in which the transformation has been chosen so as to make v_{gq} equal to zero and $\tilde{\mathbf{x}}^*$ is the desired steady-state operating point given by

$$\tilde{\mathbf{x}}^* = \begin{bmatrix} i_d^* \\ 0 \\ v^* \end{bmatrix} \tag{6.17}$$

It is observed that if i_q is regulated to zero using u_q, then the system of Eq. (6.16) becomes similar to a boost dc-dc converter.

6.2.2 Sliding Surfaces

The sliding surfaces are chosen so as to make the system similar to the boost dc-dc converter. Hence, one sliding surface is chosen to keep i_q at zero and the second is

used to regulate the output voltage. The sliding surfaces are given by

$$\begin{aligned} \sigma_d &= \hat{v} + R_s \hat{i}_d \\ \sigma_q &= \hat{i}_q \end{aligned} \tag{6.18}$$

and the switch positions are chosen depending on the signs of σ_d, σ_q, and the angular position of the source voltage phasor. The choice of control illustrated in Fig. 6.8 is given by

$$\tilde{\mathbf{u}} = \mathbf{Q}\,\mathbf{u}_s = \begin{bmatrix} \cos(\phi_r) & \sin(\phi_r) \\ -\sin(\phi_r) & \cos(\phi_r) \end{bmatrix} \begin{bmatrix} u_{sd} \\ u_{sq} \end{bmatrix} \tag{6.19}$$

where

$$u_{sd} = \begin{cases} +\sqrt{3/2} & ; \quad \sigma_d > +\Delta_d \\ -\sqrt{3/2} & ; \quad \sigma_d < -\Delta_d \end{cases}$$

$$u_{sq} = \begin{cases} +1/\sqrt{2} & ; \quad \sigma_q > +\Delta_q \\ -1/\sqrt{2} & ; \quad \sigma_q < -\Delta_q \end{cases} \tag{6.20}$$

$$\phi_r = \theta_r - \pi/6 - (\pi/3)\, s_i \quad ; \quad 0 \le s_i \le 5$$

6.2.3 Existence and Reaching Conditions

Existence conditions are found by considering the system motion in the vicinity of the sliding surfaces σ_d and σ_q. In the vicinity of $\sigma_q = 0$, $|i_q|$ is small and sliding conditions on σ_d are similar to those of a boost dc-dc converter. The rates of change of the functions σ_d and σ_q are

$$\begin{aligned} \dot{\sigma}_d &= \frac{i_d}{2C} u_d - v\omega_p + \frac{R_s}{L} v_{gd} - \frac{R_s v}{2L} u_d + R_s \omega_r i_q + \frac{i_q}{2C} u_q \\ \dot{\sigma}_q &= -\frac{v}{2L} u_q - \omega_r i_d \end{aligned} \tag{6.21}$$

in which the last two terms in $\dot{\sigma}_d$ can be neglected when the system is close to the surface $\sigma_q = 0$. Control u_d varies in magnitude between $\sqrt{3/2}$ and $1/\sqrt{2}$ in any sector, and the

conditions for sliding motion on the surface $\sigma_d = 0$ are similar to those for the boost dc-dc converter and are given by

$$\begin{aligned} L &< \frac{R_s RC v_{gd}}{v} \\ v &> 2\sqrt{2}\, v_{gd} \end{aligned} \tag{6.22}$$

However, as the magnitude of the control u_q varies between $1/\sqrt{2}$ and 0, sliding conditions for σ_q do not hold for θ_r close to the boundaries of the sectors. Though sufficient conditions cannot be found for sliding motion to exist on each individual surface, it does exist at their intersection and the conditions of Eq. (6.22) provide satisfactory criteria for the design of a sliding mode boost rectifier. Reaching is ensured using current limiting action.

6.2.4 Stability of System in Sliding Mode

The motion of the system in the sliding manifold is obtained using the power relation

$$v_{gd} i_d = \frac{v^2}{R} + Cv\dot{v} + Li_d\dot{i}_d + Li_q\dot{i}_q \tag{6.23}$$

The relation between $\hat{i}_d$ and $\hat{v}$ is

$$\hat{i}_d \approx \left\{ \frac{\hat{v}}{Rv_{gd}} + \frac{2v^*}{Rv_{gd}} \right\} \hat{v} + \left\{ \frac{C\hat{v}}{v_{gd}} + \frac{Cv^*}{v_{gd}} \right\} \dot{\hat{v}} \tag{6.24}$$

and the motion of the system in sliding mode is described by

$$\left\{ 1 + \frac{\hat{R_s} v}{Rv_{gd}} + \frac{2R_s v^*}{Rv_{gd}} \right\} \hat{v} + \left\{ \frac{R_s C\hat{v}}{v_{gd}} + \frac{R_s Cv^*}{v_{gd}} \right\} \dot{\hat{v}} = 0 \tag{6.25}$$

The conditions for the sliding system to be asymptotically stable with a stable equilibrium point at the origin are

$$\begin{aligned} R_s &> 0 \\ \hat{v} &> -v^* \end{aligned} \tag{6.26}$$

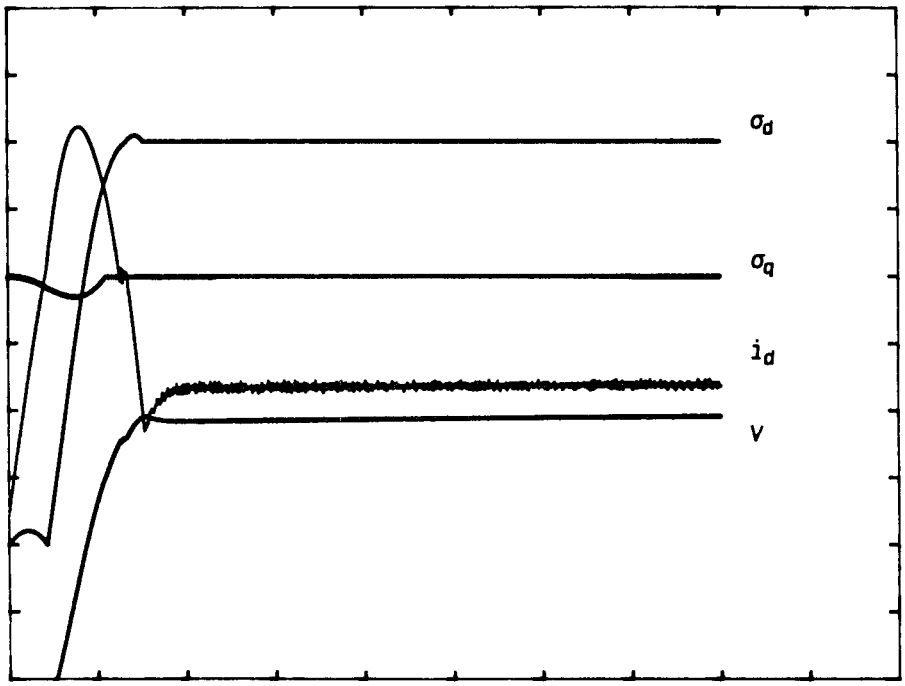

Figure 6.9: The starting transient of the three phase boost rectifier. The plot shows the sliding functions σ_d, σ_q, the output voltage v, and the component i_d of the source current.

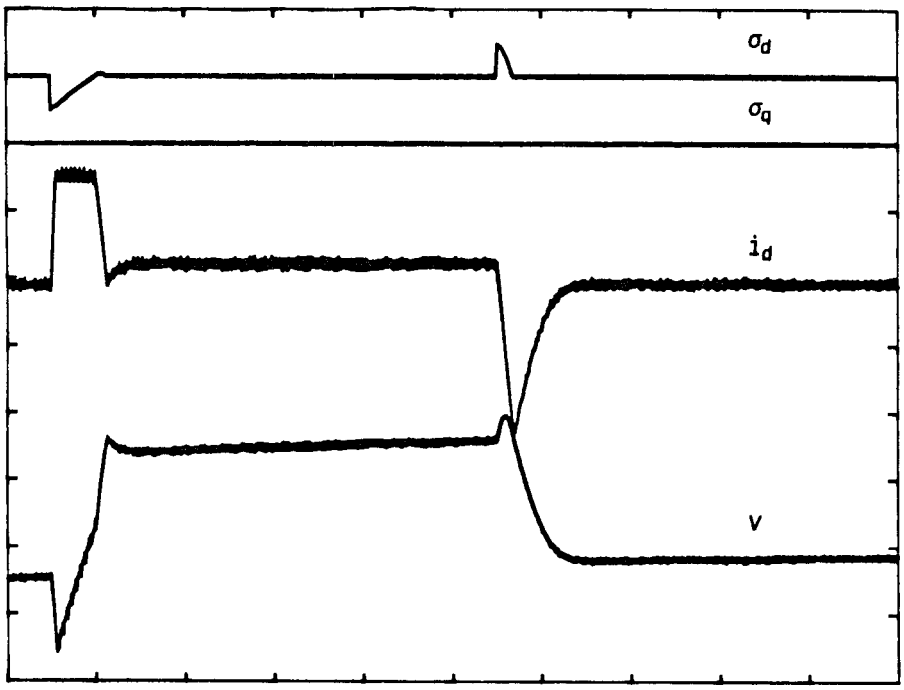

Figure 6.10: The ac input current transient for a step change in the reference v^*.

6.2.5 Simulation Results

The sliding surfaces are implemented by sensing the output voltage and inductor currents in the stationary reference frame and transforming the currents to the dq reference frame using the dq transformation. The current error $\hat{i}_d$ is then approximated by passing i_d through a high pass filter and given by

$$\hat{i}_d(s) = \frac{i_d(s)}{1+\omega_1/s} \quad ; \quad \omega_1 \ll \omega_p \tag{6.27}$$

The simulation results of the three phase boost rectifier are plotted in Figs. 6.9 and 6.10.

Figure 6.9 portrays the starting transient of the boost rectifier. The starting transient consists of three modes of operation. The first segment is the uncontrolled portion of the response while the output voltage rises to a certain minimum level, and the peak current cannot be limited during this portion of the transient. The second section of the starting transient is the current limiting mode and subsequent reaching of the sliding surfaces. The current limiting section of the starting transient of Fig 6.9 is very brief. The final section of the transient consists of motion of the system in the sliding manifold, towards the steady-state operating point. The response of the sliding mode system to a step change in the reference v^*, is shown in Fig 6.10. The response is composed of two sections: first, in current limiting mode until the system reaches the sliding surface, and finally in sliding mode to the operating point. The parameters of the system modelled are:

$$\begin{aligned} &\mathrm{L} = 1\ \mathrm{mH} \ ; \ \mathrm{C} = 100\ \mu\mathrm{F} \ ; \ \mathrm{R} = 50\ \Omega \\ &\mathrm{V_g} = 15\ \mathrm{V} \ ; \ \mathrm{R_s} = 1\ \Omega \ ; \ \mathrm{V^*} = 60\ \mathrm{V} \end{aligned} \tag{6.28}$$

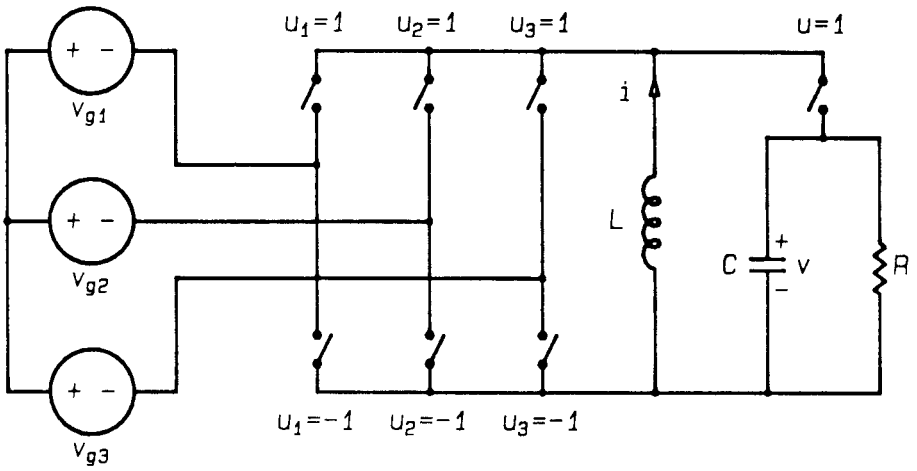

Figure 6.11: The flyback rectifier with one single-pole, triple-throw switch and quadruple-throw switch. The input currents are pulsating in this topology.

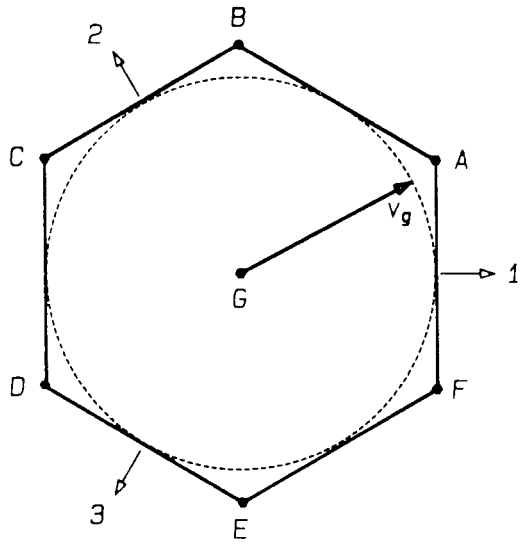

	u_1	u_2	u_3	u
A	1	0	−1	0
B	0	1	−1	0
C	−1	1	0	0
D	−1	0	1	0
E	0	−1	1	0
F	1	−1	0	0
G	0	0	0	1

Figure 6.12: The control inputs for the possible switch positions in the flyback rectifier.

6.3 Flyback Rectifier

The flyback rectifier contains one single-pole, triple-throw switch and one quadruple-throw switch, as shown in Fig. 6.11. The controls u_k can be $+1$, -1, or 0 depending on the positions of the switches S_1 and S_2. The topology constrains the controls u_k to sum to zero and there are only two independent controls available. The possible control inputs are depicted in the phasor diagram of Fig. 6.12. The input and output currents are pulsating in this topology.

6.3.1 System Description

The state space description of the system in the stationary reference frame is

$$\begin{aligned} L\dot{i} &= \sum_{k=1}^{3} u_k v_{gk} - u\, v \\ C\dot{v} &= u\, i - \frac{v}{R} \end{aligned} \tag{6.29}$$

with the balanced ac source voltages v_{gk} described by Eq. (6.2). In the dq reference frame the representation of the system is

$$\dot{\tilde{\mathbf{x}}} = \tilde{\mathbf{A}}\,\tilde{\mathbf{x}} + \tilde{\mathbf{B}}\,\tilde{\mathbf{u}} + \tilde{\mathbf{T}} \tag{6.30}$$

where

$$\begin{aligned} \tilde{\mathbf{A}} &= \begin{bmatrix} 0 & 0 \\ 0 & -\omega_p \end{bmatrix} \quad ; \quad \tilde{\mathbf{B}} = \begin{bmatrix} v_{gd}/L & 0 & -v/L \\ 0 & 0 & i/C \end{bmatrix} \\ \tilde{\mathbf{T}} &= \begin{bmatrix} 0 \\ -\omega_p v^* \end{bmatrix} \quad ; \quad \tilde{\hat{\mathbf{x}}} = \tilde{\mathbf{x}} - \tilde{\mathbf{x}}^* = \begin{bmatrix} \hat{v} \\ \dot{\hat{v}} \end{bmatrix} \quad ; \quad \tilde{\mathbf{u}} = \begin{bmatrix} u_d \\ u_q \\ u \end{bmatrix} \\ \omega_p &= \frac{1}{RC} \end{aligned} \tag{6.31}$$

In Eq. (6.31) the transformation has been chosen in phase with the ac source voltage phasor in order to make v_{gq} zero. In Eq. (6.31) it is seen that the control u_q has no effect

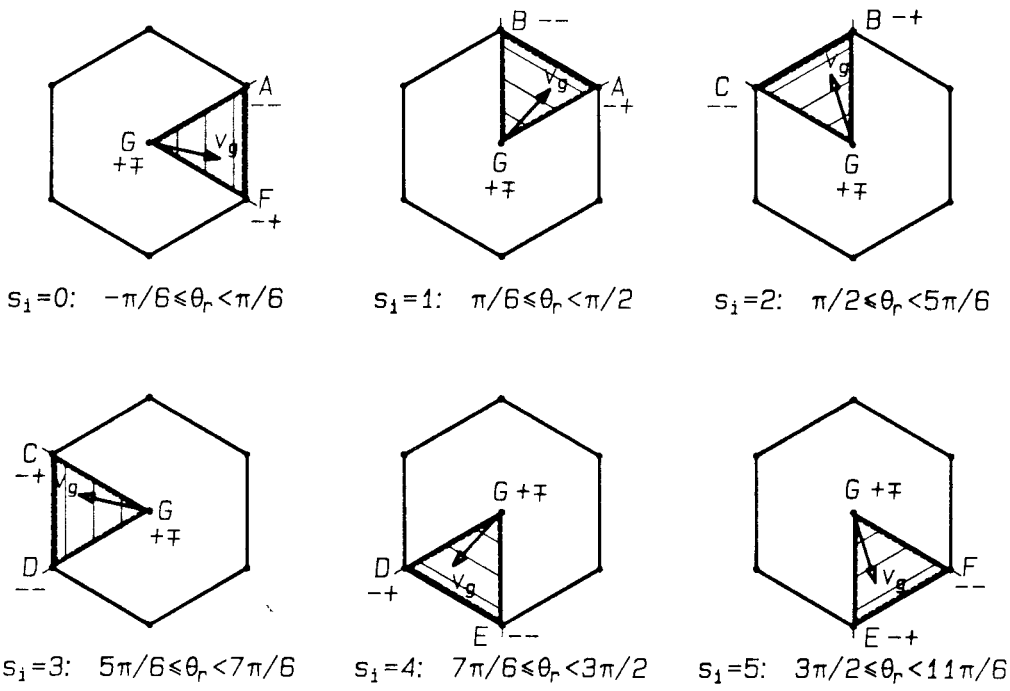

Figure 6.13: The choice of switch positions depends on σ_d, σ_q, and on the sector in which $\mathbf{v}_g$ lies.

on the output voltage, while u_d and u can be used to regulate the output voltage. The control u_q is consequently used to obtain the desired average input ac current waveforms.

6.3.2 Sliding Surfaces

The flyback rectifier of Eq. (6.31) is similar to the flyback dc-dc converter and the sliding surface

$$\sigma_d = \hat{v} + R_s \hat{i} \tag{6.32}$$

is used to regulate the output voltage. The desired average input currents are obtained by augmenting the system with the average value of u_q. The sliding surface

$$\sigma_q = x_{uq} \tag{6.33}$$

is used to maintain the average value of u_q to be zero where x_{uq} defined by

$$\dot{x}_{uq} = u_q \tag{6.34}$$

The switch positions are chosen depending on the signs of the error functions and the position of the source voltage phasor $\mathbf{v}_g$, as shown in Fig. 6.13. Only three switch positions are used in each sector in this control strategy.

6.3.3 Existence and Reaching Conditions

Sufficient conditions for existence and reaching can be obtained by considering the system to be like two single input sliding mode systems. The derivatives of the sliding functions are

$$\begin{aligned} \dot{\sigma}_d &= -\omega_p \hat{v} - \omega_p v^* + \frac{R_s}{L} v_{gd} u_d - \frac{R_s}{L} v u + \frac{i}{C} u \\ \dot{\sigma}_q &= u_q \end{aligned} \tag{6.35}$$

The existence conditions for sliding mode on σ_d are satisfied if

$$L < \frac{R_s R C v_{gd}}{\sqrt{2} v} \tag{6.36}$$

and reaching is ensured using current limiting action. If the current limit used is I_m, then L has to satisfy the inequality

$$L < \frac{R_s R C v}{R I_m + v} \tag{6.37}$$

For the control chosen

$$\begin{aligned} \sigma_q \dot{\sigma}_q &< 0 \quad \text{for} \quad \sigma_d < 0 \\ \sigma_q \dot{\sigma}_q &= 0 \quad \text{for} \quad \sigma_d > 0 \end{aligned} \tag{6.38}$$

and the rigorous conditions for sliding motion on σ_q are not satisfied. However, it is sufficient to ensure sliding motion at the intersection of $\sigma_d = 0$ and $\sigma_q = 0$.

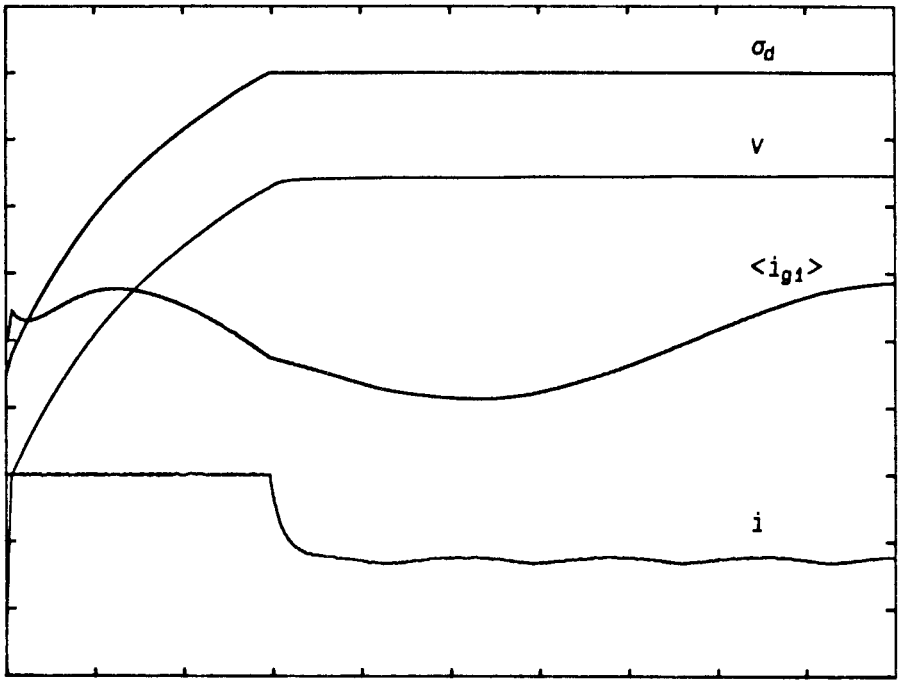

Figure 6.14: The starting transient of the three phase flyback rectifier. The plot shows the sliding function σ_d, average source current $< i_{g1} >$, the output voltage v, and the inductor current i. The ac source frequency used is 100 *Hz.*

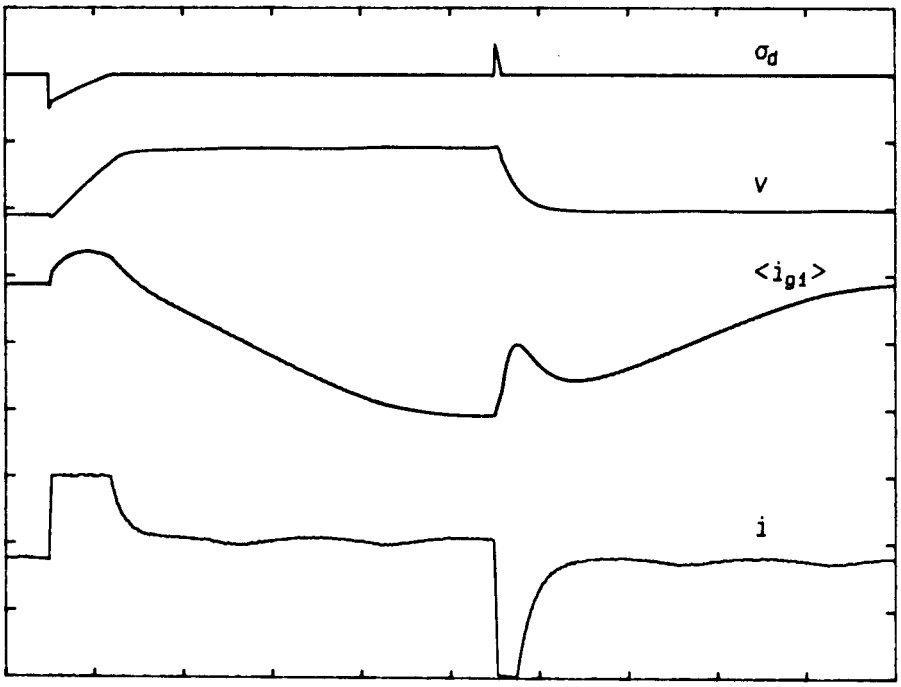

Figure 6.15: The response of the sliding mode system to a step change in the reference voltage v^*.

6.3.4 Simulation Results

The sliding function σ_d is implemented by measuring the inductor current and output voltage and passing the measured current through a high pass filter to obtain the current error $\hat{i}$. The sliding function σ_q is obtained by transforming the controls u_k to get u_q and passing through an integrator. The simulation results of the flyback rectifier using

$$\begin{aligned} &\mathrm{L} = 1 \text{ mH} \;\; ; \;\; \mathrm{C} = 100 \; \mu\mathrm{F} \;\; ; \;\; \mathrm{R} = 50 \; \Omega \\ &\mathrm{V_{gm}} = 30 \text{ V} \;\; ; \;\; \mathrm{R_s} = 1 \; \Omega \;\; ; \;\; \mathrm{V^*} = 45 \text{ V} \end{aligned} \tag{6.39}$$

are plotted in Figs. 6.14 and 6.15.

Figure 6.14 portrays the starting transient, which consists of two operating modes. In the first segment, the system reaches the sliding surfaces under current limiting action. After reaching the sliding surfaces, it moves in the the sliding manifold towards the desired steady-state operating point. In steady-state operation, the average source currents are sinusoidal and in phase with the ac source voltage. The response of the system to a step change in the reference voltage is shown in Fig. 6.15. The response again comprises current-limited motion followed by sliding motion.

6.4 Sliding Mode with Fixed Switching Frequency

It is possible to achieve sliding mode control and maintain a fixed switching frequency by using a combination of sinusoidal pulse width modulation and sliding mode control. This is done by applying sliding mode control using the duty ratio of a sinusoidally pulse width modulated rectifier. This can be done easily in the case of the buck and flyback rectifiers, as they closely resemble the corresponding dc-dc converters.

The averaged state space description of the three basic, sinusoidally pulse width modulated, rectifiers described in Chapter 1 is:

- Buck Rectifier:

$$\begin{aligned} L\,\dot{i} &= d_m\, v_m \cos\phi - v \\ C\,\dot{v} &= i - v/R \end{aligned} \tag{6.40}$$

- Boost Rectifier:

$$\begin{aligned} L\,\dot{i}_d &= v_{gd} - v\, d'_m \cos\phi + \omega_r L\, i_q \\ L\,\dot{i}_q &= v_{gq} - v\, d'_m \sin\phi - \omega_r L\, i_d \\ C\,\dot{v} &= i_d d'_m \cos\phi + i_q d'_m \sin\phi - v/R \end{aligned} \tag{6.41}$$

- Flyback Rectifier:

$$\begin{aligned} L\,\dot{i} &= d_m\, v_m \cos\phi - d'_m\, v \\ C\,\dot{v} &= d'_m\, i - v/R \end{aligned} \tag{6.42}$$

In the above description, d_m or d'_m represents the duty ratio amplitude of the switches; v_m is the amplitude of the ac source voltage; ϕ is the phase of the sinusoidal modulation of the duty ratios with respect to the source voltage. The control input in all cases is d_m and ϕ, and the duty ratio d_m is varied discontinuously between 0 and 1 (or d_{min} and d_{max}) to provide sliding mode control of the output voltage. The averaged descriptions of the buck and flyback rectifiers are identical to the buck and flyback dc-dc converters with v_g equal to $v_m \cos\phi$, and sliding control of the rectifier is identical to that of the dc-dc converter. The only additional constraint required is that the sliding frequency be small compared to the switching frequency of the pulse width modulated switches. A simple approach is not possible for the sliding control of the boost rectifier.

Good robust performance of the system can be realized using this method of control. However, it does not utilize the full capabilities of the converter as the sliding motion is constrained to operate at a lower frequency than the switching frequency itself. Consequently, the small signal bandwidth of such a controller will necessarily be only a small fraction of the switching frequency.

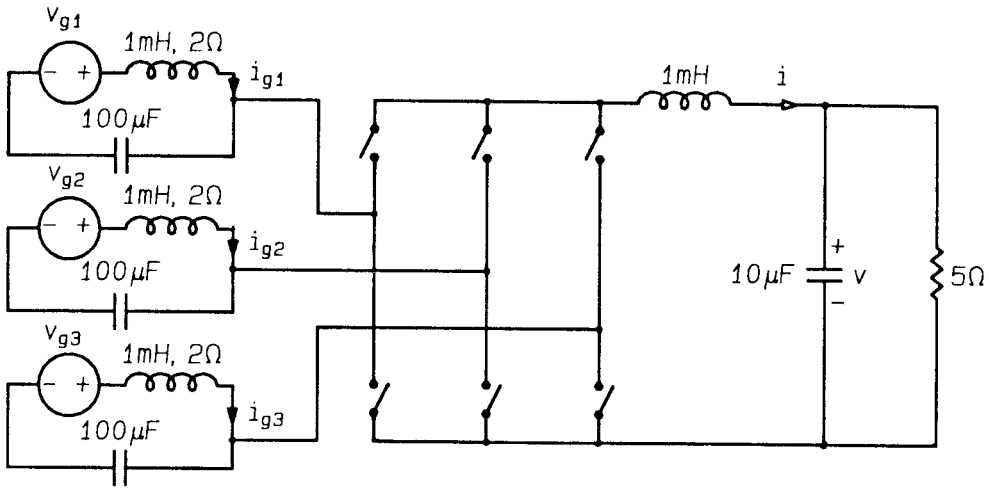

Figure 6.16: The sinusoidally pulse width modulated, buck rectifier with sliding mode control of the output used for simulations.

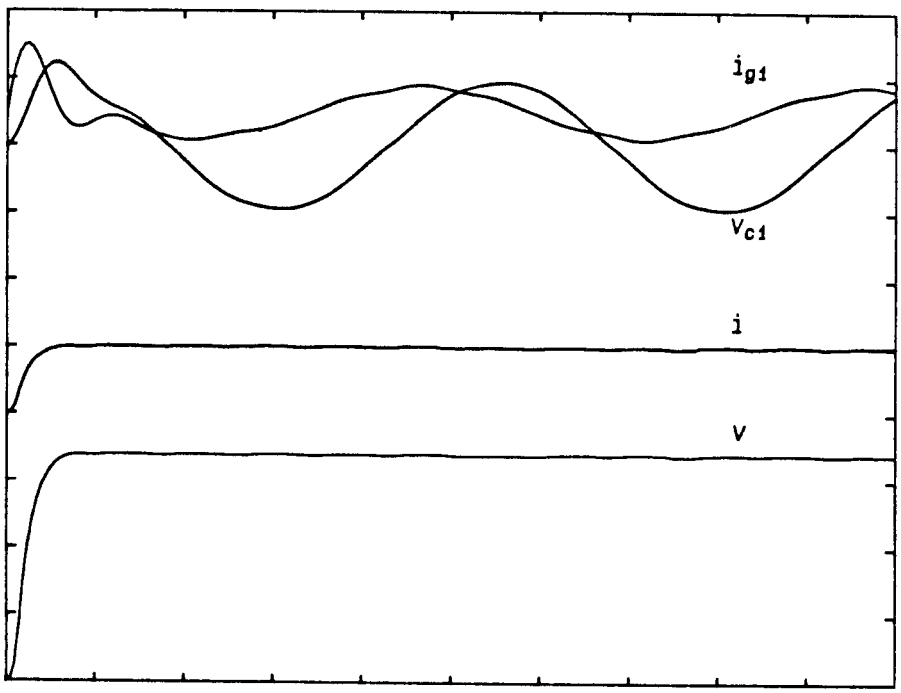

Figure 6.17: The starting transient of the sliding controlled buck rectifier.

The buck rectifier of Fig. 6.16 was simulated with the parameters shown. Figure 6.17 shows a simulation of the starting transient of the sliding mode controlled, sinusoidally pulse width modulated, buck rectifier with input filter.

Conclusion

Control and analysis techniques for fast-switching balanced polyphase inverters and rectifiers have been considered in this thesis. The concepts of current reference programming and sliding mode control of inverters and rectifiers were developed. These methods of control are utilized to enable and simplify the control of balanced polyphase converter systems that are multiple-input multiple-output, nonlinear systems.

The low frequency model of the converter was found using describing functions in the rotating dq reference frame. The low frequency representation of the system is in general nonlinear and the system input-output pairs are not decoupled from each other. Current reference programming simplifies the system by reducing the effective order of the system and improves the dynamic response of the converter. In some converters the current programming loop helps to decouple the outputs from one another and eliminates some of the nonlinearities present in the converter. Consequently, the design of regulators using MIMO control techniques is simplified considerably. However, design of the controller employing the small-signal, linear models is not adequate to ensure the stability or performance of the system in the face of large signal disturbances or transients.

Sliding mode control of the switching converter was used to ensure the stability and performance of the system in the presence of large signal transients. The conditions for sliding motion were satisfied by proper choice of switch positions and design parameters. The existence and reaching conditions ensure the stability of the system during large signal transients. The linear ripple and small-signal approximations made in state

space averaging techniques are not necessary, and both the large and small signal motion of the system were characterized using the sliding system formulation. The sliding system guarantees that the average motion of the converter converges to the desired response described by the equivalent control.

The equivalent control represents the low frequency behavior of the system, and small signal models can be obtained from it. The sliding domain of operation of the system is, however, not easy to obtain in an analytic closed form owing to the complexity and high order of balanced polyphase converter systems. Although some of the analytic conditions derived are conservative, they are useful for design purposes. The state-plane trajectories cannot be utilized to obtain the sliding domain and reaching conditions, as in the case of the basic dc-dc converters, because of the higher order of polyphase systems.

The two control methods developed perform the task of regulation through two vastly different approaches. In a current programmed system, the objective of sinusoidal ac voltage and current waveforms is achieved using an open loop, sinusoidal pulse width modulation scheme. An external feedback controller is then employed to provide regulation. Thus, the system design and testing is separated into two distinct segments and is simplified. However, global stability and performance cannot be guaranteed. The sliding mode system, however, achieves both objectives simultaneously using a closed loop controller. The design process is simple using the derived conditions, but the system is not easy to test and debug as it cannot be operated open loop to test subcomponents of the system. However, proper design of the sliding system ensures global stability and performance for the operating range of the system.

Appendix A

Variable Structure Systems in Sliding Mode

The n^{th} order variable structure system is considered to be of the form

$$\dot{\mathbf{x}} = \mathbf{f}(\mathbf{x}, t) + \mathbf{B}(\mathbf{x}, t)\,\mathbf{u} \tag{A.1}$$

where the functions $\mathbf{f}$ and $\mathbf{Bu}$ satisfy the Lipschitz conditions everywhere except on the discontinuity surfaces. Each component of the m-dimensional control input $\mathbf{u}$ is discontinuous and the m discontinuity surfaces used to determine the control inputs are given by

$$\mathbf{s} = \mathbf{G}\,\mathbf{x} \tag{A.2}$$

and the control inputs are chosen according to

$$u_i = \begin{cases} u_i^+ \;\; ; \;\; s_i > 0 \\ \\ u_i^- \;\; ; \;\; s_i < 0 \end{cases} \quad ; \quad 1 \leq i \leq m \tag{A.3}$$

Sliding motion of the system is related to the convergence of the states of the system towards the manifold $\mathbf{s} = 0$, as shown in Fig. A.1.

Definition 1 *A domain* $\mathbf{S}$ *in the manifold* $\mathbf{s} = \mathbf{0}$ *is a sliding mode domain if for each* $\epsilon > 0$ *there exists a* $\delta > 0$ *such that any motion starting in the n-dimensional* δ*-vicinity of* $\mathbf{S}$ *may leave the n-dimensional* ϵ*-vicinity of* $\mathbf{S}$ *only through the n-dimensional* ϵ*-vicinity of the boundaries of* $\mathbf{S}$.

The sliding surfaces and the controls must satisfy the following necessary conditions for sliding motion to exist at the intersection of the discontinuity surfaces.

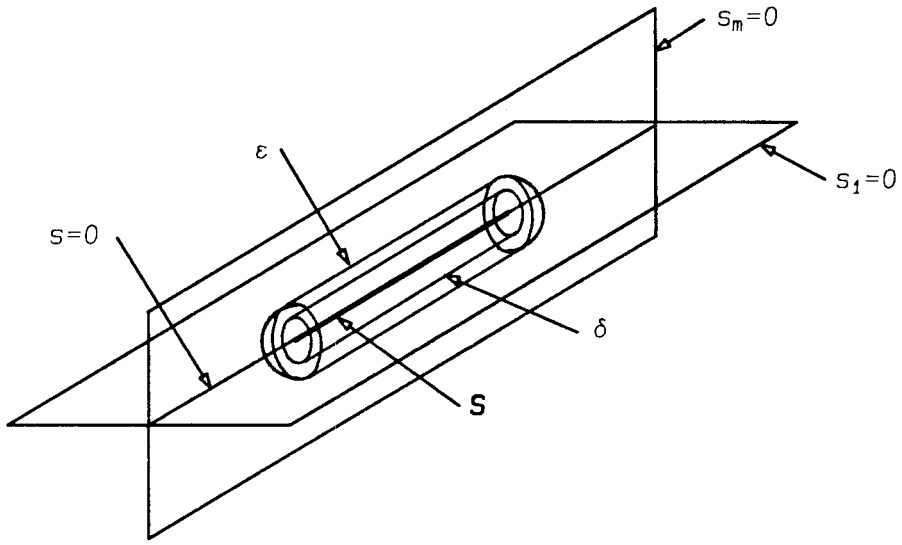

Figure A.1: Definition of domain of sliding mode in a multiple-input, variable structure system.

Theorem 1 *For sliding motion to exist in the sliding manifold* $\mathbf{s} = 0$ *it is necessary that:*

1. *There exists a solution* u_{eq} *for the equivalent control defined by*

$$\mathbf{s} = \mathbf{Gf} + \mathbf{GBu}_{eq} = 0$$

2. *The components of* $\mathbf{u}_{eq}$ *satisfy the inequalities*

$$\min(u_i^+, u_i^-) \leq u_{i_{eq}} \leq \max(u_i^+, u_i^-)$$

Theorem 2 *For the* $(n-m)$*-dimensional domain* $\mathbf{S}$ *in the manifold* $\mathbf{s} = 0$ *to be a sliding domain, it is sufficient that in some n-dimensional domain* $\mathbf{\Omega}$, $\mathbf{S} \subset \mathbf{\Omega}$, *there exists a continuously differentiable function* $v(\mathbf{x}, \mathbf{s}, t)$ *satisfying the following conditions.*

1. v *is positive definite with respect to* $\mathbf{s}$ *for any* $\mathbf{x} \in \mathbf{S}$ *and* t

$$\inf_{\|\mathbf{s}\|=R} v = h_R \ , \qquad \sup_{\|\mathbf{s}\|=R} v = H_R \ ,$$

where h_R and H_R are positive quantities (for $R > 0$) depending only on R.

2. *The time derivative of v has a negative supremum on small enough spheres $\|\mathbf{s}\| = R$ excluding points on the discontinuity surfaces, where this derivative does not exist.*

The above theorem is an analog of the Lyapunov stability theorem on the motion of the system, projected on the subspace $(s_1, \ldots, s_m)$, and there are no standard methods to find the function v in the general case.

If the sliding conditions are satisfied over the complete state space, then reaching of the sliding manifold is assured. However, if the sliding conditions are satisfied only in the vicinity of the sliding manifold, then reaching has to be ensured using different conditions. The following necessary condition has to hold for the system to reach the discontinuity surfaces.

Theorem 3 *For the variable structure system to reach the discontinuity surfaces, it is necessary that the equilibrium points of each structure do not belong to the existence domain of that structure.*

If existence conditions for sliding motion are satisfied on each individual discontinuity surface, and the motion of the system in sliding mode is asymptotically stable, then the system will reach the sliding manifold if it reaches any of the discontinuity surfaces.

Theorem 4 *For the asymptotic stability of the motion of the variable structure system in sliding mode along the manifold $\mathbf{s} = 0$, it is necessary and sufficient that the system with $\mathbf{u} = \mathbf{u}_{eq}$ computed with $\mathbf{s} = 0$ is asymptotically stable.*

Bibliography

[1] B. D. Bedford and R. G. Hoft, *Principles of Inverter Circuits,* John Wiley and Sons: New York, 1964.

[2] B. K. Bose, ed., *Adjustable Speed Ac Drive Systems,* IEEE Press: New York, 1981.

[3] S. B. Dewan and A. Straughen, *Power Semiconductor Circuits,* John Wiley and Sons: New York, 1975.

[4] J. Zubek, "Pulsewidth Modulated Inverter Motor Drives with Improved Modulation," IEEE Tran. Industry Applications, vol. IA-11, November/December 1975, pp. 695–703.

[5] G. S. Buja and G. B. Indri, "Optimal Pulsewidth Modulation for Feeding Ac Motors, " IEEE Tran. Industry Applications, vol. IA-13, no. 1, January/February 1977, pp. 38–44.

[6] J. B. Casteel and R. G. Hoft, "Optimum PWM Waveforms of a Microprocessor Controlled Inverter," IEEE Power Electronics Specialists Conference, 1978 Record, pp. 243–250 (IEEE Publication 78CH1337-5).

[7] F. Barzegar and S. Ćuk, "A New Switched-Mode Amplifier Produces Clean Three Phase Power," Proc. Ninth International Solid-State Power Conversion (Powercon 9), July 1982, pp. E3.1–15.

[8] F. C. Schwarz and W. L. M. Chateleux, " A Multikilowatt Polyphase Ac/Dc Converter with Reversible Power Flow and without Passive Low Frequency Filters," IEEE Power Electronics Specialists Conference, 1979 Record, pp. 448–458 (IEEE Publication 79CH1461-3 AES).

[9] K. Ngo, S. Ćuk, and R. D. Middlebrook, "A New Flyback Dc-to-Three-Phase Converter with Sinusoidal Outputs," IEEE Power Electronics Specialists Conference, 1983 Record, pp. 377–388 (IEEE Publication 83CH1877-0).

[10] Khai. D. T. Ngo, "Low Frequency Characterization of PWM Converters," IEEE Power Electronics Specialists Conference, 1985 Record, pp. 195–203 (IEEE Publication 85CH2117-0).

[11] D. C. White and H. H. Woodson, *Electromechanical Energy Conversion,* John Wiley and Sons: New York, 1959.

[12] R. D. Middlebrook and Slobodan Ćuk, "A General Unified Approach to Modelling Switching-Converter Power Stages," IEEE Power Electronics Specialists Conference, 1976 Record, pp. 18–34 (IEEE Publication 76CH1084-3 AES).

[13] A. Capel, G. Ferrante, D. O'Sullivan, and A. Weinberg, " Application of the Injected Current Model for the Dynamic Analysis of Switching Regulators with the New Concept of LC^3 Modulator," IEEE Power Electronics Specialists Conference, 1978 Record, pp. 135–147 (IEEE Publication 78CH1337-5 AES).

[14] Cecil W. Deisch, "Simple Switching Control Method Changes Power Converter into a Current Source," IEEE Power Electronics Specialists Conference, 1978 Record, pp. 300–306 (IEEE Publication 78CH1337-5 AES).

[15] Shi-Ping Hsu, Art Brown, Loman Rensink, and R. D. Middlebrook, "Modelling and Analysis of Switching Dc-to-Dc Converters in Constant-Frequency Current-Programmed Mode," IEEE Power Electronics Specialists Conference, 1979 Record, pp. 284–301 (IEEE Publication 79CH1461-3 AES).

[16] R. D. Middlebrook, "Topics in Multiple-Loop Regulators and Current-Mode Programming," IEEE Power Electronics Specialists Conference, 1985 Record, pp. 716–732 (IEEE Publication 85CH2117-0).

[17] Art Brown and R. D. Middlebrook, "Sampled-Data Modelling of Switching Regulators," IEEE Power Electronics Specialists Conference, 1981 Record, pp. 349–369 (IEEE Publication 81CH1652-7).

[18] B. H. Cho and F. C. Lee, "Measurement of Loop Gain with the Digital Modulator," IEEE Power Electronics Specialists Conference, 1984 Record, pp. 363–373 (IEEE Publication 84CH2000-8).

[19] R. Mahadevan, S. El-Hamamsy, W. M. Polivka, and S. Ćuk, "A Converter with Three Switched-Networks Improves Regulation, Dynamics and Control," Proc. Tenth International Solid-State Power Conversion (Powercon 10), March 1983, pp. E1.1–E1.19.

[20] V.I.Utkin, *Sliding Modes and their Application in Variable Structure Systems,* Mir Publishers: Moscow, 1974 (English translation, Mir, 1978).

[21] Faruk Bilalović, Osman Musić, and Asif Sabanović, "Buck Converter Regulator Operating in the Sliding Mode," Proc. Seventh International PCI'83 Conference, pp. 331–340.

[22] Ram Venkataramanan, Asif Sabanović, and Slobodan Ćuk, "Sliding Mode Control of Dc-to-Dc Converters," International Conference on Industrial Electronics, Control, and Instrumentation (IECON '85), 1985 Record, pp. 251–258 (IEEE Publication 85CH2160-0).